

# AutoPhysio

A companion active knee brace for early phase home-based  
anterior cruciate ligament (ACL) rehabilitation



Chih Jung Lee (**CJL**), Ryan Cherian (**RJC**), Will Taylor (**WT**), Yoonsang Lee (**YSL**)

3rd Year Project Report

Trinity Term 2024

# Contents

---

<b>1</b>	<b>Introduction</b>	(co-authored)	<b>3</b>
1.1	Motivation (John) . . . . .		3
1.2	AutoPhysio goals & overview (Ryan) . . . . .		3
1.3	Report outline (Yoonsang) . . . . .		4
<b>2</b>	<b>Background</b>	(co-authored)	<b>6</b>
2.1	Industry overview (Yoonsang) . . . . .		6
2.2	The anterior cruciate ligament (John) . . . . .		10
2.3	Electromyography (EMG) (John) . . . . .		12
<b>3</b>	<b>Emulation of physiotherapy</b>	(Ryan)	<b>15</b>
3.1	Informal operation & functionality . . . . .		15
3.2	Formal representation as a Finite State Machine . . . . .		20
3.3	Calculation of output torque in each state . . . . .		21
3.4	Boolean logic governing state transitions . . . . .		24
<b>4</b>	<b>Estimation of exertion</b>	(Ryan)	<b>30</b>
4.1	Statistical model . . . . .		30
4.2	Feature selection . . . . .		35
4.3	Data collection and maintaining calibration . . . . .		36
4.4	Clustering algorithm . . . . .		37
4.5	Analysis of model and areas for improvement . . . . .		37
<b>5</b>	<b>Delivery of determined torque</b>	(Ryan)	<b>40</b>
5.1	Motor circuit . . . . .		40
5.2	Motor control & safety . . . . .		43
5.3	Computing system design considerations . . . . .		45
<b>6</b>	<b>Mechanism considerations</b>	(Will)	<b>48</b>
6.1	Design objectives and functions . . . . .		48
6.2	Alternative designs . . . . .		49
6.3	Setup and initial basic calculations . . . . .		51
<b>7</b>	<b>Motor mechanism design</b>	(Will)	<b>55</b>
7.1	Investigation of four bar linkages for driving rotation . . . . .		55
7.2	Preferred design - single joint exoskeleton . . . . .		64
7.3	Summary and scope of mechanism . . . . .		71

<b>8 Measuring muscle activity</b>	<b>(John) 72</b>
8.1 General specifications . . . . .	72
8.2 Sleeve design . . . . .	73
8.3 Connection design . . . . .	79
8.4 Filter design . . . . .	81
8.5 Areas for improvement . . . . .	85
<b>9 Machine learning for personalised rehabilitation</b>	<b>(Yoonsang) 86</b>
9.1 Theoretical data generation for initial training . . . . .	86
9.2 Predictive analysis for recovery progress . . . . .	91
9.3 Personalised rehabilitation training plans . . . . .	94
<b>10 Machine learning for device safety</b>	<b>(Yoonsang) 97</b>
10.1 Anomaly detection in movement patterns . . . . .	97
10.2 Intelligent sound analysis for pain detection . . . . .	100
<b>11 App design</b>	<b>(John) 103</b>
11.1 Purpose of App . . . . .	103
11.2 Frontend design . . . . .	103
11.3 Backend system design . . . . .	106
11.4 Areas for improvement . . . . .	107
<b>12 Conclusion</b>	<b>(co-authored) 108</b>
12.1 Risk assessment (Yoonsang) . . . . .	108
12.2 Project ethics (Yoonsang) . . . . .	109
12.3 Summary (John) . . . . .	110
<b>13 References</b>	<b>111</b>
<b>14 List of Figures</b>	<b>119</b>
<b>15 List of Tables</b>	<b>120</b>

# 1 Introduction

(co-authored)

## 1.1 Motivation (John)

This project is inspired by one of the AutoPhysio team members' experience of suffering an anterior cruciate ligament (ACL) tear back in 2017. Consultation with the member's surgeon Dr. Lim Jit Kheng in Mount Elizabeth hospital in Singapore revealed multiple insights:

1. Repeat injuries are more common among patients with non-optimal rehabilitation strategies
2. It is inconvenient to adhere to rehabilitation plan due to distance, price, and clashes in schedules
3. Rehabilitation can absolutely be improved through monitoring quantitative metrics

More globally, the ACL is one of the most commonly injured structures in the body, with over 250,000 individuals suffering from an ACL tear per year in the USA alone [1]. Given its ubiquity, making refinements on the recovery progress can provide massive positive impact on the global physiotherapy market. The opportunity for innovation lies in Dr. Lim's insights (as well as through observation of ACL physiotherapy generally), where technology serves as a path to improvement for "evidence-based rehabilitation" [2].

## 1.2 AutoPhysio goals & overview (Ryan)

Motivated by John's injury and a demand for improved recovery methods, this report entails a proposal for our device, *AutoPhysio*, designed to enhance and partly automate physiotherapy for patients recovering from reconstructions for ACL ruptures. This overarching goal is threefold. Firstly, AutoPhysio aims to **improve accessibility to ACL physiotherapy** by facilitating convenient at-home sessions that do not disrupt daily routine. More specifically, the design targets post-surgery exercises that improve range of motion, primarily knee extensions. Secondly, the product should maintain patients' motivation throughout their recovery by **gamifying rehabilitation** via interactive feedback and engaging patient targets. Finally, its ultimate aim is to **increase the speed and efficacy of recovery**. To prevent the technology from being prematurely dismissed as "not worth the effort", it is necessary to encapsulate all these goals within an intuitive and hassle-free product.

AutoPhysio's novel solution consists of a physical device that resembles an enhanced knee brace with unique features: a motor positioned at the knee joint, a rotary encoder, and an elastic sleeve of EMG sensors encircling the hamstrings and quadriceps. The device has an on-board processing chip dedicated to

analysing the data from these sensors, controlling the motor, and interfacing with both the physical input via physical buttons and the AutoPhysio app, accessible by the patient and their healthcare provider.

AutoPhysio's database hosts a machine learning model trained on historical data from previous ACL rehabilitation cases. This generates a tailored, adaptive training plan entailing physiotherapy sessions over the duration of a patient's recovery. Akin to traditional in-person therapy, a session contains multiple sets, with each set having three main parameters: target angle of extension, target number of repetitions and target patient exertion. Our model selects each sessions' parameters based on data from the patient's performance thus far, in order to ensure effective training while minimising the overall recovery time.

The generated physiotherapy sessions are loaded on our mobile application, and to conduct one, a seated patient simply fits our module to their brace and starts the session via the app. Once the module receives the session's three parameters from the app, a context-aware algorithm uses the EMG sleeve, encoder and motor to assist the patient safely and smoothly reach these targets. After each session, the patient's data is processed and relayed to the app, informing the patient and doctor of their progress. In order to adapt to fluctuations in patient performance, our model may then suggest updates to the training plan on the app, which will be approved or adjusted by the doctor, e.g. extending the duration of recovery.

Beyond immediate benefit, AutoPhysio would also gradually collect quantitative data<sup>1</sup> on the recovery period and training logs for several patients who have experienced ACL ruptures. Thus, widespread adoption of AutoPhysio devices could not only directly revolutionise present-day patient recovery, but also enable research which back-propagates into the design of optimal rehabilitation plans for the future.

### 1.3 Report outline (Yoonsang)

Following the introduction, the report provides background on the knee brace and rehabilitation device industry, anterior cruciate ligament injuries, and the role of electromyography (EMG) in rehabilitation.

The main body of the report offers a detailed technical discussion on various aspects of the AutoPhysio device. **Ryan**'s chapters concern how our device performs physiotherapy sessions to safely emulate in-person therapy. This includes its design as a finite state machine which acts as the overarching blueprint for our device. He then details its implementation, by estimating exertion with statistics, deriving controlled circuitry to deliver appropriate torque, and computing it all in close to real-time. With this, the rest of the report concerns fleshing out the machine's dependencies. **Will** compares several brace designs and

---

<sup>1</sup>(anonymised)

mechanisms to withstand the torque from the motor and comfortably transfer it to the patient's limb. He then selects and presents the optimal mechanism in further technical detail. To obtain the required quantitative measurements of muscle activity, **John** explores how electromyography (EMG) signals could be acquired comfortably and accurately. With the physical implementation complete, **Yoonsang** then investigates the generation of personalised rehabilitation plans, containing the three set parameters required by the device to determine its operation in sessions. This necessitates a discussion on the generation of theoretical training data. He also covers general machine learning applications such as pain and anomaly detection to emphasize the safety of the AutoPhysio device. **John** describes the design and functionality of the mobile app, for facilitating interaction between the patient and the AutoPhysio system. He also provides insight into the practical application of biofeedback in rehabilitation, by covering the structure of the database that supports the app, the required data, and the machine learning models.

The report concludes with a discussion of the risks and ethical considerations associated with the project, closing with a summary of the benefits and prospects of the AutoPhysio device.

## 2 Background (co-authored)

### 2.1 Industry overview (Yoonsang)

#### 2.1.1 Importance of knee braces

Knee braces provide support, stability, and relief for post-ACL injuries. However, several studies highlight that the sole reliance on bracing may have limited effect [3, 4, 5]. In fact, some studies say that using braces and putting off weight-bearing after ACL surgery could worsen the long-term function of the knee, as measured by the International Knee Documentation Committee (IKDC) [3]. In a study group of 969 individuals, there were no significant differences in clinical outcomes between patients assigned early bracing and those not [4]. Similarly, there is insufficient evidence to support the daily use of knee braces immediately after ACL reconstruction [5]. These studies suggest that an accelerated rehabilitation program with early weight-bearing and range of motion exercises is advantageous for recovery.

Braces play a critical role in safeguarding the graft used in ACL reconstruction while maintaining functionality, mobility, and proprioception [6]. According to a survey conducted by the American Academy of Orthopaedic Surgeons, 60% of physicians recommend using a brace for the initial six weeks post-reconstruction, with 62.9% advising brace use during sports activities post-surgery [7]. Braces also effectively protect against low-intensity anteroposterior displacement and sub-physiological rotational movements, offering additional protection during the recovery process [8].

Knee braces are more than physical supports; they also play a significant role in the psychological aspect of rehabilitation [9, 10]. The sense of stability a brace provides can significantly boost a patient's confidence in moving and using their injured knee during the critical early stage of recovery. Psychological support is crucial for overcoming the fear of re-injury, which acts as a common barrier to effective rehabilitation. Engaging in rehabilitation exercises and returning to daily activities with a brace can help patients rebuild trust in their knee's strength and functionality [11].

The combination of advanced technology and knee braces will enhance their effectiveness [12, 13]. Innovations such as adjustable tension, custom fit, and integration with physiotherapy protocols allow more personalised rehabilitation programs. These technological advancements will not only improve the mechanical functionality of the braces but also contribute to more engaging and motivating recovery experiences for patients.

In conclusion, while the application of knee braces in ACL recovery is nuanced, with studies indicating varying degrees of effectiveness, their overall contribution to a comprehensive rehabilitation strategy is undeniable. Knee braces offer physical support and protection and extend psychological support to patients, providing a sense of security and encouraging mobility. The evolving technologies in brace design emphasise the importance of a holistic approach in ACL rehabilitation, particularly highlighting the need for a balanced integration of information technologies to optimize patient clinical outcomes.

### **2.1.2 Knee braces market size and growth projections**

The global knee braces market was valued at USD 1.7 billion in 2023 world-wide and is expected to grow at a compound annual growth rate (CAGR) of 5.2% from 2025 to 2030 [14]. This market expansion is driven by the rising prevalence of orthopedic conditions, increasing sports-related injuries, and growth of the elderly population. Functional knee braces dominate the market due to their ability to enhance knee stability, especially for individuals with ACL injuries. The market is also experiencing a shift towards custom-fit, lightweight, and intelligent technological integration, catering to a range of medical needs and consumer preferences.

### **2.1.3 Types of medical knee braces by uses**

According to the American Academy of Orthopaedic Surgeons, knee braces are categorised as prophylactic, functional, rehabilitative, or unloader/offloader [15]. Prophylactic knee braces are designed to prevent or reduce the severity of knee injuries during high-risk sports and activities. Athletes typically use them for injury prevention. Functional knee braces are used post-injury or post-surgery to provide stability and support to the knee. They are essential for individuals recovering from ACL injuries or undergoing ACL reconstruction surgery. Rehabilitative knee braces limit the knee's motion while allowing for a controlled range of motion during rehabilitation. These braces support the rehabilitation process by preventing further injury. Lastly, unloader/offloader knee braces are designed to relieve pain for individuals with arthritis.

### **2.1.4 Types of medical knee braces by materials**

Selecting an appropriate knee brace is crucial for a safe and efficient recovery process after an ACL injury. Within the categories mentioned in section 2.1.3, the market offers a variety of braces, each designed to meet specific needs from mild support to significant stability and protection.



Figure 1: (a) Bauerfeind sleeve brace, (b) Össur hinged brace, (c) Spring Loaded spring brace [16, 17, 18]

Sleeve braces, shown in figure 1a, are made from elastic material designed to be pulled over the knee. They provide compression to help control swelling and pain. These braces are suited for mild to moderate knee instability or use in the early stages of rehabilitation. The advantages are comfort and ease of use. On the downside, they offer limited support, are prone to wear and tear, and can retain heat, which might be uncomfortable for some users.

Hinged braces, shown in figure 1b, feature metal or plastic hinges to significantly assist knee stability. They are designed to control knee movement, providing robust support. These braces help prevent knee hyper-extension and support rotational stability. However, their bulkiness is a disadvantage, which may limit movement and comfort. Additionally, some users may find hinged braces complex to put on and adjust due to their design.

Spring-loaded braces, shown in figure 1c, have springs that reduce pain and help movement. They absorb the body weight when the knee is bent and release the energy when the knee extends. However, due to the complex mechanism, they are easy to break.

AutoPhysio works alongside the structural knee brace types, as shown in figure 1b and 1c. This makes our motorised mechanism significantly easier to design, and improves safety of use.

### 2.1.5 Key competitors in the knee brace market

The major knee brace market leaders are DJO Global™, Össur®, and Bauerfeind® [19]. DJO Global™, now part of Enovis™, is known for its extensive range of knee braces, including the DEFIANCE III brace specifically designed for ACL injuries, featuring advanced technologies like the 4-Points-of-Leverage-System. Össur® is another leader in the industry, with products like the REBOUND brace, which dynamically reduces strain on the ACL. Bauerfeind® provides the GenuTrain brace with advanced knitting techniques for a comfortable fit and effective joint stabilisation.

## 2.1.6 Electronic devices

Recently, diverse electronic devices have been developed to help the rehabilitation process by analysing and assisting with the patient's motion, rather than directly supporting and protecting the patient's knee.



Figure 2: (a) Continuous Passive Motion (b) HAL-SJ (c) exoRehab [20, 21, 22]

**Continuous Passive Motion** (CPM) involves machines that move a joint passively without the patient's effort. The device moves the knee joint through a fixed range of angles and speeds to help the recovery post-surgery, aiming to enhance the range of motion and prevent stiffness of the joint [20]. However, in the long term, CPM does not show advantages over physical therapy in terms of range of motion and patient satisfaction. [23] This might stem from its passive nature, limiting its effectiveness in promoting long-term functional recovery and muscle strength compared to active rehabilitation methods.

**Single-joint hybrid assistive limb** (HAL-SJ) is designed for post-ACL reconstruction rehabilitation, starting 18 weeks after surgery, to minimise risk of additional damage [21]. This means that HAL-SJ is not suitable for rehabilitation immediately after surgery, and its strap-based attachment can lead to stability issues.

**exoRehab** is a smart knee care solution designed by EXOSYSTEMS [22]. It combines electrical stimulation with gamified, personalised training content to aid in knee joint muscle recovery. However, as it focuses primarily on analysis and does not offer mechanical support, it may not be suitable for immediate use post-ACL reconstruction surgery.

AutoPhysio is a hybrid solution that combines the physical assistance of CPM and HAL-SJ with the analytical capabilities of exoRehab, aiming to provide comprehensive support throughout the rehabilitation process.

## 2.2 The anterior cruciate ligament (John)

The anterior cruciate ligament (ACL) is a ligament that resides in the knee, originating at the tibia and attaching to the femur [24]. As seen in figure 3, it acts with three main ligaments (Lateral collateral ligament (LCL), Medial collateral ligament (MCL), Posterior cruciate ligament (PCL)) as stabilisers in a dense network of musculoskeletal parts. Crucially, the ACL resists anterior tibial translation and internal rotational loads as well as valgus angulation, thereby preventing the tibia from sliding in front of the femur and providing rotational stability to the knee [25]. The tension that arises from these is so great that an ACL rupture is usually accompanied by an audible loud “pop” [2].

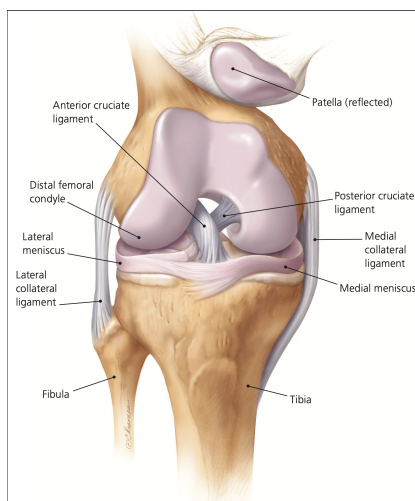


Figure 3: An anatomy of the knee. Adapted from Calmbach and Hutchens 2003 [26].

Beyond the mechanics, the ACL is thought to support dynamic knee stability via Ruffini and Pacinian corpuscles, the Golgi tendon organs, and free nerve endings [27]. These mechanoreceptors contribute to “proprioception” which is defined as the afferent information arising from the internal peripheral area of the body and contributing to postural control, joint stability, and specific conscious sensations [28].

### 2.2.1 Injury

Given the ACL’s importance, sustaining an injury there can be massively debilitating to the patient. An ACL injury is diagnosed using a combination of information from patient history, clinical examination, and medical imaging via Magnetic Resonance Imaging (MRI). Quality of life becomes severely affected, a result of muscle atrophy, instability, and decreased range of motion. This can also manifest long-term, where knee pains, knee osteoarthritis, and fear of re-injury lead to an inability to return to pre-injury activities [2]. To ensure best results, the patient must follow a recovery process upon diagnosis.

## 2.2.2 Recovery process

### Pre-surgery

Upon diagnosis, the patient can choose to schedule an ACL Reconstruction surgery. For best results, the surgery is performed after swelling subsides, muscle strength is increased, and range of motion is restored. Therefore, rehabilitation is required prior to surgery, typically under the guidance of a physiotherapist. The NHS suggests exercises which are classified by their purposes, namely

- Exercises to regain movement (range of motion)
- Strengthening exercises (Quadriceps, Hamstrings, Gluteal, Calf)
- Balance exercises (for proprioception, e.g. single leg stand)
- Aerobic exercises (e.g. using the stationary bike and elliptical trainer)
- Plyometric exercises (for agility, e.g. two-legged jump, single-legged hop)

The role of the physiotherapist is to use symptoms of swelling or pain to adjust intensity and frequency of the exercises, fine-tuning the speed of recovery for reconstruction surgery [29].

### Post-surgery

The goal of post-surgery rehabilitation is to prepare the patient for their return to pre-injury activities with the new graft. Unlike in pre-surgery where the rehabilitation duration is well-defined, recovery duration in post-ACLR is tailored by the physiotherapist or surgeon to the patient's long-term goals. The early phase (first few weeks) is crucial, dedicated to:

- Restoring range of motion (ROM)
- Building quadriceps muscle activation
- Normalising walking with crutches and then without crutches
- Controlling the patient's pain and swelling

The patient should take regular pain relief to keep to the rehabilitation schedule [30]. After the initial phase, the intensity and frequency of exercises can go up, along with the addition of more load-bearing exercises to rebuild strength lost from muscle atrophy. By conducting rehabilitation in a routine and measured pace, the patient increases their likelihood of returning to pre-injury activities and, importantly, lowers their chances of re-injury [2].

## Psychological support

With any injury, there is a mental aspect to focus on during recovery. Fear is a common psychological byproduct of a traumatic ACL injury which deters patients from engaging actively in movement as well as in later stages in the lack of confidence to return to pre-injury lifestyle [9, 10, 2]; recovery is not simply biomechanical, further emphasising the physiotherapist's role of pacing the rehabilitation to accommodate for both physical and psychological healing. Another common problem is the patient's motivation to participate in consistent rehabilitation [31, 2]. Gamification is an element that has been added to rehabilitation in areas such as strokes [32, 33] and a range of musculoskeletal injuries (impingement syndrome, rheumatoid arthritis, osteoarthritis, lower back pain, fibromyalgia, fracture and ligament reconstruction) [34] with positive results in encouraging patients to adhere to routine recovery exercises.

## Salient exercises for product design

In the context of a rehabilitation product, mimicking the physiotherapist-recommended exercises empowers the patient to recover from the comfort of their home. Given the prime objectives in early-phase rehabilitation for both pre-surgery and post-surgery [29, 30], the product's design should focus on knee extensions, an exercise strongly recommended by the NHS for both the restoration of range of motion and the building of quadriceps. The exercise involves straightening the knee at a measured pace, which requires quadriceps activation and pain endurance for the patient. If the pain becomes too much for the patient, the physiotherapist would assist in returning the tibia back to its original position. The result of repeating this exercise over a few weeks is a prominent improvement in the range of motion where pain is tolerable throughout as well as in the strength of the quadriceps muscles. If our design is successful, the device could upscale to assist with other exercises.

### 2.3 Electromyography (EMG) (John)

EMG is the recording of muscle electrical activity by measuring the electrical potential created during muscular contraction. This electrical potential arises due to stimulation by peripheral motor nerves that carry signals from the brain or spinal cord to the skeletal muscle fibres [35]. These motor nerves innervate muscle fibres which group to form muscles. As such, EMG signals of motor nerves can be detected from a general area of the muscle it innervates.

These signals can be detected invasively by using intramuscular electrodes or non-invasively through

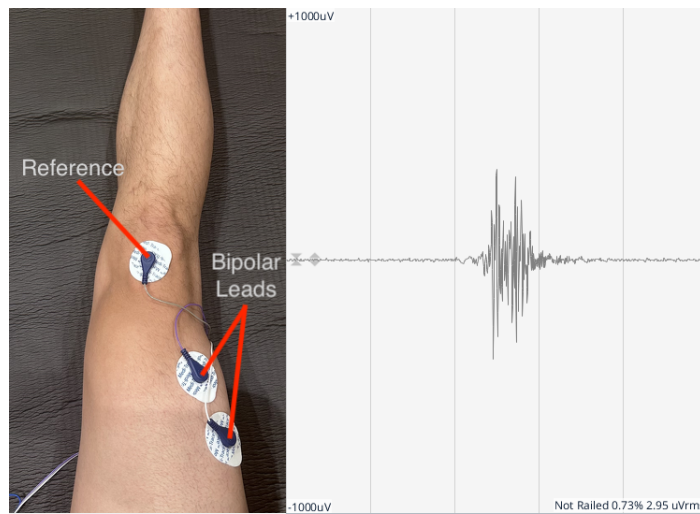


Figure 4: Left: a labelled picture of sEMG electrodes placed on one of AutoPhysio's team members's quadriceps. Right: the corresponding EMG signal upon muscle flexion.

electrodes applied on the skin surface to gather a superposition of signals [36]. AutoPhysio uses the latter method (also known as surface EMG or sEMG) to create a comfortable recording experience during training. The sEMG setup involves three electrodes: two for measuring potential difference, and one as reference (ground); the reference electrode is placed in a neutral area to work as the baseline, while the other two work as positive and negative leads to measure potential difference with respect to the reference-established baseline. figure 4 demonstrates the rough positioning of the necessary electrodes as well as the resulting EMG signal upon muscle flexion.

### 2.3.1 Potential use cases

On their own, single-channel EMG signals already show potential in providing meaningful data for analysis. In particular, studies demonstrate its relationship with upper leg muscle strength [37, 38] and fatigue [39]. These will be useful in the monitoring of rehabilitation progress. EMG has also been used for motion recognition and prediction which could prove useful for making real-time adjustments as well as in post-training analysis [40, 41].

A combination of multiple EMG channels not only aids in the aforementioned analyses, but also presents new perspectives on muscle performance. The derived quantity co-contraction index (CCI) provides further information on recruitment patterns via comparison of normalised EMG signals between muscle pairs [42]. This is calculated using Equation 1.

$$CCI = \frac{EMGS}{EMGL} (EMGS + EMGL) \quad (1)$$

where EMGS is the normalised magnitude of the EMG signal in the less active muscle and EMGL is the normalised magnitude of the EMG signal in the more active muscle. CCI measures the amount of overlap between activities of the two muscles considered. High CCI represents a high activity in both muscles across a large time interval, while low CCI represents either low activity in both muscles, or a high activity in one and low activity in the other. Higher CCI of opposing muscle groups could cause higher joint compression [43], which might compromise joint integrity in the long term.

AutoPhysio focuses on the quadriceps and hamstrings as mentioned in Chapter 2.2.2. The quadriceps comprise the vastus medialis (VM), rectus femoris (RF), vastus lateralis (VL), and vastus intermedius (VI), while the hamstrings comprise the biceps femoris long head (BFlh), biceps femoris short head (BFsh), semitendinosus (ST), and the semimembranosus (SM). Muscles for EMG recording will be selected from these, and CCI will be measured for each quadriceps-hamstrings pair.

### 2.3.2 EMG profile

While it is easy to spot EMG spikes in time-series data, it is affected by various noise sources (baseline noise, interference noise, and artefacts) [36]. Apart from it appearing 30 to 150 ms earlier than movement [44], other unique identifiers lie in the EMG signal profile. The frequency spectrum for EMG signals is from 10 to 500 Hz [45], with signals above 350 Hz exhibiting very low energies [46]. For the lower end of the EMG frequency range, several studies apply a higher cutoff frequency at 20 Hz [47, 48], recognising that the 0 to 20 Hz motor unit firing rate adds noise [44, 49].

As for sEMG amplitude, the range is 0 to 10 mV (-5 to +5 mV) prior to amplification [45, 49]. Its difference from an appropriate baseline makes it highly distinguishable as in figure 4.

### 3 Emulation of physiotherapy (Ryan)

*This chapter pertains how our device conducts physiotherapy. I begin by informally explaining the functionality that our device aims to achieve and then establish the need for context-aware and multi-modal operation. This requires a finite state machine to determine the torque to output in each state and conditions for transitions between them. Once formally constructed, the machine is able to determine exactly what torque to provide at any point during a physiotherapy session. It thus represents AutoPhysio's overarching design task.*

#### 3.1 Informal operation & functionality

In section 2.2, John thoroughly explored the traditional in-person physiotherapy practice for the early stages of ACL rehabilitation. In order to achieve our goals, AutoPhysio is designed to emulate this practice, as it is the most successful rehab method evidenced by medical research insofar. The table below summarises John's review and highlights how the psychological aspects of physiotherapy cannot be addressed physically, as a matter of safety. A patient may hesitate to extend their leg due to fear, lack of motivation, or any other psychological reason. Thus, our motorized brace is designed to *only assist in leg extension if the patient is actively consenting*. These psychological roles of therapy, which are primarily motivational, are addressed through gamification in our app, a topic John will cover in chapter 11. Therefore, the device itself focuses solely on emulating the physical functions of a physiotherapist, outlined in the second column.

Table 1: Summary of the physical and psychological roles of physiotherapy sessions

Goals of physiotherapy sessions	Mode of delivery	
	Physical means	Psychological means
Increase range of motion	Assist the patient's motion to gradually extend range of motion over time	-
Re-strengthen	Moderate the amount of assistance appropriately	-
Restore confidence	With patient consent, make incremental progress	Overcome fear through reasoning and demonstration of therapist's experience
Provide motivation	-	Verbal motivation and encouragement
Prevent overenthusiasm	Sense and prevent the patient from pushing past a threshold for optimal recovery	Advise on training in moderation

To fulfill the first three physical roles, in traditional physiotherapy, therapists devise patient-specific training

plans containing a gradual progression of knee extensions, exemplified in figure 5b below. As mentioned in section 1.2, these plans entail sets of a target number of repetitions ('reps') to a target angle of extension and at an approximate target muscular effort [50]. The therapist then helps patients follow this training plan through in-person physiotherapy sessions, where they infer how to optimally aid and control patients' movement during repetitions [51]. Throughout the session, therapists are continuously aware of the patient's exertion, in order to fulfill the last physical role – preventing overexertion.

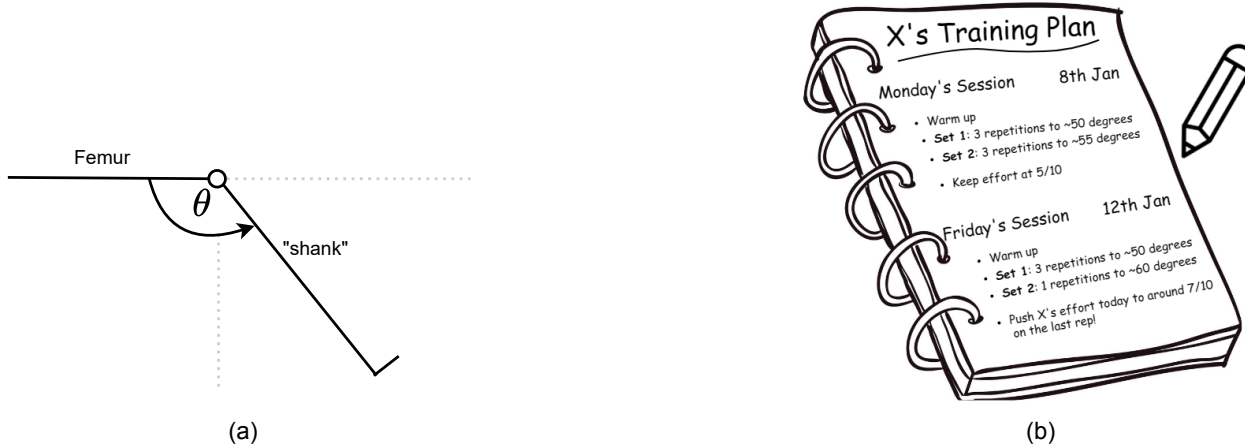


Figure 5: (a) Simplified diagram of leg extension, (b) cartoon illustrating exemplar sessions from a rehab. plan

With a model devised by Yoonsang in chapter 9 that is capable of generating such a training plan, we can obtain these three set parameters  $\bar{\theta}$ ,  $\bar{\varepsilon}$  and  $\bar{N}$ . The remainder of this section dissects the intricacies of therapy sessions, in order to formalise how our device goes from these three targets to reliably and safely performing a session that realises the physical goals in table 1.

### 3.1.1 The overall structure of a session

The session begins when the user dons the brace and turns on AutoPhysio. Upon booting, the device enters the standby mode as denoted in figure 6 overleaf. If Yoonsang's model generates a set due for completion, it would be available on the app for the user to initiate it. This prompts the transmission of the target parameters  $\bar{\theta}$ ,  $\bar{\varepsilon}$  and  $\bar{N}$  to the device. Upon receipt, the device checks if a warm-up has been recorded. If not, it starts logging EMG data, and requests the user to warm up via the app. This request is intentionally vague, asking the user to perform unassisted knee extensions to a comfortable and easy angle, until they feel ready.

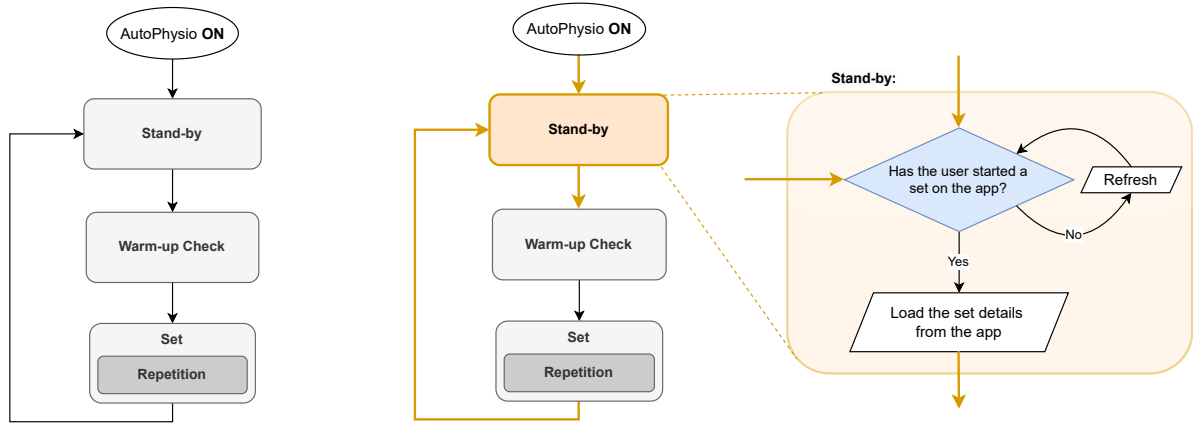


Figure 6: left: (a) Summary of sessions, right: (b) Stand-by mode

*The warm-up is important for three reasons.* Firstly, a warm-up is vital to prevent injury in rehabilitation. Secondly, unassisted reps are an important part of physiotherapy (alongside the primary goal of assisted reps to improve range of motion) [52]. Finally, the warm-up data entails important EMG information which needs to be analysed for later use in the algorithm. To detect when a user has warmed up, the device simply counts the number of times the resting region ( $\theta_{rest} \leq \theta \leq \theta_{rest} + tolerance$ ) is left and returned to. After three counts, it considers the user as warmed up, stops logging and finds the average EMG amplitude from the data.

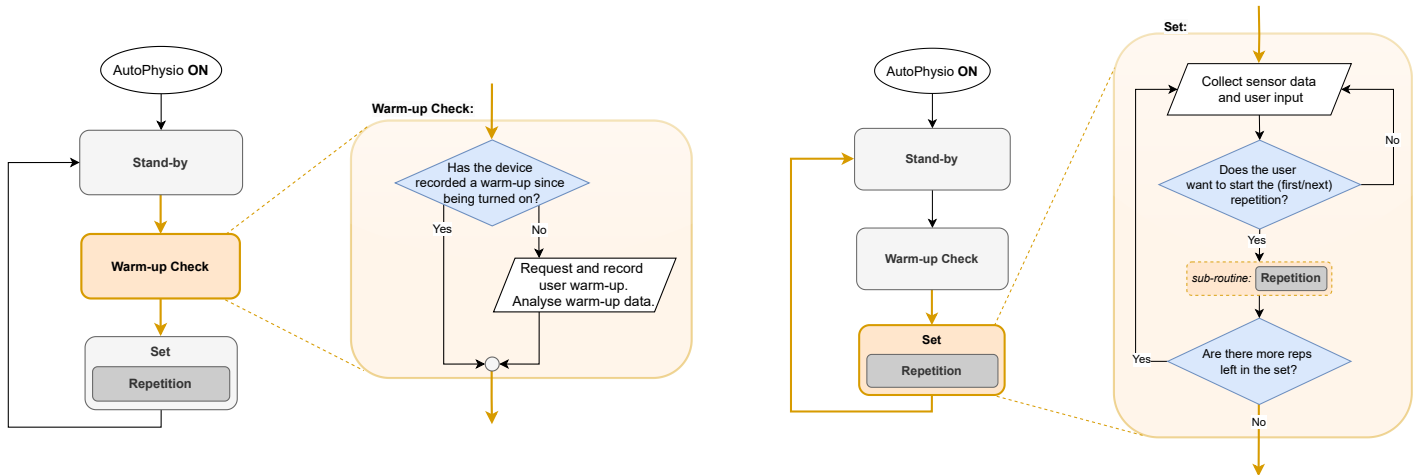


Figure 7: left: (a) Warm-up mode, right: (b) Set mode

After a warm-up is recorded and analysed, the device is ready to start the repetitions in the set. However, the user is free to continue warming up, and the device waits for the user to explicitly initiate the first rep via the start/stop button, before entering the rep state. After each rep, the device loops through the remaining reps to complete. If none remain, the set is complete, and the device returns to the stand-by state, where another set may be generated.

### 3.1.2 The physiotherapy procedure during repetitions

Performing a repetition is the most involved part of the session. We aim to emulate the traditional procedure evidenced in the sources of section 2.2, for knee extensions in the early stages of rehab.

When a patient initiates the movement, the physiotherapist starts providing an assistance which both, gives the patient confidence in the fact that they have support if required, and helps them to extend. The amount of assistance provided depends on the amount the therapist wants the patient to exert (target exertion), and the amount they think the patient is exerting, which they gauge from audiovisual signals and their own experience. The aim is to provide support which maintains the patient's exertion to the target. If it is very early stages, they will provide a large amount of assistance (on the order of magnitude of the limb's self-weight) in order to keep the patient's exertion to a safe level. The goal is that the patient gets stronger and is able to provide more force with less exertion. Thus the assistance required at a constant target exertion, should drop naturally over time. For instance, in week 1, a high amount of assistance may be required for the user to exert 5/10 effort, but in week 4, the amount of assistance will reduce for the same 5/10 exertion. To re-build strength, rehab plans may cycle between low target exertion, and high target exertion, similar to training plans in sport [53].

The therapist's perception of a patient's exertion, is a combination of gauging effort and overcoming dull pains. However, given any indication of a *sharp* pain, the therapist immediately switches from assisting the extension, to supporting the leg to go to wherever the patient feels comfortable. A therapist will also enforce a break if a patient is trying to push past pain that they should not ('over-exerting'). During a pause like this, they inform the patient to take the rep easier. This gives rise to the existence of 'pauses' within the repetition. The patient may also verbally request to pause, asking the physiotherapist to support their leg. This could be when they experience a sudden small sensation of pain, or are fatigued from pushing, but still have some effort left and would not like to completely end the repetition yet.

In either scenario - an implicit or explicit switch to this paused state - after some rest, the patient may choose to try to extend their leg to the target angle again. The patient could cycle between these states multiple times, but after a certain number of 'attempts', the physiotherapist will interject and stop the repetition, since this indicates that the target angle was unrealistic [54]. Equally, the patient may also choose to end the rep at any point, be it whilst 'paused' or mid-'attempt'. At the end of the rep, the physiotherapist takes the full weight off patient (much like in the paused phase), and then slowly lowers the leg to the rest angle.

### 3.1.3 Conversion into a sequence of actions

The procedure above is intuitive to trained physiotherapists, however it needs to be formalised into a robust sequence of actions in order for a device to compute it. This will complete the remaining part of our structure: repetitions. In the flowchart that follows, there are multiple complex functions that occur. I will design an implementation of these in the next chapter.

Initially the device is disengaged, providing no torque until the patient gives direct indication they are done warming up and wish to begin the rep. At this point the device must start providing an assistance to help the patient in their attempt to reach the target angle, whilst also maintaining the patient's exertion level to the target. If at any point, the user retracts due to pain, or wishes to take a break, we must then switch into a pause phase within repetitions, during which the device must provide the user with support that allows both full support and free movement. Thus, we recognise two loops in the flowchart, both of which the user must be able to end the rep from.

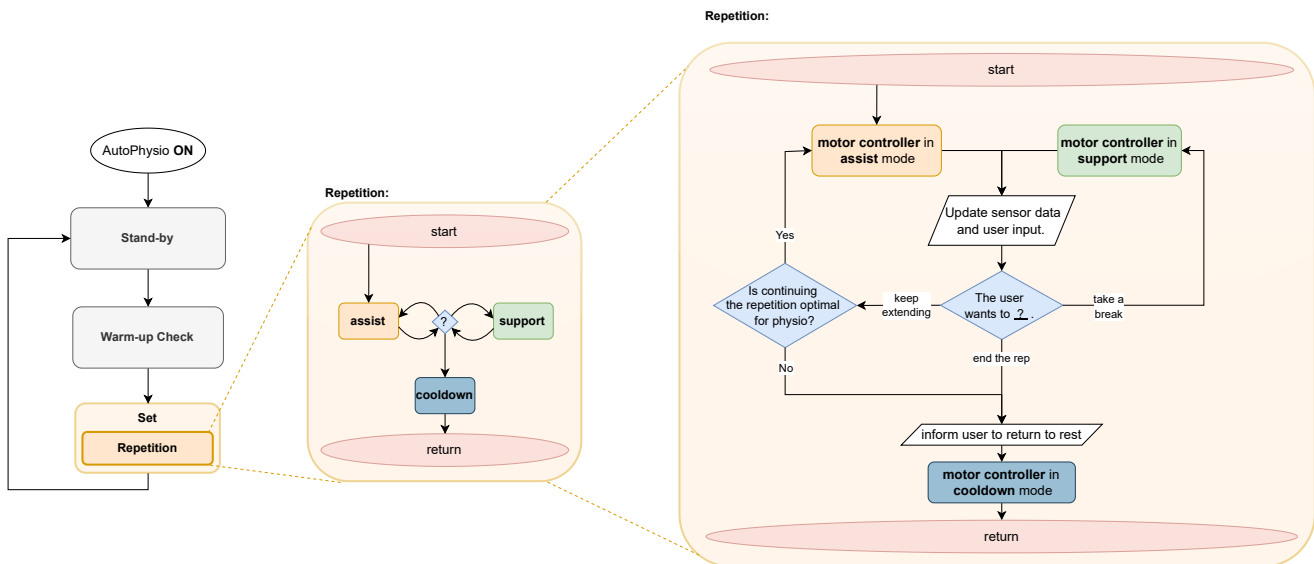


Figure 8: Flowchart of the procedure during a repetition

To exit and enter these loops, the device needs to continuously observe the patient's state and determine what they want to do at any point. There are three options here: keep extending, take a break (pause), or end the rep. As discussed, in order to keep extending, the user must also not be overexerting themselves, as this would not be optimal for rehab. Thus the device must be able to infer whether continuing a rep is safe and optimal rehab. The device must use this to make a decision and update the motor controller's mode of operation at any point.

The final piece of the puzzle is ending the rep. During this phase, the motor must cool-down: slowly and safely siphoning the support it was providing at the point the rep was ended. We note that whilst the two loops require continuously calculating the assistance based on the current data, the assistance provided when ending the rep no longer depends on the live data, as the support is simply waned off gently.

### 3.2 Formal representation as a Finite State Machine

From these flowcharts, it is now clear that for the successful emulation of therapy sessions, AutoPhyio's behaviour must be governed by four overarching operating modes which it can switch between. The desired functionalities of these modes are summarised in table 2 below, where as a matter of safety, the motor is disconnected from the power supply in at least one state.

Table 2: The desired functionality for the four modes of AutoPhysio's operation

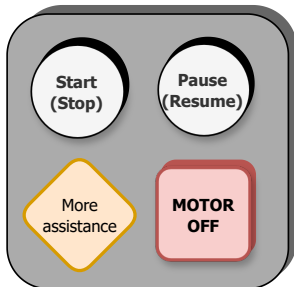
Motor States - desired functionality		
DISENGAGED		Free leg movement and disconnected from power supply for safety
ON	assist	Provide assistive torque whilst patient extends to maintain exertion at the target
	support	Leg is both fully supported and fully free to move
	cooldown	Take the full weight off patient and slowly lower the leg to rest angle

In order to formalise this such that it can be implemented through a processor, there are two overarching tasks. First, design output torque functions that achieve the functionality of these modes and second, design the decision making process that selects the system's operating mode at any point in time. From fig. 8, it is clear that this process is largely governed by the answers to the two blue question nodes: *understanding what the user indicates they want to do, and inferring whether continuing a repetition is safe and optimal for their recovery*. It is then implicit that a device interface is necessary, buttons for which are shown in figure 9.

This formalisation into finite states and *transition functions* between them, is a concept from a branch of *Finite Automata* theory, which would be specifically categorised as developing a *Finite State Machine* (FSM). These are very useful models for sequential programs, such as lexers. Furthermore, FSMs are also incredibly useful for digital logic design, which would be necessary if we were to transform our product from software to hardware by designing a new integrated circuit.

A finite state machine  $M$ , comprises of a finite set  $S$  of states, with a set of inputs  $\Sigma$  called an *alphabet*, and

a set of transitions  $\delta$  between states, indicated by an arrow between them. The transitions are functions of the alphabet as indicated below. The mathematical description is given below – more intuitively, each state represents a description of the status of the system. For more detail on FSMs, please refer to Oxford’s CS and Cambridge’s Engineering departments [55, 56].



$$M := (S, \Sigma, \delta, s_0, F) \quad (2)$$

$$\delta : S \times \Sigma \mapsto S$$

$$\text{initial state } s_0 \in S$$

$$\text{final states } F \subseteq S$$

Figure 9: AutoPhysio’s user interface

Although a *non-deterministic* FSM is simpler to build since every state and transition need not be derived rigorously, I shall construct a *deterministic* FSM. This is primarily because non-determinism means the system has ‘ambiguity’, such that the system could be in multiple states at once. This is not desirable here: we require AutoPhysio to remain in one state, only transitioning to another state when certain conditions are met. It must also run with low latency without much computational power. Despite their ease of creation, non-deterministic FSMs are harder to implement, since they require much runtime memory. Therefore, they are also usually slower to run, as many states must be processed simultaneously.

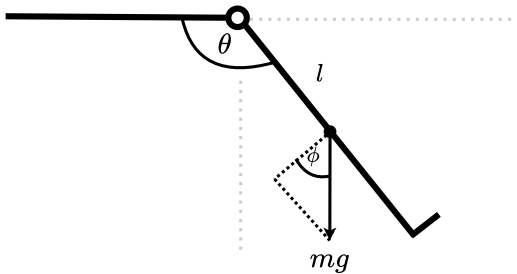
The constructed FSM will also need to be a *Moore* machine, due to the stability gained from having the system’s output depend solely on the state it is in (as opposed to both the state and input like in *Mealy* machines). This stability is necessary since preemptively transitioning between multiple states incorrectly may disrupt or even harm the patient. Although the output is indirectly dependent on the input in both types of machines (since output depends on state and state transitions depend on input), the difference is that a Mealy machine has multiple outputs whilst remaining in the same state. This is undesirable in our use case, and therefore it is important that machine we construct is also Moore. In the next two sections we will discuss this construction.

### 3.3 Calculation of output torque in each state

The first state is the Disengaged mode, where the torque to be sent to the user is zero as the rep hasn’t started. This is also the safety state, so the power supply to the motor circuit must be completely cut off.

Next, the Support and Cooldown states share some similarities. In Support mode, the patient is to be

both fully supported *and* free to move. By providing a *continuously updating* torque which completely matches the self-weight torque at each position, patients are able to relax all muscles, and only contract when they wish to move. Calculating this torque is simply a matter of geometry. In the figure below, I provide a first-order approximation by treating the lower leg as a point mass at its centre of mass, to arrive at  $T_{\text{self}}$  in eqn. 4.



$$\phi = \pi - \theta \quad (3)$$

$$\begin{aligned} T_{\text{self}} &= mgl \cos(\phi) \\ &= mgl \cos(\pi - \theta) \\ &= -mgl \cos(\theta) \end{aligned} \quad (4)$$

In Cooldown mode, the device takes the full support of the leg at its current position, so that the user relaxes completely, and gently lowers the leg at a comfortable velocity. The velocity at which this is done can be set by the patient's doctor. Thus we note that in the Cooldown state, the torque is not a function of the current live data, and just a function of time and the initial measurement. This reflects the flowchart from figure 8. Using the  $T_{\text{self}}(\theta)$  expression above, we can calculate this torque-time function as follows via a simple change of variables.

$$\theta(t) = \theta_0 - \omega t \quad (5)$$

$$T(t) = T_{\text{self}}(\theta_0 - \omega t) = -mgl \cos(\theta_0 - \omega t) \quad (6)$$

We are now left with determining the torque to provide in the Assist state. This state aims to control the patient's exertion and maintain it to the target for the set. It therefore requires a quantification of the patient's current exertion, for which I will design a statistical model in chapter 4. Given such a measurement of the patient's exertion, we can then derive a controller to provide an assistance that aims to maintain exertion to the target. Since target exertion is constant for each rep, this is much like a set-point control problem, where we have a sensor of the variable we are interested in (exertion), an actuator (assistive torque), and of course, a system. Aside from the patient, the system also comprises the brace mechanics and the dynamics of the exertion model. Providing there is very little flex in the brace, its mechanics can be assumed to be negligible. Since both model and patient dynamics are unknown, and simulation is beyond the scope of this report, we treat them as one system.

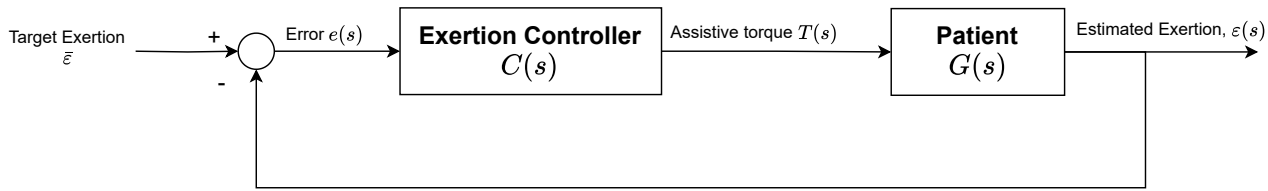


Figure 10: The system to be controlled in the Assist state

The remaining system is inherently non-linear, since even ignoring pain and assuming that exertion is proportional to the self-weight torque  $T_s(\theta)$ , this is already similar to the classic pendulum system from P1. As the aim is to extend to a large angle, small-angle linearisation about an equilibrium point is pointless. However, PID controllers can still produce a reasonable result [57], and a fair degree of inaccuracy is tolerable, as controlling exertion precisely is not vital. We will explore alternatives in section 3.3.1. This leaves finding the optimal gains of the controller which is an implementation-side task since, for unknown system dynamics, we would require test data or simulations.

This controller is safe since any motor support requires a non-zero exertion, which means a patient must be trying to extend their leg. For additional safety, the controller must have a set upper limit. We limit the maximum amount of torque assistance a patient can receive to the self weight of the patient's leg. This way, a motor will never be able to push a patient past an angle they don't wish to be at.

Table 3: Summarising the implementations for each state's output torque calculation

Motor States - implementation		
<b>DISENGAGED</b>		$T = 0$ , and no net current in the motor circuit ( $i_{\text{net}}(t) = 0$ )
ON	<b>assist</b>	$T = \text{ExertionController}(\bar{\varepsilon}, \varepsilon)$
	<b>support</b>	$T = -mgl \cos(\theta)$ $\theta_{\text{rest}} \leq \theta \leq \bar{\theta}$
	<b>cooldown</b>	$T = -mgl \cos(\theta_0 - \omega t)$ $0 \leq t \leq (\theta_0 - \theta_{\text{rest}})/\omega$

### 3.3.1 Evaluation of and alternatives to the exertion controller

Given the degree of non-linearity, it is plausible the controller does not work. However, sophisticated control methods can be developed for non-linear systems (linear quadratic regulators) and unknown systems (Kalman filtering). Thus, this should be achievable in further iterations. Nonetheless, it is important to devise an alternative method of delivery if this does not work out in implementation. An equally good solution would be to provide a torque that is proportional to the self-weight. The proportion would be a

constant during a repetition and devised by the training plan. Using this method, we could still maintain the patient's exertion through gamification on the app. This would involve a small animation that notifies the patient to try harder or try less hard according to the exertion we measure.

### 3.4 Boolean logic governing state transitions

We now move to the second task, designing the conditions for all transitions between states. We established that the decision making process is largely governed by *understanding what the user indicates they want to do, and inferring whether continuing a repetition is safe and optimal for their recovery*. This subsection will result in mathematical logic statements, which are included in fig. 11 for the reader's reference.

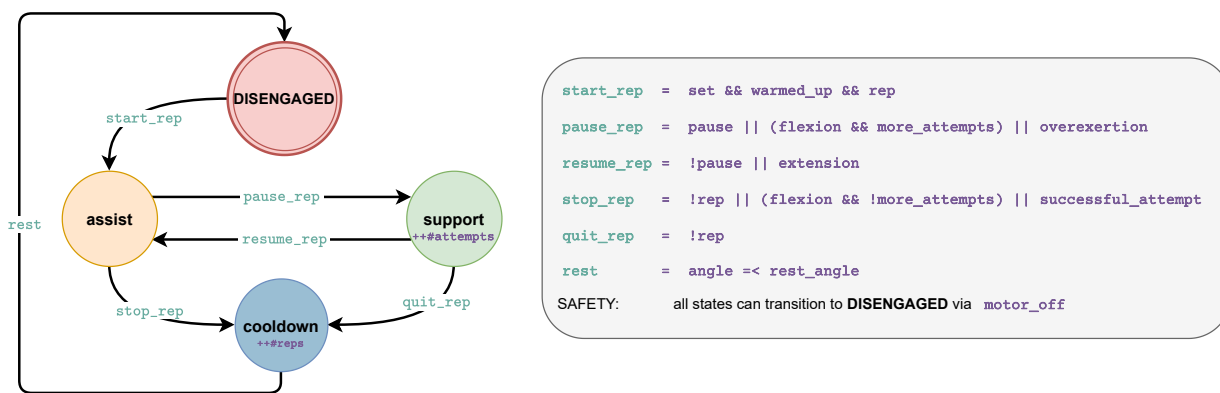


Figure 11: Finite State Machine for the motor - safety transitions not illustrated for clarity

Throughout this design, we will work under the pessimistic assumption that our memory system is volatile, i.e. it does not retain stored information after power is removed. Thus, when the device first turns on, all variables (e.g. the number of repetitions completed) are set at 0 or false. This will allow our system to work with less dependency, which ensures robustness to misfires such as memory faults during boot.

First, we consider the transition function from the Disengaged state into the Assist state, which denotes the '*starting*' of the rep. For this to occur, three things need to have happened. First, a set must be active, denoted by a boolean 'set', which is assigned to true if the number of reps completed is less than the number of target reps. Both these variables will be 0 initially, until the training plan is loaded onto the device and the number of target reps is updated. Second, the device must have recorded and analysed a warm-up, such that the variable for the average EMG amplitude is non-zero. Finally, the user must directly indicate that they wish to move from the warm-up phase to start the rep by pressing the

start/stop button. This button toggles the boolean called ‘rep’, which governs whether a rep is ongoing.

Now, we have the transitions out of the Assist state. The transition to the Cooldown state denotes the *stopping* of the rep, whilst the transition to the Support state is when the rep is *paused*. The easiest way to detect when to stop or pause the rep is using direct user input.

We have already covered the start/stop button which toggles the ‘rep’ boolean. In order to have transitioned into the Assist state, the rep boolean must be true, which means the button must have been pressed. Therefore, if pressed again, the rep boolean toggles to false. The other button, pause/resume, toggles a separate boolean which indicates if the rep is paused, called ‘pause’. This is one way to detect when the user wants to pause the rep and whether the machine should transition to the Support state. However there are other ways in which a rep could pause. The most important event is if the patient experiences a sudden pain and jolts their leg back, since this reaction requires a real-time response. Following this subsection, in 3.4.2, Yoonsang discusses the method which detects retraction through the encoder and motor controller. The outcome of this is a boolean that represents if the user is retracting, which we call ‘retraction’. Instead of immediately stopping the rep, the device switches to pause mode (i.e. the Support state), so that the patient can try again. However, as mentioned earlier, therapists only allow patients to try again if they haven’t already tried too many times [54]. A variable that sets the number of attempts a patient is allowed would be set by their physiotherapist. We can then define a boolean which denotes whether the user has more attempts left. Then, if the user retracts, this boolean governs whether the machine transitions to the Support or Cooldown state.

However, there are still other ways in which a transition could occur to these states. As discussed in the previous section, if physiotherapists detect that a patient is overexerting, they will pause the rep and tell the patient to stop pushing so hard or to take the rep easier. In the next subsection, 3.4.1, I will design an implementation of this function that relies on the same statistical model for exertion that the exertion controller does in the Assist state. This outputs a boolean which can be included in the transition function from Assist to Support. However, this quantification is simply an estimate and it is therefore much more safe if we also enforce the set’s target angle as a conservative upper limit for the patient’s range of motion. This is well-suited, since the training plan generates depending on the user’s history, so if the user is meeting the target fairly easily for a couple of sessions, the next session may contain a higher target to allow the patient to safely recover at a faster rate. Thus, when the angle of extension passes the generated target angle, the device must consider it a successful attempt, stopping the rep and moving

into the Cooldown state where the torque is slowly siphoned. Therefore, we now also create a boolean to indicate whether the target angle has been surpassed which we include in the transition function from Assist to Cooldown.

Now we have the transitions out of the Support state: back to Assist, and to Cooldown. The first can be considered as *resuming* the rep, and the second as *quitting* the rep (in contrast to *stopping* the rep directly from the Assist state). We designed the Support state such that the user is both completely supported and free to move. Since they are therefore not being actively pushed, the transitions out of the state state can afford to be simple, as quick decisions (faster than human reflex to press a button) are not necessary. Thus, to quit the rep, as before, the user can simply press the start/stop button to toggle the ‘rep’ boolean to false. Likewise, to resume the rep and try again, the user simply presses the pause/resume button again, which toggles the pause boolean back to false.

However, for user convenience, the device is also designed to detect when the patient’s leg has started moving forward again. Thus, in addition to designing the method that detects retraction, Yoonsang also designs a similar method to detect flexion, which updates a boolean ‘flexion’, that indicates whether the patient has started extending their leg again. We also note that when a rep is resumed, the variable counting the number of attempts must be incremented, in order to update the boolean discussed earlier that denotes whether the user has exceeded the number of attempts their physiotherapist allows.

Lastly, we’re left with the transition from the Cooldown state to the Disengaged state, denoting the user is at *rest*. This occurs when the user’s leg reaches a pre-defined ‘rest angle’, which is considered to be the angle from which the user first starts the rep. At this point we also increment the number of reps completed in order to keep the ‘set’ boolean updated.

The result is shown in figure 11. As required, our machine is *deterministic*, because there is no point where the machine can be in multiple states, i.e. a single input corresponds to a single individual transition. The FSM is also a *Moore* machine, since its output (i.e. the motor controller’s mode of operation) is only dependent on the state. In fact, even if the output was re-defined to be the specific torque sent to the user at any point, our machine would still be Moore, since the variables that change the output (e.g. *floats* that represent the EMG amplitudes or the current angular position) are not part of the machine’s recognised alphabet  $\Sigma$ . So even from a rigorous mathematical perspective, the machine remains Moore, since the output of the machine is still independent of its alphabet.

However, the machine is not quite a blueprint that is ready to be implemented yet, as it is not fully spec-

ified. Although most the variables in the transition functions can be implemented trivially in software using analogue or digital input pins, the ‘overexertion’, ‘retraction’ and ‘flexion’ variables require further specification. I will discuss this next.

### 3.4.1 Overexertion

The point of this function is to detect when the patient is pushing themselves too much. This is a frequent problem in sports injury rehabilitation, as athletes are keen to push past pain in attempt to speed up their recovery and get back to sport. In physiotherapy, the therapist’s role is to detect when patients are trying too hard, to notify them and then pause the rep so they can try again.

As mentioned in 3.3, our model for exertion allows us to quantify exertion and thus determine when the patient is exceeding the target. By accumulating only the positive difference over time, we can get a measure for overexertion. We select only the positive difference because overexertion should not be able to be countered by underexertion - i.e. taking time in the rep to push yourself too hard can not be bought by spending some time pushing yourself too little. Any time spent over the target counts towards the overexertion, regardless of time spent under the target. More formally then, we can define the accumulated overexertion,  $\mathcal{E}(t)$ , below.

$$\mathcal{E}(t) = \int_0^t (\varepsilon - \bar{\varepsilon})^+ dt \quad \text{where } (x)^+ = \max\{0, x\} \quad (7)$$

Then, the doctor in charge of the rehabilitation can set a tolerance  $t$ , for the amount of overexertion allowed at any point in time, such that our boolean ‘overexertion’ can be assigned true when the accumulated overexertion exceeds the tolerance times the time. For instance, if we allow for 10% overexertion at any point in time, we can set an upperbound on overexertion at  $0.1t$ . The doctor may adjust this tolerance according to their knowledge of the patient’s desire to return to sports quickly, or immaturity in respect to how much they will naively overexert themselves in hope that it will speed up their recovery.

In section 3.4, I also noted that this measure of overexertion is reliant on the measure for exertion, which itself is only an estimate. Thus, this is not a completely safe detection of overexertion. However, since we are also enforcing the target angle as an upper-bound, this is acceptable.

### 3.4.2 Extension and flexion (Yoonsang)

In rehabilitation, the patient's comfort and safety are essential. Integrating software to automate the activation and termination of physiotherapy sessions will enhance the therapeutic experience, minimising the need for manual intervention.

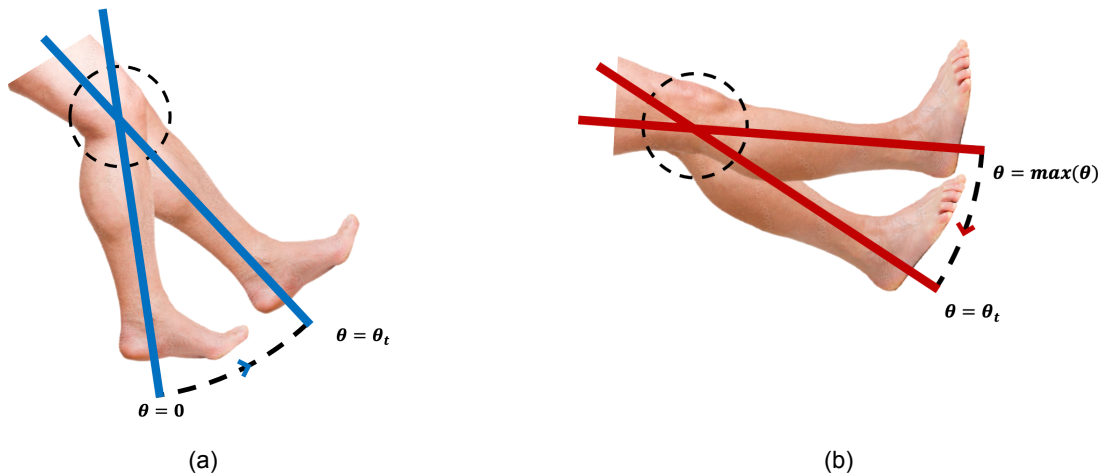


Figure 12: (a) Motor support activation (b) Motor support termination

The AutoPhysio device tracks the knee's angular movement to facilitate precise control over the rehabilitation process. The angular displacement of the knee at time  $t$ , relative to its initial position, is defined as  $\theta_t$ . As shown in figure 12a, motor activates when  $\theta_t$  surpasses a predefined angular threshold, referred to as  $\theta_{start}$ . This specific angle is carefully chosen to correspond with the patient's deliberate intent to initiate a rehabilitation session, ensuring that the device responds to actual rehabilitation efforts rather than accidental movements.

Patients can customize their  $\theta_{start}$  setting. This personalisation allows the patients to tailor their rehabilitation experience, aligning it more closely with their individual recovery goals and comfort preferences. To prevent potential accidents by inadvertent device activation, the system only allows  $\theta_{start}$  to be above a minimum safety value. This minimum value is set to prevent unintended device activation, offering a balance between safety and the flexibility for personal adjustment based on individual rehabilitation needs.

$\Delta\theta_{stop}$  is the angle by which the patient needs to lower their leg from  $\max(\theta)$ , defined as the maximum angle the patient's knee achieves during the rehabilitation session, to signal to the device that they want to stop the motor. It is set to provide a clear and deliberate action that the patient can easily perform when they want to cease the motor's assistance.

Unlike a static threshold,  $\max(\theta)$  is continually updated to reflect the maximum movement point. As patients approach their limit, their legs might not move smoothly in a single direction but oscillate as the muscles engage and relax. For instance, during an exercise session, the angle of the leg might follow a sequence like 60, 62, 64, 69, 75, 74, 78, 76, 72, and 74 degrees. In such cases, the software is designed to recognize the peak within the oscillation, 78 degrees, as the current  $\max(\theta)$ . This peak is critical because it represents the true limit of the patient's range of motion in the session. If the patient sets  $\Delta\theta_{stop}$  as 15 degrees, the motor will cease to assist or slow down when the patient's leg lowers to an angle of  $\theta_t = \max(\theta) - \Delta\theta_{stop}$ , which would be  $78 - 15 = 63$  degrees in our example (shown in figure 12b). This adjustment ensures that the motor support does not exceed the weight of the patient's leg, allowing the patient to lower their knee using only the strength of their leg, thereby ensuring both safety and the effectiveness of the exercise.

$\Delta\theta_{stop}$  must be set to a value greater than the amplitude of these oscillations to distinguish between involuntary shaking and the patient's intentional movement to lower the leg. If  $\Delta\theta_{stop}$  is too small, the motor might stop or slow down during the natural oscillations, interrupting the exercise unnecessarily. Conversely, if it is too large, the motor might continue running when the patient intends to stop, potentially leading to strain or injury. The primary function of  $\Delta\theta_{stop}$  is to ensure the patient's safety and comfort. By setting an appropriate threshold, the device can quickly respond to a significant decrease in the range of motion, indicating that the patient wishes to end the session. Establishing this threshold requires collaboration with physiotherapists and further research to align with best practices in ACL rehabilitation, ensuring patient safety without interrupting rehabilitation sessions unnecessarily.

To further refine the safety mechanisms in place, another potential solution could be integrated into the  $\Delta\theta_{stop}$  functionality of the AutoPhysio device. This enhancement involves the automatic termination of motor assistance when sustained minimal oscillations at the peak angle of movement are detected, indicative of potential distress or exhaustion. Such a feature would be particularly useful in scenarios where a patient might struggle to actively decrease their leg's angle to the designated  $\Delta\theta_{stop}$  due to fatigue. By detecting prolonged tremble-like movements near the maximum angle, signs that the patient may no longer be able to participate actively, the device would automatically disengage its support. This solution would complement the existing  $\Delta\theta_{stop}$  settings, using similar detection methods to provide a more nuanced response to the patient's physical state, ensuring that the therapy remains safe and effective without requiring manual intervention.

## 4 Estimation of exertion

(Ryan)

*With the full blueprint for our machine complete, we must design an implementation to realise its novel functionality using available technologies. The first task is deriving an estimate for the patient's exertion which is necessary for the controller in section 3.3 to provide the amount of assistive torque needed to maintain the patient's exertion at the target. This chapter will detail how AutoPhysio collects data on select features for use in a statistical model to estimate exertion.*

### 4.1 Statistical model

We wish to quantify exertion,  $\varepsilon$ . In literature, exertion is most commonly measured using verbal responses from a patient. This is termed 'rate of perceived exertion' (RPE). Although this is usually bounded 0 through 10 for ease of communication, normalisation makes this equivalent to a range of 0 to 1. In our device we aim to be able to estimate the value of the patient's exertion without explicit input from the patient, as this is cumbersome and infeasible. As such our goal is a statistical model who's output is a bounded scalar value from 0 to 1.

However, collecting labelled data points to build such a model is also quite inconvenient as it requires recording RPE feedback from the patient, and since this is perceived exertion, it would also vary with the patient's psyche. Furthermore, building a model for a continuous output range, requires a significant volume of data. Alternatively, to increase the accuracy and convenience of data collection, we will quantise the output-space of our model, such that we collect only two classes of data points  $C_1$  and  $C_0$ .

Let  $C_1$  be data points at which the patient cannot continue extension without further support, and let  $C_0$  denote the opposite. A more thorough discussion on the data collection will be presented later, but for now, data for the first class can be collected trivially with a button that a patient presses only when they cannot keep extending without further support. Data for the second class can be collected from all the points recorded before the user presses the button. Then, by definition, a patient's exertion is *directly and monotonically* mapped to the their probability of pressing the button to indicate they need support.

$$\varepsilon \mapsto \mathbb{P}(C_1) \tag{8}$$

This is because the maximum value of exertion is now being directly mapped to 100% probability of pressing the button, and the minimum value is directly mapped to 0% probability of pressing the button.

It is monotonic because a slower increase in exertion is equivalent to a slower increase in probability. We can verify this since, if a variable is changing that makes a patient's exertion increase very slowly, then the distribution of button presses will be spread out over a larger range and thus too, the probability of a button press increases slowly. Therefore we are justified in defining the value of the patient's exertion as the probability of being in  $C_1$ . We then need to find the probability distribution of pressing the button,  $p(C_1)$ .

We shall assume that exertion (or equivalently, the probability of pressing the button), is related to some features,  $\mathbf{F} = [F_1, \dots, F_n]$ . Relating exertion to any individual feature is insufficient, as we *cannot assume* a one-to-one mapping for any feature in isolation. Simply put, this means exertion may be multi-variate such that it can be both high and low for the same value of  $F_1$ . This is known as *many-to-one*, and is illustrated in fig. 13a below, where for  $F_1 = 0$ , the probability density could be both high or low depending on  $F_2$ . Furthermore, the mapping may also be *many-to-many*, such that there are multiple locations in the space where exertion is high. This is illustrated in fig. 13b.

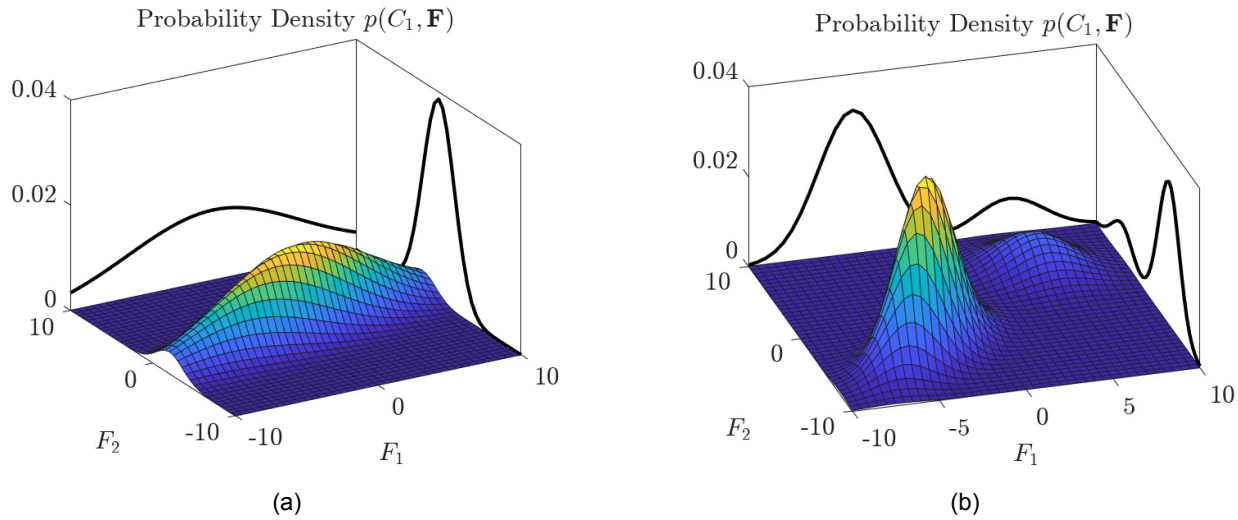


Figure 13: Illustrations showing how the distribution of  $C_1$  may be: a) multi-variate, & b) also multi-modal

Instead, if we sufficiently sample all dimensions of the  $n$ -dimensional feature space by collecting enough data, we can build a better generative model of exertion in this space. Essentially, *if we know both  $F_1$  and  $F_2$ , we have more information to determine the probability of being in  $C_1$* . Thus, from the data collected, both classes are distributed over the feature space with *densities*  $p(C_1, \mathbf{F})$  and  $p(C_0, \mathbf{F})$ .

Finally then, the goal of our model is to output the *absolute* probability of being in  $C_1$ , given any arbitrary feature vector,  $\mathbf{F}^*$ . As explained in equation 8, this then is our estimated value of exertion.

$$\varepsilon(\mathbf{F}^*) := \mathbb{P}(C_1 | \mathbf{F} = \mathbf{F}^*) \quad (9)$$

Computing this probability first requires finding the 'class-conditional probability density' function,  $p(C_1 | \mathbf{F})$ , from the collected data. I will do this through Bayesian inference. Then we must go from this probability density to an absolute probability from 0 to 1,  $\mathbb{P}(C_1 | \mathbf{F}^*)$ . To do this, I will treat the density as a scalar field  $\epsilon(\mathbf{F})$  over the  $n$ -dimensional feature space, such that given a new location  $\mathbf{F}^*$ , I can then determine what volume to integrate over in order to output in the desired probability.

#### 4.1.1 Obtaining $p(C_1 | \mathbf{F})$ through Bayesian inference

To obtain the density function, we must start from some training data. As mentioned earlier, the data points collected in calibration give some distribution for both classes over the feature space. We have already established that it is possible for points where the button is pressed to be located in different 'clusters', shown below.

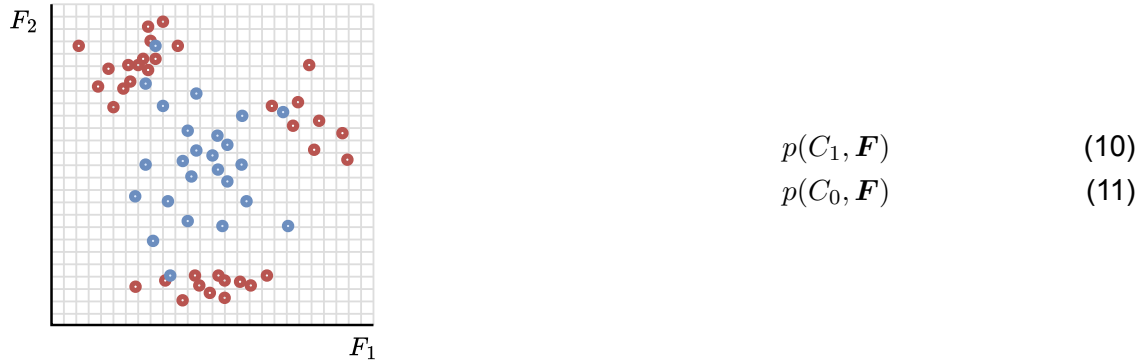
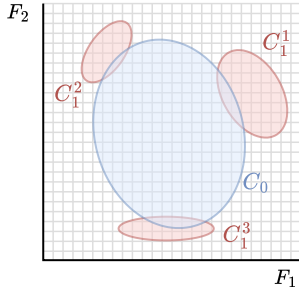


Figure 14: Example collected data (simplified to 2D)

We will assume that each of these class 1 clusters correspond to noisy measurements of particular points in the space, past which the user cannot progress without further assistance. Since a human is in control of these presses, we will also assume the noise is Gaussian. This assumption, who's validity will be discussed later, then allows us to model the system as a type of *Gaussian mixture model*, where, the points belonging to each cluster  $C_1^j$  are normally distributed around the mean location of that cluster. By using an unsupervised learning algorithm to determine the number of clusters, and then by considering the data points for each cluster in isolation, we can find the mean and covariance for each cluster.

The  $p(C_0, \mathbf{F})$  distribution is less categorical. Since  $C_0$  is simply all the locations where the patient does *not* need assistance, this means that the mass of the distribution tapers off near the  $C_1$  clusters. It also means

that it will have a main region of support far from each  $C_1$  cluster. Thus, as a first order approximation, we will assume this is also normally distributed. We then also need to find the mean and covariance of the  $C_0$  distribution from the data. In further iterations where we have collected data, it would be possible to investigate the best model to fit the distribution  $p(C_0, \mathbf{F})$ .



$$p(C_1^j, \mathbf{F}) = \mathcal{N}(\mathbf{F} | \mu_1^j, \Sigma_1^j) \quad (12)$$

$$p(C_0, \mathbf{F}) = \mathcal{N}(\mathbf{F} | \mu_0, \Sigma_0) \quad (13)$$

Figure 15: Clusters

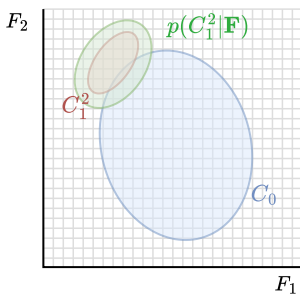
We then end up with the distributions illustrated above. With these, given any point in the feature space  $\mathbf{F}$ , we can find the posterior probability density that this point belongs to a particular cluster  $C_1^j$ , using Bayesian inference. For now, we will also assume that it is not possible to be in multiple  $C_1$  clusters at the same time. In further iterations this assumption can be worked around simply by extending the following classification method from binary to  $n$ -ary. Under this assumption, for the  $j^{\text{th}}$  cluster we ignore all other  $C_1$  clusters, leaving just the  $C_1^j$  and  $C_0$  distributions. Then using Bayes' formula, we calculate the probability of being in  $C_1^j$  given a point in the feature space. Since we have quantised down to two classes,  $C_1^j$  and  $C_0$ , this simplifies easily in equation 15.

$$p(C_1^j | \mathbf{F}) = \frac{p(C_1^j, \mathbf{F})}{p(\mathbf{F})} \quad (14)$$

$$= \frac{p(C_1^j, \mathbf{F})}{\sum_i p(C = C_i, \mathbf{F})} = \frac{p(C_1^j, \mathbf{F})}{p(C_0, \mathbf{F}) + p(C_1^j, \mathbf{F})} \quad (15)$$

Earlier in equations 12 and 13, we already derived models for the joint distributions in the above equation. The parameters for these models, the means and covariances, can be worked out trivially from the collected training data. We can now complete equation 15 to get equation 16 below. With this, we can infer the probability density that a new point in the feature space is in  $C_1$  for each cluster  $j$ . For ease of notation, we define this as  $\epsilon_j$  which we can treat as scalar potential field.

So far then, we began by clustering all our class 1 data. Then we treated each cluster of class 1 in



$$\epsilon_j := p(C_1^j | \mathbf{F}) = \frac{\mathcal{N}(\mathbf{F} | \boldsymbol{\mu}_1^j, \boldsymbol{\Sigma}_1^j)}{\mathcal{N}(\mathbf{F} | \boldsymbol{\mu}_0, \boldsymbol{\Sigma}_0) + \mathcal{N}(\mathbf{F} | \boldsymbol{\mu}_1^j, \boldsymbol{\Sigma}_1^j)} \text{ for all } j \quad (16)$$

Figure 16: Class posterior PDF

isolation, meaning for each analysis we had binary classes,  $C_1^j$  or  $C_0$ . By modelling the two joint distributions as Gaussian, we used Baye's to infer the distribution describing the posterior probability density of belonging to each cluster  $C_1^j$  given any feature vector, illustrated in green in the figure above.

Now, given a specific location  $\mathbf{F}^*$ , for each cluster we must select the volume of feature-space to integrate over to be able to output an *absolute* probability that this point belongs to that cluster of class 1. We then select the largest probability from the integrals over each field, since the patient can only be in one cluster. This tells us the probability of being in  $C_1$ .

#### 4.1.2 Obtaining $\mathbb{P}(C_1 | \text{bm}\mathbf{F} = \mathbf{F}^*)$ from $p(C_1 | \mathbf{F})$

Up to now we have been using standard statistical techniques. Selecting a volume to integrate over is non-trivial since there is no unique volume given one point in the space. The aim of our volume integral is to reach 100% probability as we get further into the region of the cluster. One way to select this is to split the space in half, and integrate over everything in the direction where it becomes less likely to be in  $C_1$ . The more traditional alternative method is '*discriminant function analysis*', however this does not result in a bounded function, which we require. The drawbacks of the volume integral method I have chosen will be discussed in section 4.5.

Continuing this method, we must first find the direction in which the feature vector becomes more likely to be classified as  $C_1$ . Since our distributions are conveniently Gaussian, we can simply take the a vector from the centre of mass of one distribution to the centre of mass of the other, where the centres of mass are simply the means. With this vector  $\bar{\mathbf{v}}$ , we then have a general direction in which it becomes more likely to be  $C_1$ .

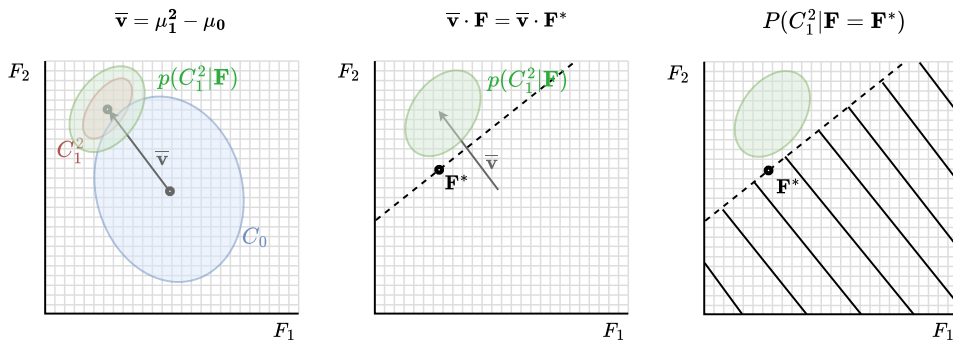


Figure 17: Integral over the volume split by the hyperplane at  $\mathbf{F}^*$  perpendicular to  $\bar{\mathbf{v}}$

Then for any particular point  $\mathbf{F}^*$ , we define a hyperplane past which it becomes more likely to be  $C_1$ :  $\bar{\mathbf{v}} \cdot \mathbf{F} \geq \bar{\mathbf{v}} \cdot \mathbf{F}^*$ . Using this hyperplane, we can integrate our distribution over all dimensions from  $-\infty$  up to this plane. With this, we finally arrive at our estimate for exertion.

$$\varepsilon(\mathbf{F}^*) := \mathbb{P}(C_1|\mathbf{F} = \mathbf{F}^*) = \operatorname{argmax}_j \iiint_{\mathbb{R}^n} H(\bar{\mathbf{v}} \cdot \mathbf{F} - \bar{\mathbf{v}} \cdot \mathbf{F}^*) \epsilon_j(\mathbf{F}) d\mathbf{F} \quad (17)$$

where  $H$  is the Heaviside function (unit step), (18)

$$\text{and } \epsilon_j(\mathbf{F}) = p(C_1^j|\mathbf{F}) = \frac{\mathcal{N}(\mathbf{F}|\boldsymbol{\mu}_1^j, \boldsymbol{\Sigma}_1^j)}{\mathcal{N}(\mathbf{F}|\boldsymbol{\mu}_0, \boldsymbol{\Sigma}_0) + \mathcal{N}(\mathbf{F}|\boldsymbol{\mu}_1^j, \boldsymbol{\Sigma}_1^j)} \quad (19)$$

## 4.2 Feature selection

With the model, we must now select the features. Each feature must both: have *some* relationship with exertion, and be normalised (bounded). Additionally, we do not wish to have too many features since the amount of data required grows exponentially with dimensions - the ‘curse of dimensionality’.

### 4.2.1 $F_1$ and $F_2$ - EMG signals

In the background section, John established and evidenced that the amplitude of EMG signals is related to both voluntary contractions and myoelectric muscle fatigue (MMF). A further paper also relates perceived effort to EMG signals in localised muscle groups [58]. In the scenario of knee extensions, the patient is extending their leg using their quadriceps. Thus, the voluntary contraction is the quadriceps. However, in times of pain, it is well established [59] that *reflexive contractions* occur in the antagonistic muscle - in this case, the hamstrings. It is also important to acknowledge the need to normalise EMG [36]. This is one of the objectives of the warm-up phase - to collect EMG data which we can use as a normalisation point.

Given the above as background, it is clear that both the EMG from the quadriceps and the EMG from the hamstrings relate the patient's exertion during knee extensions. As such, our first feature  $F_1$  will be the normalised amplitude of the EMG from the quadriceps. Furthermore, we have already discussed that the aim of providing assistance is to help the patient extend their range of motion despite both pain and muscular weakness. Thus, the model for exertion should reflect when a patient is trying to overcome pain. As we have also established that under pain it is likely that both muscles are contracting, our second feature  $F_2$  will be the *sum* of the normalised amplitudes from both the quadriceps and hamstrings.

#### 4.2.2 $F_3$ - Frequency of vibrations from tremor

It has also been documented that muscle fatigue is related to physiological tremor [60, 61]. Tremor is a lack of smooth movement. Additionally, "smoothness of movements has been used to gauge motor performance (movement quality) in both healthy (Balasubramanian et al., 2010) and patient (Rohrer et al., 2002; Kahn et al., 2006a) populations" [62]. As such, our chosen third feature  $F_3$ , is the frequency of vibrations in the patient's motion. We can normalise and bound this by the highest frequency of trembling recorded in humans.

#### 4.2.3 $F_4$ - Velocity of the movement

It is also well established that when fatigued, the amount of force muscles can provide decreases [63]. Therefore from Newtons law, the acceleration they create also decreases. By normalising this using the highest recorded velocity for the patient, we can then achieve a bounded variable that is related to exertion. Our final feature  $F_4$  is then chosen to be the difference between current velocity and the maximal recorded velocity for the patient.

I also performed an informal qualitative study on the relation between velocity and exertion at Oxford University Athletic Club. The study included a small group of eleven elite or semi-professional athletes. Although only one athlete in my study had torn their ACL, all eleven athletes reported significant drop in the speed of movement during exercise when recovering or over-exerting past previous strength levels.

### 4.3 Data collection and maintaining calibration

As mentioned earlier, to collect data points from the  $C_1$  class, we simply record the feature vector when the 'More Assistance' button is pressed. We can collect data points from the  $C_0$  class by taking samples of the feature vector at all points prior to the button press. This then calls for a phase in the product's

life-cycle where it calibrates to the user by collecting this data.

In this calibration phase, the set-up is the same as usual, except in the assist state we do not have any data to know what assistance to provide we provide to control the patient's exertion. Thus, instead in this phase we provide a pre-determined torque – a set fraction of the self-weight at each angle. We must also ensure to introduce enough variance to capture all the clusters in the feature space. To do this, we do two things. We request different speeds from the patient, and for each speed, we provide different fractions of the self weight. This then allows us to capture the  $j$  different clusters of  $C_1$  classes.

Notably, this model also allows us to easily continue learning beyond the calibration phase, by simply adding more labelled points when the user presses the button. We will already have captured enough  $C_0$  points since these will be the majority, so we will only add the  $C_1$  points to the models. To update the model, we then re-run the clustering algorithm, and re-calculate the mean and variance of each cluster.

#### 4.4 Clustering algorithm

This is the unsupervised task of the model, since we do not know how many clusters we will obtain. For simplicity, we will assume that there are only a few *different* regions of the feature space, where the user presses the button to indicate they need more assistance to progress. Under this assumption, the number of clusters is low. We will also assume that the clusters are well spread out such that there is little to no overlap. It is still possible to cluster without these assumptions, but we make them to make clustering easier for an initial design.

Since we have assumed no overlapping clusters, a quick and robust clustering algorithm is K-means. We can then use elbow detection to select K (the number of clusters), by starting from a low K and gradually increasing it to find the point when the total error suddenly drops.

However, we cannot rule out the possibility of having overlapping clusters. In this case, it is more appropriate to use support vector clustering with a non-linear kernel [64]. This is a task for implementation upon obtaining data.

#### 4.5 Analysis of model and areas for improvement

There are several areas for improvement. To begin with I'll start with an analysis of our model. We have essentially created a *generative classification model* for our output labels  $C$  and input feature vector  $F$ . The generative approach means we are '*parametrising*' our distribution - i.e. describing the distributions

as certain defined models (e.g. Gaussian, Poisson etc.) and fitting them using parameters,  $\theta, \phi$ . Mathematically speaking, this can be expressed and expanded to a multiplication of the marginal distribution of the outputs  $C$  and the class-conditional distribution of the inputs  $F$ , as shown in eqn. 20.

$$P(C, F|\theta, \phi) = P(C|\theta) \cdot P(F|C = C_i, \phi_i) \quad (20)$$

It has been proved that the marginal distribution over the outputs is simply the proportion of each classes [55]. The class-conditional distribution is more complex and must be defined for each class. In our case, as explained earlier, we have taken normal distributions for all clusters of class 1,  $C_1^j$ . We also took normal distributions for  $C_0$ . Then our parameter vectors for both these distributions simply becomes:

$$\begin{aligned} \phi_i &= [\mu_i, \Sigma_i] & s.t. \quad P(F|C = C_0, [\mu_0, \Sigma_0]), \\ & & P(F|C = C_1^j, [\mu_1^j, \Sigma_1^j]) \end{aligned} \quad (21)$$

These choices must be evaluated. Firstly, the  $C_0$ -conditioned distribution being Gaussian is a big approximation. In truth we do not know what this distribution looks like, and would need to collect data in order to get a better approximation. Secondly, the  $C_1^j$ -conditioned distributions were set as Gaussian processes because they are believed to be modelling human error. However, human error might be skewed. For instance, when stopping a stopwatch at an exact time, some humans may consistently stop earlier than the time, and some may stop later than the time. This skew can be added into the model's parameters such that,  $\phi_1^j = [\mu_1^j, \Sigma_1^j, \sigma_1^j]$ .

However, the more parameters for each model the more data we need for each model. Thus, it makes sense to do this in a later iteration when we have collected enough data.

Thirdly, moving past modelling them as Gaussian distributions, when determining the model parameters, we are assuming no prior information. We simply find the mean and variance for each distribution, and set these as our parameters. This means the approach we have taken to set these parameters is *Frequentist* - i.e. a maximum likelihood estimate. Whilst this approach is valid, some would argue that a *Bayesian* approach with an uniform distribution prior (no information on prior) would be more appropriate. Thus in our product we should test both options.

The final salient point of analysis is an evaluation on the volume integral. The approach I detailed involves an integral to try and find an absolute probability of being in class 1 given a feature vector. The issue of

this approach is that saying that the feature vector  $\mathbf{F}^*$  covers the range between the defined hyperplane and  $-\infty$ , is somewhat fictitious. Also the definition of a vector that indicates the direction in which the probability of being class 1 increases, also may not hold up to scrutiny if our distributions are not Gaussian. Another drawback is that the complex nature of this integral, makes the model clunky and slow, especially for non-Gaussian distributions. This is all in an attempt to find the absolute probability. Instead of focusing on this absolute probability, it is also possible to use a (non-)linear *discriminant function* to allocate any particular feature to one class or the other. The magnitude of the discriminant function tells us how confident we are that it is that class. In our case, it has been shown that a linear discriminant function can be defined as shown in eqn. 23 below [65].

$$g(\mathbf{F}) := \ln \frac{p(C_1^j | \mathbf{F})}{p(C_0 | \mathbf{F})} \quad (22)$$

$$= -\frac{1}{2}(\mathbf{F} - \boldsymbol{\mu}_1^j)^\top \boldsymbol{\Sigma}_1^j (\mathbf{F} - \boldsymbol{\mu}_1^j) + -\frac{1}{2}(\mathbf{F} - \boldsymbol{\mu}_0)^\top \boldsymbol{\Sigma}_1^j (\mathbf{F} - \boldsymbol{\mu}_0) + k \quad (23)$$

where symbols have been previously defined and  $k$  is a constant

It is possible to use this as our measure of exertion, however we would then need to be able to map exertion monotonically to the discriminant function. This is a task that could be explored in a future implementation.

## 5 Delivery of determined torque

(Ryan)

*The transitions and torque functions designed so far are key to calculating the right torque at the right time, but we have not yet discussed how AutoPhysio can physically provide this. Use of a motor has been mentioned, however the requirements of our device make a specific implementation non-trivial. In this chapter, I discuss the technicalities and present a solution which involves a controlled motor circuit. This leads to a discussion on a cascaded system for exertion control in the Assist state. Finally, I discuss how this comes together on a processing system, with certain considerations necessitated by a near real-time implementation. Thus, by the end of this chapter we will have determined how our device operates, and can progress in the rest of the report to design the finer implementation details.*

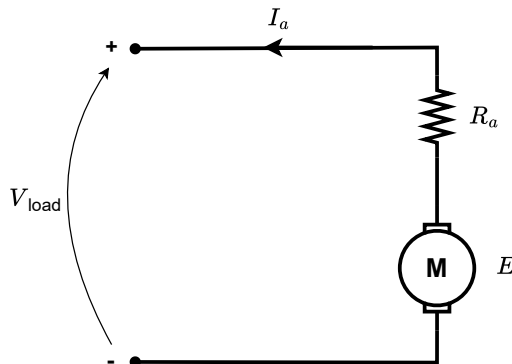
### 5.1 Motor circuit

AutoPhysio's knee joint holds a motor whose rotor is being driven by both the user and the power supply. This is most evident in the Assist state where the motor assists a user-driven motion. Thus, the electromagnetic system is somewhere between the generator and motor regime. Here, user-driven motion generates an electromotive force (EMF) and backwards torque; the opposite of what we desire. Even in the most simple state, Disengaged, providing zero torque is not trivial, since when the user moves (for example, in the warm-up), they generate an EMF and backwards torque.

These problems are similar to the ones faced by electric vehicles or regenerative braking scenarios[66]. In these scenarios, DC motors are used with additional circuitry that allows for dual torque control from both power supply and external driver. Thus, AutoPhysio also uses a DC motor and in this subsection I will design such a circuit that outputs the current required to provide the actual desired net torque, countering any backwards torque generated by the user's motion. With an ideal implementation, this will facilitate both free movement for the user and the addition of a variable net torque to the movement at any point.

In typical separately-excited DC motor circuits, a power supply sends current into the motor at a certain voltage. This causes a torque in the direction of motion and a velocity governed by the well-established motor equation (eqn. 24). In a generator circuit, the motor acts as the power supply and sends current into a load. Under Lenz's law this also generates a backwards torque, against the direction of motion. The relationship here is simply the reverse, such that for the same direction of rotation, current now goes

the other direction. The electrical power generated is the mechanical power consumed (eqn. 25).



$$k_m = \frac{E}{\omega} = \frac{T}{I_a} \quad (24)$$

$$V_{\text{load}} I_a = T\omega \quad (25)$$

Figure 18: Equivalent circuit for a separately-excited DC generator and the corresponding governing equations. Symbols have their usual meanings:  $k_m$  is the motor constant,  $T$  is torque,  $E$  is back-EMF,  $I_a$  is armature current.

The generative effect is far from desirable for AutoPhysio. In the Disengaged state where the power supply is disconnected, if the circuit was closed, users would still have to overcome the backwards torque that they generate from their motion. In the assist state this gets more disruptive, as the desired torque we wish to send, may not be what the user experiences due to the generative motion, which is effectively a disturbance from a control theory perspective. The disruptive EMF is given simply from the motor (generator) equation:  $E(t) = \frac{\omega(t)}{k_m}$ , from which we can work out that the net current and torque below, such that the torque experienced by the user will change as they move.

$$i_a(t) = \frac{V - E(t)}{R_a} = \frac{V - \omega(t)/k_m}{R_a} \quad (26)$$

$$T(t) = k_m i_a(t) = \frac{k_m V - \omega(t)}{R_a} \quad (27)$$

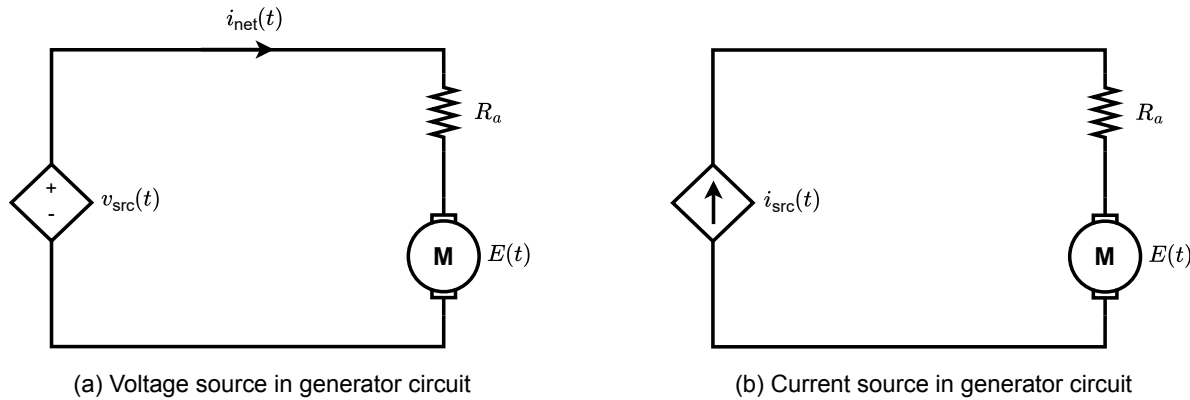
However, consider the situation when a user is driving the motor at  $\omega$  but that it was open circuited. The result would be such that no current could flow and therefore no power is consumed and therefore the rotor could rotate freely. This is in fact the ‘open-circuit generator’ scenario in equation 28: no current is allowed to generate in the motor coils, so the Lorentz force is 0 and the rotation  $\omega$  is unhindered, or ‘free’. We can see this from considering the power equilibrium:

$$T\omega = EI_{\text{net}} = 0 \quad (\because I_{\text{net}} = 0) \quad (28)$$

$$\therefore T = 0 \text{ for all } \omega$$

Similarly, if we had a voltage source that managed to match and negate the EMF at all times, then no

current would flow and the rotor could again rotate freely. From another perspective, the voltage source provides the same EMF required by the motor equation to make the motor spin at  $\omega$ , thus the driver would now need to rotate faster than  $\omega$  to generate any EMF and experience any backwards torque.



It then becomes clear that in order to control the torque (backwards or forwards) on the rotor, we must simply control the current in the circuit (into or out of the motor). This way, as long as the net current is controlled to the same target value, user-driven motion will not affect the torque being sent to the motor. We can do this using a variable current source in the circuit which aims to maintain the current in the circuit and thus the torque on the motor. This then becomes a control problem, where we control the current to achieve a target net torque. Thus, our circuit is as follows in figure 19b, where we use a multiplexer to set the target torque depending on the current state of our machine.

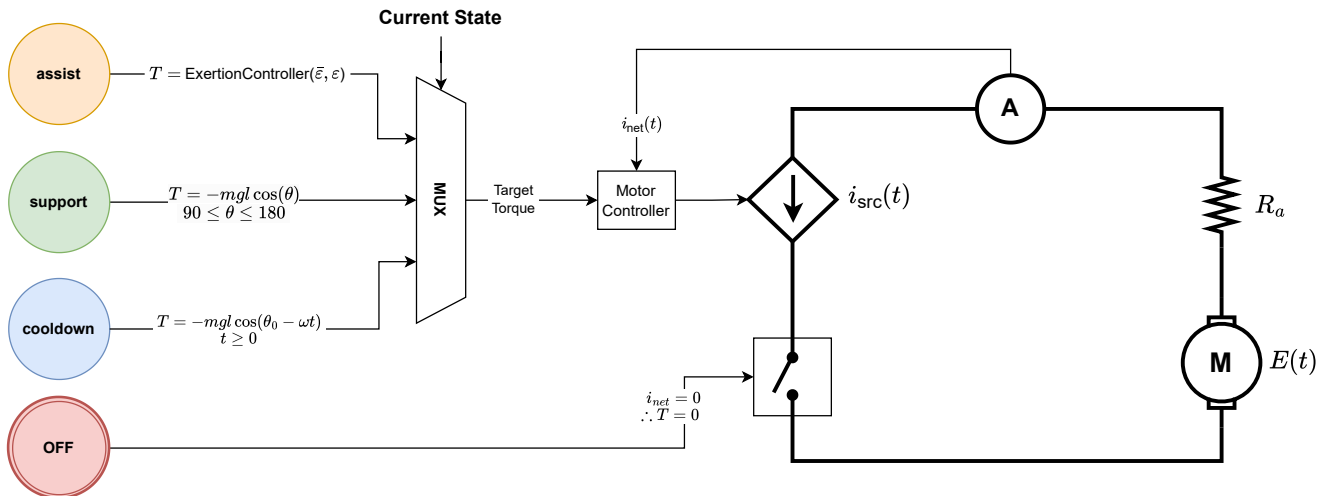


Figure 20: Overall Schematic

## 5.2 Motor control & safety

In theory, simply using a variable current source that dictates the current in the circuit, would allow us to set the torque as we wished, regardless of user motion. In reality however, most current sources are actually voltage source controllers, where the actuator is the voltage source, the sensor is an ammeter and the signal being controlled is the current. This results in the following control block diagram for the motor system.

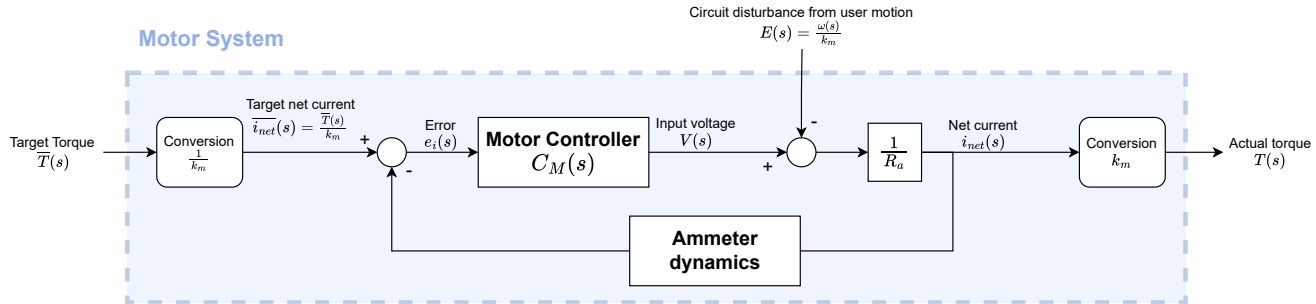


Figure 21: System for the control of motor torque to a desired torque

However, most motors come with their own controllers which are capable of controlling the current input to the motor. These controllers also come with additional safety features, such as detecting overheating. In section 7.2.1, Will selects a motor capable of providing the desired levels of torque. In our design we will assume use of the manufacturer-provided controller in order to control the current safely.

### 5.2.1 Cascaded control in the assist state

With this controller, we can achieve the desired torque output by all states. However in the Assist state in particular, the desired torque is calculated by another control system, the exertion controller, which was detailed in section 3.3. We thus have two *cascaded* controllers, where the motor controller (fig. 21) is the secondary (inner) loop of the primary (outer) exertion controller. Although we decided to use the manufacturer's motor controller, figure 22 shows how these two controls simplify into one system, via block diagram reductions.

This result shows that we could achieve an *integrated* controller using a voltage source as an actuator directly, instead of using an input torque and sending this through another controller. Integrated control systems are more responsive than cascaded systems, due to the lack of a back-and-forth time delay recurring between the two controllers. They also achieve an optimal control for the whole system, as opposed to two optimal controls for the sub-systems which may not be the global optimal. However,

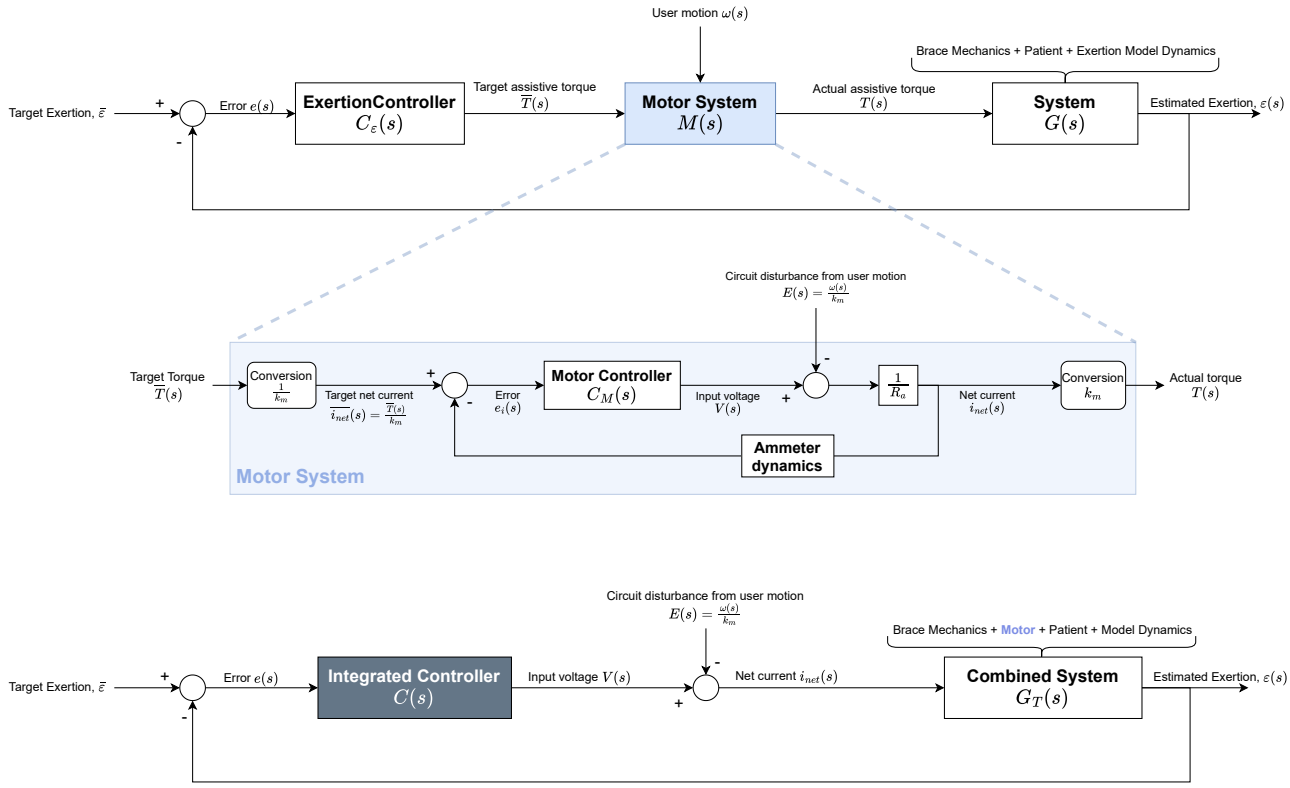


Figure 22: Block reduction from a cascaded to an integrated control system

splitting the system into a primary and secondary is often a less complex implementation task as it is easier to understand the processes separately. In our case, since the manufacturer's controller also comes with built-in safety features, we decide to continue using it at this proof of concept stage. In later design iterations, we may incorporate these features into our own Integrated Controller to ensure a safe system that is more responsive than two cascaded loops.

### 5.2.2 Safety

Earlier, we incorporated an upper limit on the torque from the motor. To consider this in our circuit, we can now determine the maximum current that should be allowed to flow into the motor,  $i_{\max}$ . This can be incorporated into the motor controller from the manufacturer.

$$i_{\max} = T_{\text{self}}/k_m \quad (29)$$

$$= -mgl \cos(\theta)/k_m$$

We also need to ensure that there is a method to cut-off the motor from the power supply at any point the user requires. In fig. 20, we see how this is achieved through hard-wiring the Disengaged state as a switch in the circuit. Thus, if the motor-off button is pressed at any point, the switch is opened

immediately without needing to pass through a processor, and no current flows resulting in nil net torque. Simultaneously, after the processor has processed that the Disengaged state has been entered, it then sets the target torque to zero, preventing the controller from draining power due to a non-zero target torque since the ammeter continues to feedback  $I_{\text{net}} = 0$  under open-circuit.

Finally, the motor should only ever be in operation between the pre-determined rest angle  $\theta_{\text{rest}}$  and target angle  $\bar{\theta}$ . We note that this safety range has already been achieved by the transitions in our FSM, since it is not possible to be in any of the active motor states when the user is outside of this range.

### 5.3 Computing system design considerations

Thus, our overall system is as illustrated below. We have several inputs, which get buffered onto the chip. They get pre-processed, synchronised and logged to memory. From this, we can calculate the torque to provide for any given state, which is in turn decided by the state machine based also on this data. This output target torque is sent to the controller which sets the current in the motor circuit, and finally, through the brace mechanism, the patient receives the assistance.

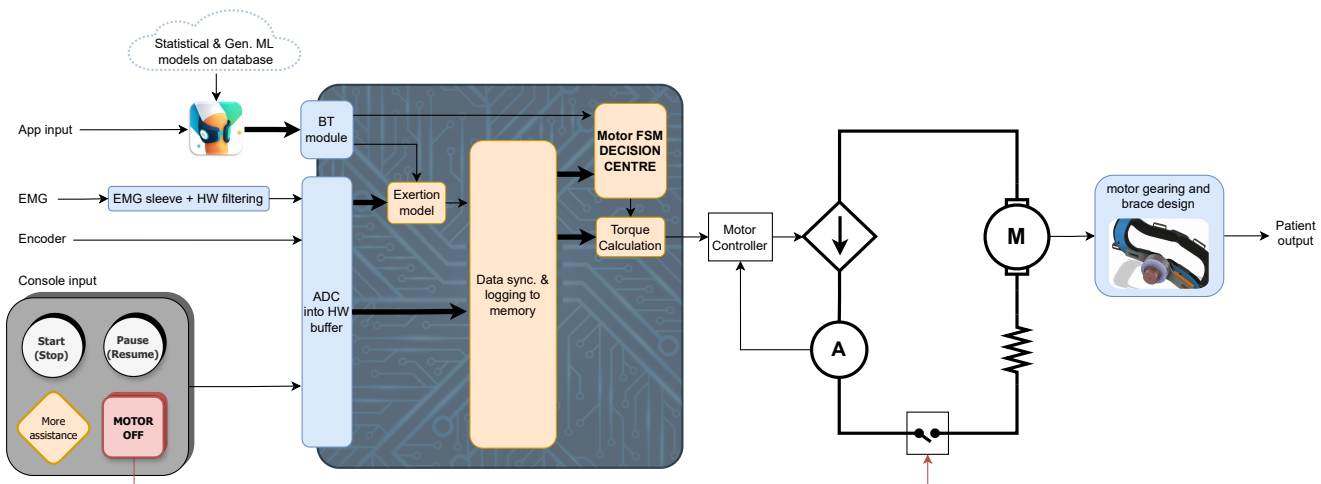


Figure 23: Overall schematic for AutoPhysio

#### 5.3.1 Further electronics: positional sensor and ADC

Whilst the motor has been discussed in great depth already, there remain a few electronic components that need to be considered. As we are using a DC motor and not a servo, we require an alternative method to determine the angular position and thus derive angular velocity and acceleration. While an IMU would be useful in three-dimensional movements, our system is to be used in a singular axis of rotation - the leg extension. Thus we can use an angular encoder to get a very precise signal with high SNR. This

can be used to derive angular velocity and acceleration, as opposed to calibrating and denoising a very noisy IMU, let alone accounting for sensor drift common to IMUs [67]. The choice between absolute and incremental encoders is rather inconsequential, since both will work for our system. An incremental encoder may be less robust in the case of a power outage, but as components are easier to maintain care of. In both cases, the output data will be in the form of quadrature pulses, which can be read easily for most microcontrollers via open-source libraries.

As John has discussed, the EMG inputs will simply provide a continuous, bounded voltage signal to the chip. We then require an ADC at a set sampling rate. Most microcontroller's have an in-built ADC. We will return to the sampling frequency in the next section.

### 5.3.2 Firmware & System-on-Chip (SoC)

The complexity of an algorithm relates each loop to the computation time. The rate limiting step in our algorithm is the estimation of the exertion, as it requires an involved integral. There are also several processes that we wish to occur at the same time, or in *parallel*. True parallelism is physically impossible on a single-core processor since it can only process one instruction at any time. Instead parallelism simulated, as I will discuss below. Both of these factors mean that sensor data is in reality accessed slightly out of sync, and therefore operations would be slightly inaccurate or 'non real-time' if programmed completely sequentially.

Although our device is non-critical, the length of the algorithm results in a non-negligible delay which will affect comfort. We also need to collect all the data in order to send it to the cloud for analysis after sessions. Thus the software would need to be implemented such that data is collected, or 'logged', in sync. We also need to do this (and other tasks) as quickly as possible, such that other services are also able to compute. Therefore we require synchronisation, parallel simulation and high performance compute.

A buffer system preserves the order and synchronisation of collected data. A first-in-first-out (FIFO) system is appropriate. To avoid adding this to the list of processes, a low-hanging fruit for speed-up would be through a hardware implementation. Much VHDL/verilog IP is available for this. Another simple improvement is using a look-up table (LUT) for the motor states.

Simulating parallelism to perform multiple tasks 'simultaneously' on a single-core processor is non-trivial. To begin this, we would list all the processes and threads that need to be running. Then we can assign

a priority to each one, and build a task scheduler that decides when to start, stop, and swap between all these tasks. We then define how it handles system interrupts (ISRs), such as button presses.

To implement this, we could either use a Real Time Operating System (RTOS) or write our own a task-scheduler program. The general idea is to **schedule tasks** as above. Using an RTOS abstracts away the creation of the task scheduler, however the operating system itself occupies both RAM and flash memory on the micro-controller. In this scenario an RTOS such as ‘FreeRTOS’ could be used to create a prototype, abstracting away the intricacies of task management and Operating Systems. Later, a more compressed task scheduling program could be written by hand, incorporating system interrupts. This would be clean and without the extra bulk of a kernel and an OS.

With a method for simulating parallelism, we can then use the clock speed of the chip to estimate the compute time for all processes and determine where improvements need to be made. After this, we can work out the best and worst-case *throughput* rates of our chip. This will decide the sampling frequency of the ADC that we can use for the interface with the EMG peripherals. We can then compare this with the data production rate to determine if this is sufficient. It will also decide the amount of both RAM and storage required to log all the data. This requires knowledge of the architecture of the board we will use and deliberate selection between a micro-controller, microprocessor or CPU-based System-on-Chip (SoC).

A final consideration is to achieve the high performance compute of input data signals through use of algorithms which split integration into parallel tasks. This would allow us to compute the exertion estimate quicker. One of the features we need to collect for our algorithm is the amplitude and frequency of vibrations. Collecting this from raw encoder input using fast Fourier transform (FFT) is possible, however, we could also use a hardware filter to get the frequency range of interest and simply take the overall magnitude of this bandwidth.

Once all the source code (firmware) is complete, we would compile and link it to instructions, and then to machine code. This binary would contain the whole program’s behaviour, including the RTOS kernel and thus the desired parallelism. As usual, we then ‘flash’ the controller with the binary so that the controller runs the program.

# 6 Mechanism considerations

(Will)

This chapter covers introductory considerations for the design of a mechanism to drive rotation about the knee. In this chapter I also detail the torque requirements of the mechanism, which will be used for motor selection in the next chapter, and are critical for safety of the device.

## 6.1 Design objectives and functions

It is crucial that the design objectives are set out clearly before preliminary designs are considered. Here are the key objectives for the design of a mechanism to drive rotation of the leg.

- The mechanism is detachable such that the knee brace can be used as normal in daily routine.
- The mechanism is *independent to any specific knee brace*, and as such can be fitted and unfitted to most / any brace, with no, or minimal permanent alterations.
- The mechanism assists with and measures data about range of motion exercises. The mechanism *does not* aim to provide enough torque for targeted strengthening of any muscle groups in the leg.
- The mechanism is as quick and as easy as possible to attach and detach, and there should be no ambiguity as to its installment, or possibility for user failure.
- The module should be lightweight and comfortable, and manufacturing of any parts should be as simple as possible (e.g. 3d printing or using off the shelf parts).
- The assistive mechanism should be capable of providing a maximum torque which is of the order of that generated by the dead weight of the lower leg when fully extended, and thus capable of manipulating the leg.
- There must be a way to *measure the angle of the knee*. This is an essential piece of data for the control algorithm and ML model.
- Points of safety: There needs to be a physical kill switch which is accessible to the patient at all times. The mechanism should also be physically limited between certain ranges, in case the existing knee brace limits fail. The module should be battery powered, not connected to mains.

## 6.2 Alternative designs

There are several design possibilities which I have touched upon during my research which could be explored further, but will be discounted due to not meeting the design criteria or other reasons. These designs could be explored as an alternative approach to solving the problem of at-home rehabilitation for leg injury recovery, and they also give a little bit more context to the designs which will later be discussed, so it is worth briefly mentioning them here.

*Direct drive of pivot*



Figure 24: Knee pivots (external)

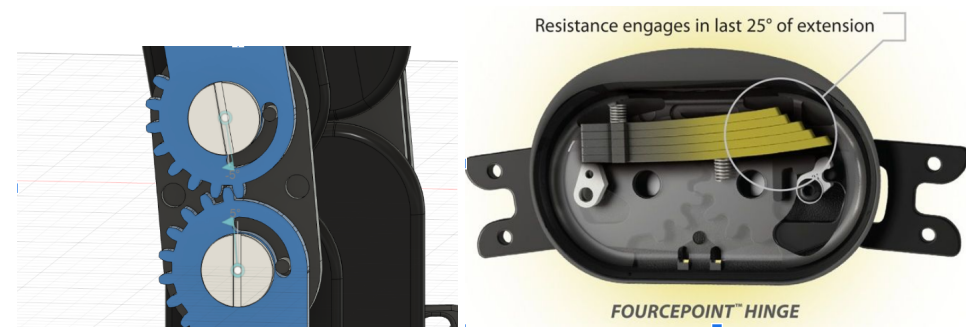


Figure 25: Knee pivots (internal)

As demonstrated in figure 24, there is great variety of pivot housing designs in modern knee braces. Figure 25 shows a basic mesh gearing between the upper and lower brace on the left, and in the right image a brace with additional bending bars to provide resistance in certain ranges of motion. It is clear that designing a method to drive this geared pivot directly would be futile, since it would require breaking open the brace housing and modifying existing parts or features in the brace. It is worth also noting that the use of a rotary actuator connected directly into the pivot between top and bottom brace bars is not suitable for this design; we have already stated we want the mechanism to be easily detachable, and this

would not be the case with a permanent actuator.

#### *Leg rocking mechanism*

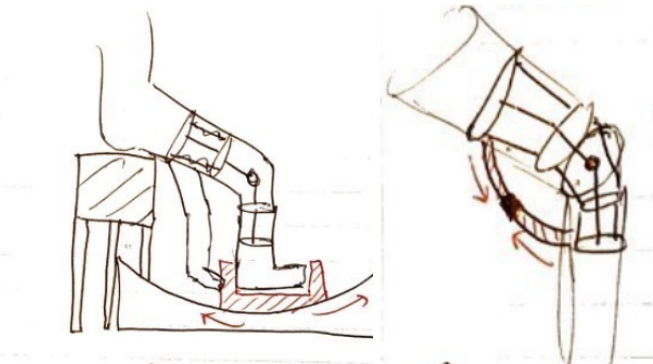


Figure 26: Left: Leg rocker. Right: Piston extension.

Another possible way to approach this is to build a rig / external unit to facilitate the manipulation of the leg. In this design, the shoe is held in place and slides along a curved housing unit up and down. The shoe holder could be pulled upwards (extension) with one string, and downwards (flexion) with another string for full range of motion control. There are several reasons this design is not considered further. Firstly, due to the fixed shape of the rig, it is not bio-mechanically compatible with various leg lengths. Secondly, the unit is overall very bulky and does not constitute 'wearable technology'. This design also doesn't provide a good way to measure the angle of the leg, which is essential for our project.

#### *Hydraulic piston extension*

Designs with any working pressurised fluid or extending pistons to generate torque and manipulate the leg are also discounted. We want to use a servo motor so that we have simple control of motion, and also an easy way to measure the angle of rotation of the leg.

#### *Pulley and spool*

A more flexible design can be achieved by using a pulley and spool system, consisting of a string wrapping around a spool which is driven by a motor. One end of the string will be attached to the lower brace, and will wrap around a pulley offset from the brace pivot. The string will then be wound around a spool, which is rotated by a motor. Mechanical advantage can be gained by decreasing the spool diameter, such that the motor rotates more times per unit length of string wound.

A pulley system, however, only facilitates lifting the leg up, i.e. extension, which limits the scope of the design. It could potentially be modified with a string on the underside of the lower leg in order to assist with

flexion exercises (e.g. heel slides), however this makes the design complex and not easily removable. This design might also be tricky to fit, since it would require a pulley and spool to be fitted separately. The string could also get tangled when removing or attaching the parts so it might take longer to set up. Measuring knee angle would also likely require a secondary encoder (the motors encoder wouldn't give an accurate reading of the knee angle).

Mechanisms where the motor is mechanically linked to the brace are preferable, since it makes fitting easier and measurement of the knee angle more robust.

### 6.3 Setup and initial basic calculations

Now that the design goals and project has been introduced, it is necessary to begin to more clearly define the module / mechanism that we wish to create.

It is first important to understand the structure and mechanics of the orthotic knee brace. All knee braces have a structural top and bottom bar which are rigid and strong. During daily activities and leg motion, forces are transferred from the leg via the strapping of the brace into these structural members. This distribution of force reduces pressure in the knee for recovery. Our mechanism will exert forces onto these rigid bars, which will be distributed by the strapping in order to comfortably assist leg extension or flexion. This is the reason we still need the knee brace for the design at all; Without the brace, making an ergonomic mechanism to rotate the leg would be extremely challenging.

The structural bars are connected by a simple 1:1 geared pivot to allow rotation and expansion of the knee during leg motion. Since the radius of the gears is small compared to the length of the knee brace and leg, the geared pivot can be approximated as a simple pivot for preliminary calculations and design. This slightly reduces the complexity of calculation.

#### 6.3.1 Torque requirement of mechanism

Our design requires that the maximum torque of the mechanism is of the order of the dead weight of the lower leg when horizontal; this ensures enough assistance is provided.

The torque requirement should be calculated for males. The reasoning for this is twofold: The vast majority of ACL injuries occur in males (as is clear in literature), and if the design is strong enough to manipulate a male leg it will also be suitable for manipulating lighter weights, as expected with a female

leg. Anatomical data gathered from Plagenhoef (1983) provides data shown in figure 4: [68]

Table 4: Anatomical data (relevant data indicated)

	Men N = 35		Women N = 100		Man Prox	Woman r Dist	Man Prox	Woman r Dist	Man k Prox	Man k Dist	Woman k Dist
<b>Table 4</b> <b>Segment Weights as Percentages of Total Body Weight</b>											
One segment	Mean	SD	Mean	SD							
Hand	0.65%	0.06%	0.5%	0.026%							
Forearm	1.87	0.2	1.57	0.1							
Upper arm	3.25	0.49	2.9	0.32							
Foot	1.43	0.13	1.33	0.02							
Shank	4.75	0.53	5.35	0.47							
Thigh	10.5	1.21	11.75	1.86							
Whole trunk	55.1	2.75	53.2	4.64							
Head and neck	8.26		8.2								
Thorax	20.1		17.02								
Abdomen	13.06		12.24								
Pelvis	13.66		15.96								

\*Length of shank alone = 100%  
\*Length of forearm alone = 100%  
\*Hip joint to hip joint = 100%  
\*Hip to shoulder length = 100%  
\*Shoulder to shoulder length = 100%

<sup>a</sup>Hip to shoulder length = 100%  
<sup>b</sup>Length of forearm and hand = 100%  
<sup>c</sup>Hip joint to hip joint = 100%  
<sup>d</sup>Hip to shoulder length = 100%  
<sup>e</sup>Radius of gyration about knee = 100%  
<sup>f</sup>Man = 81000 gms or 178½ lbs, and 180 cm or 5 ft 11 in.  
<sup>g</sup>Woman = 61290 gms or 135 lbs, and 170 cm or 5 ft 7 in.

From the data (35 men) we can conclude the following approximate information for our model of the lower leg:

- Weight of shank and foot (lower leg) is 6.18% of total body weight. Using the standard weight of 81kg from the study, the lower leg mean weight for a man is **m = 5kg**.
- The centre of mass from the knee (proximal) is 61% of the length of the lower leg - found as 0.445m in the study. So the centre of mass of the lower leg is expected to be **I = 0.27m** from the knee.
- The radius of gyration about the knee (proximal) is 74% of the length of the lower leg. This corresponds to a radius of gyration of **r = 0.33m**.

So the mean and standard deviation of torque provided by the dead weight of the lower leg when horizontal, and therefore our design specification for the mechanism, is simply:

$$T_{deadweight} = mgl \approx 13Nm \pm 1.5Nm$$

### 6.3.2 Torque provided by leg muscles

According to the EN-ISO 13482 standard for low risk robotics, the torque provided by a robotic mechanism should only be about 50% of human capabilities. This ensures that, if there is a malfunction in the motor controller, the user can always override the motor torque with the strength of their own leg. Data for maximum human flexion and extension torques are shown in fig 27. The study was conducted with a group of athletic males and females, so their capabilities are likely greater than an ACL patient who's

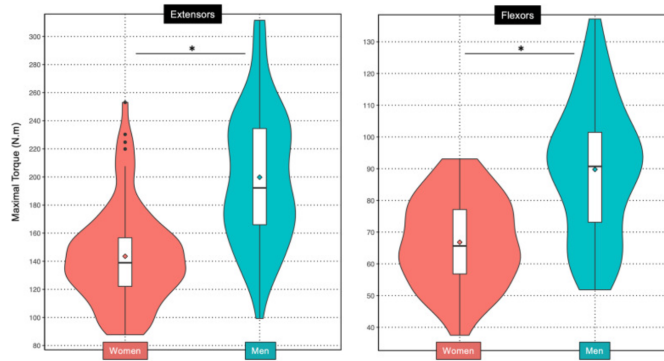


Figure 27: Flexion and extension torque for males and females [69].

muscles have atrophied slightly due to injury, and therefore we must show that the safety factor is larger.

If we take the weakest group for the weakest exercise (female and knee flexion) the maximum torque that can be delivered by the muscles is about 40Nm. This means that our mechanism should have an upper bound of about 20Nm to comply with robotics standards, which is well above the dead weight of the shank, and well above what we will need in our design. This analysis indicates that our mechanism will be operating in safe and effective torque ranges, i.e. enough to assist the leg, but not more than can be manually resisted. Therefore in the case of a control failure or too much pain during exercise, the patient will be able to flex muscles to halt the motor, and have time to manually turn off the power.

We might also be interested in calculating the actual torque which is produced by the patient during exercises for research purposes and for training our machine learning model later down the line. Since we measure the angle of the motor,  $\theta_{motor}$ , we can also find the angle of the leg,  $\theta$ , which is the inner angle between upper and lower leg. Since we measure the angle continuously, we can use a numerical method to define the second derivative of the angular rotation with respect to time, as in equation 30

$$\theta = f(\theta_{motor})$$

$$\frac{d^2\theta}{dt^2} \approx \frac{\theta_{i-1} - 2\theta_i + \theta_{i+1}}{\Delta t^2} \quad (30)$$

Here  $\Delta t$  is the time between readings of the angle, which will be known when we choose our encoder and controller system. The controller might alternatively give us the angular acceleration directly.

Now that we have the angular acceleration of the leg, we can write the system dynamics of the lower leg pivoting around the knee, as shown in figure 28. The system dynamics are given in equation 31.

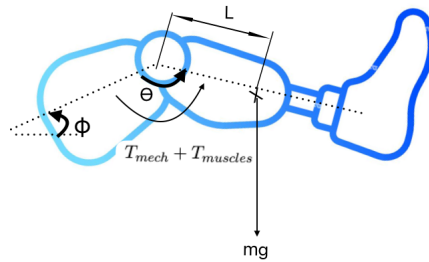


Figure 28: Simplified leg dynamics

$$T = I\ddot{\theta}$$

$$T_{mech} + T_{muscles} - mgl \cos(180 - \theta - \phi) = mr^2\ddot{\theta}$$

$$T_{mech} + T_{muscles} + mgl \cos(\theta + \phi) = mr^2\ddot{\theta} \quad (31)$$

Where  $T_{mech}$  is the torque provided by our mechanism, which is related to motor torque (since we know the current we deliver to the motor).  $T_{muscles}$  is the torque provided by the leg muscles,  $l$  is the distance to centre of mass,  $r$  is the radius of gyration,  $\theta$  is the inside angle between upper and lower leg,  $\phi$  is the angle that the upper leg is inclined to relative to the global horizontal.

The dynamics of the leg system can be used to estimate the torque which is applied by the upper leg muscles during either flexion or extension, given that we know or can calculate all the other terms in the equation.

The limitations of this analysis are:

- The torque from the inside ligaments of the knee are not accounted for, so we might not be accounting for all the rotational forces on the leg.
- We need to know the angle of the upper leg to the global horizontal,  $\phi$ , if we want to account for the weight of the lower leg in the calculation. This arises from the fact that our measurement  $\theta$  is only a relative angle, so we need  $\phi$  as well to know which way gravity acts in the global frame.
- We have ignored the weight of the knee brace and its contribution to the moment of inertia, since its mass is small compared to the mass of the lower leg ( $\approx 0.5\text{kg}$  total, so about  $0.25\text{kg}$  for lower half, so less than 5% of lower leg weight).

# 7 Motor mechanism design

(Will)

This chapter outlines the main design for the mechanism which will be driving rotation of the leg. I have assumed that the patient is wearing an orthotic (structural) knee brace, as shown in 29. The significance of this is that the leg is constrained to a safe path by the brace, so the design task is reduced to simply driving rotation, and considerations of twist or expansion of the knee joint become less relevant, since this is accounted for by the knee brace. The two designs I consider are a four bar linkage and an exoskeleton joint.

## 7.1 Investigation of four bar linkages for driving rotation

Figure 29 shows the basic structure of a four bar linkage for modification to the knee brace - colour coded appropriately and named *frame(1)*, *input(2)*, *coupler(3)* and *output(4)* - as per convention. The main objective of the four bar mechanism is to provide a mechanical advantage from the motor to the knee brace. We must also be very careful that there isn't an abnormally large mechanical advantage anywhere within the working range of the mechanism, since this is very dangerous.

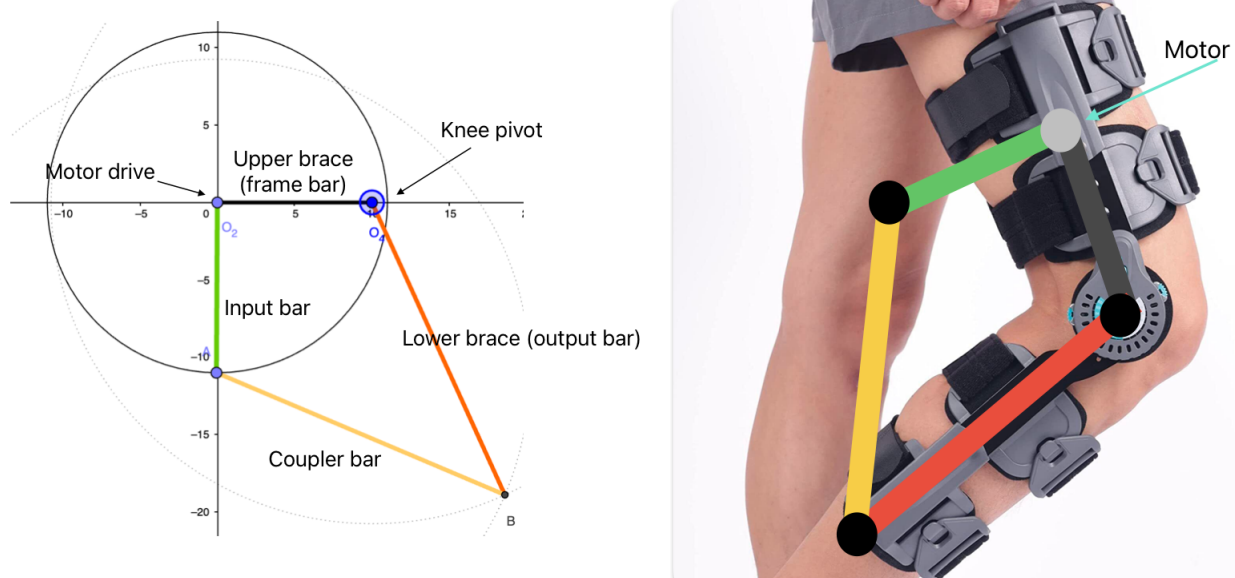


Figure 29: four bar linkage for driving knee brace. Left: example of a potential four bar mechanism. Right: a similar mechanism overlaid onto the knee brace to show where pivots could be.

Using a free online tool (geogebra), I was able to analyse and investigate possible linkages which could provide mechanical advantage.

Initial testing was done with the frame bar length set to a fixed value of 10cm, and the input bar was shorter than the output bar for mechanical advantage. Lengths were then adjusted so that the input bar sweep a larger angle than the output bar. With  $r_1 = r_2 = 10$ , and  $r_3 = r_4 = 20$ , the mechanical advantage can be calculated by considering the ratio of angular velocity from the input (motor) to the output (knee pivot). This is equivalent to considering the small changes in angle to the output caused by rotating the input a small amount.

*(The reason this simple analysis can be done is because we have a single rotational input which is coupled to a rotational output via the mechanism, so due to energy conservation it must be that the product of torque and angular velocity is constant around both pivots).*

By simply measuring small changes in angles with the online tool, I estimated the mechanical advantages at different positions of the mechanism (angles measured here as anticlockwise from the x-axis).

- input angle =  $270^\circ$ , mechanical advantage = 1.45
- input angle =  $315^\circ$ , mechanical advantage = 1.36
- input angle =  $355^\circ$ , mechanical advantage = 1.34

It is clear that this analysis is limited, and ideally we want a general method to quickly find the mechanical advantage in terms of the lengths of the bars and the input angle.

### 7.1.1 Solving four bar linkage with MATLAB

The governing equations for a four bar linkage which are easiest to solve computationally are the loop closure vector equations. This is simply the constraint that the four bars in the linkage must all connect back to one another. I.e. the vector sum of the lengths of the bars, as well as the vector sum of the velocities of the bars, are zero. This is illustrated in figure 30.

$$r_1 e^{i\theta_1} + r_2 e^{i\theta_2} + r_3 e^{i\theta_3} + r_4 e^{i\theta_4} = 0$$

With  $\theta_1 = 180^\circ$ , this simplifies to:

$$-r_1 + r_2 e^{i\theta_2} + r_3 e^{i\theta_3} + r_4 e^{i\theta_4} = 0 \quad (32)$$

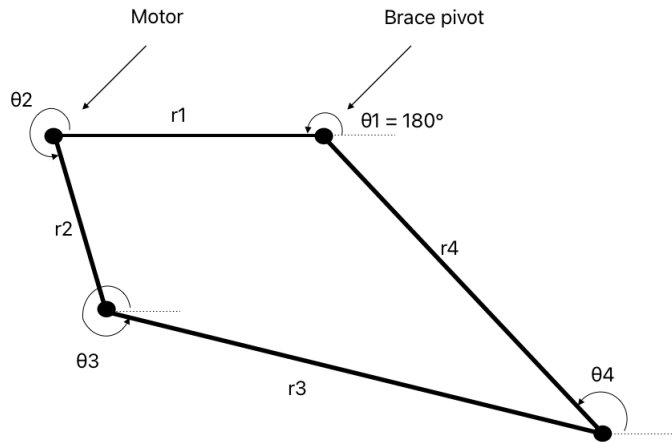


Figure 30: Loop closure angles convention.

Differentiate w.r.t time for velocity loop closure equation:

$$r_2 \dot{\theta}_2 e^{i\theta_2} + r_3 \dot{\theta}_3 e^{i\theta_3} + r_4 \dot{\theta}_4 e^{i\theta_4} = 0 \quad (33)$$

By taking real and imaginary components of equations 32 and 33, we end up with 4 equations. This allows us to have 4 unknowns in the equations, out of the possible list of parameters:  $r_1, r_2, r_3, r_4, \theta_2, \theta_3, \theta_4, \dot{\theta}_2, \dot{\theta}_3, \dot{\theta}_4$

- $r_1 = 10, r_2 = 10, r_3 = 20, r_4 = 20$ , all lengths are set (units don't matter as we will scale all lengths later)
- $\theta_2$  will be varied between  $0^\circ$  and  $360^\circ$ ,  $\dot{\theta}_2$  is arbitrarily set to 1 rad/s.
- $\theta_3, \theta_4, \dot{\theta}_3, \dot{\theta}_4$  are unknowns

The method is to solve for the unknowns at a certain values of  $\theta_2$ , and then find the mechanical advantage as the ratio of input to output angular velocities, as in equation 34.

$$MA = \frac{\dot{\theta}_2}{\dot{\theta}_4} \quad (34)$$

I used a function solving method in Matlab, in order to find the unknowns for my system of equations. I plotted the solution of the linkage to show that my equations were set up and solved correctly, as shown in 31. Then I modified the code to solve the equations at every input angle of the mechanism,  $0^\circ < \theta_2 < 360^\circ$ , and plotted this against the mechanical advantage. This is the most important plot in

order to decide bar lengths, because it shows how the mechanical advantage varies at every position of the mechanism.

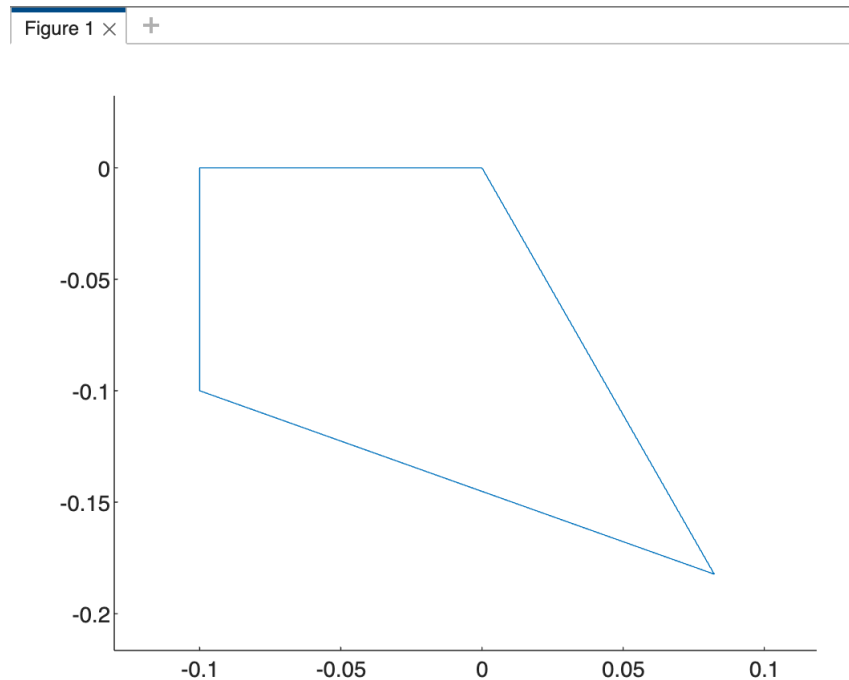


Figure 31: Plotting the solution to the four bar compatibility equations to show my MATLAB script is working (bars connect to form a closed loop).

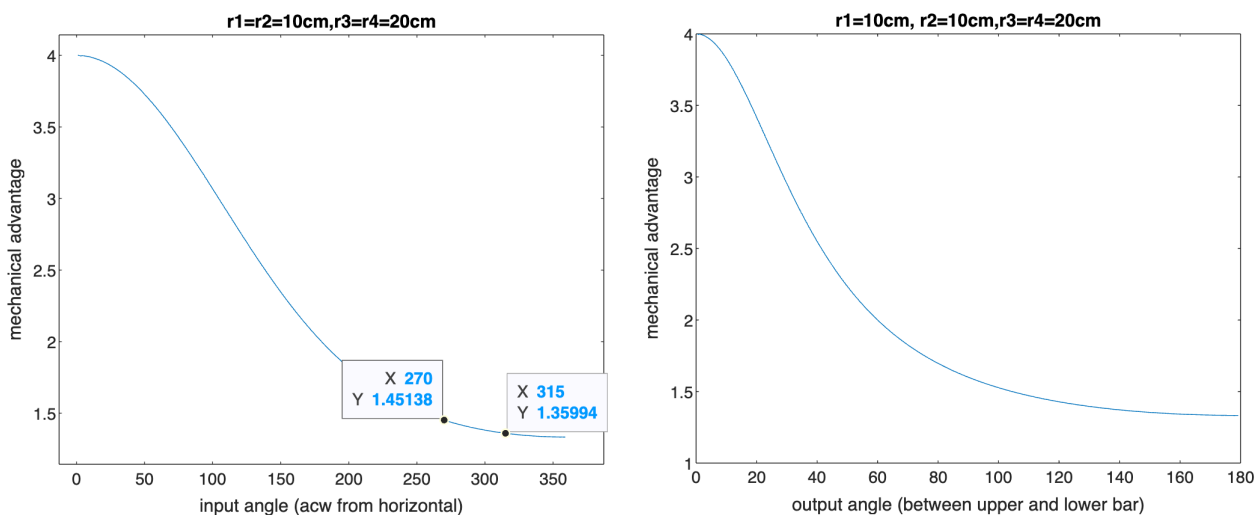


Figure 32: mechanical advantage for initial set of bar lengths. Left: mechanical advantage vs input angle. Right: mechanical advantage vs output angle.

Figure 32, on the left, shows how mechanical advantage varies over the entire range of motor input angles for the initial set of lengths proposed. On the right is the plot of mechanical advantage vs output angle,  $\theta$ , the inner angle between upper and lower brace. Full flexion at  $\theta = 0^\circ$  (impossible) and full extension at  $\theta = 180^\circ$ .

There is a discontinuity between  $0^\circ$  and  $360^\circ$ , and this is because the mechanism has an impossibly fast jump at this configuration (due to  $r_1 + r_2 = r_3 + r_4$ ). It can also be seen that the mechanical advantages at inputs of  $270^\circ$  and  $315^\circ$  agree with our previous calculations using the small angle changes, so the code is working as intended.

Next we should try varying the lengths of certain bars (perhaps using an online tool as a reference for what is and isn't plausible), and use the mechanical advantage vs output angle plot to select a suitable mechanism. We are looking for high and uniform mechanical advantage across all possible output angles:  $20^\circ < \theta < 180^\circ$ . It is not expected (or physically possible) to get a uniform mechanical advantage with a mechanism such as a four bar linkage.

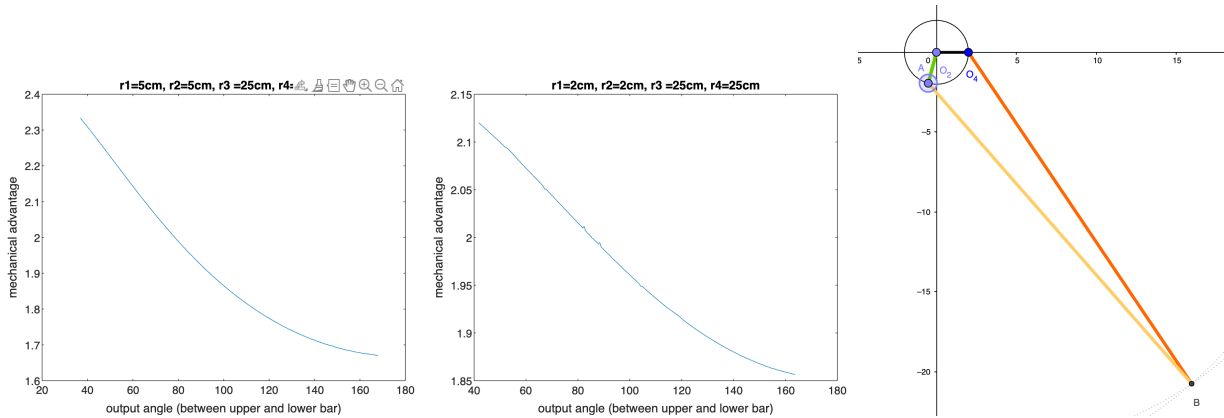


Figure 33: more testing with different bar lengths. Left:  $r_1=r_2=5$ ,  $r_3=r_4=25$ . Middle:  $r_1=r_2=2$ ,  $r_3=r_4=25$ . Right: Configuration of the 'two short two long' mechanism.

### 7.1.2 Insights from analysis

Figure 33 indicates that making the frame and input bar both very small, and the output and coupler bar both very long (what I call a 'two short two long' mechanism) *yields a near constant mechanical advantage of about 2*. The trade off is that the internal forces in the longer bars increase as the difference between lengths becomes more extreme, especially at large output angles. Also, such an extreme design is not feasible in the real world, due to space constraints.

From analysis it seems that the mechanical advantage always decreases as the output angle approaches  $180^\circ$ , and this makes sense intuitively since the thing we want to rotate (the lower brace) is further away from the motor, so it's more awkward to deliver torque there. There might exist mechanisms where this is not the case, however in my testing I was not able to find any practical mechanisms with this property.

Selection of an appropriate four bar linkage involves a trade off between the ideal case of a constant

mechanical advantage of 2 (two short two long), and having all bars in sensible proportion.  $r_1 = r_2 = 5, r_3 = r_4 = 20$  seems reasonable, and provides a theoretical minimum mechanical advantage of about 1.6 at full extension. In reality this configuration has a considerable drawback, since as the extension tends to  $180^\circ$ , the internal forces tend to infinity in order to provide a normal component of force when all bars are aligned in the longitudinal direction. This might not be a problem if we constrain our extension of the leg to, say,  $175^\circ$ , but in this case we still need to be aware that the internal forces will become large as our mechanism tends to its terminal state.

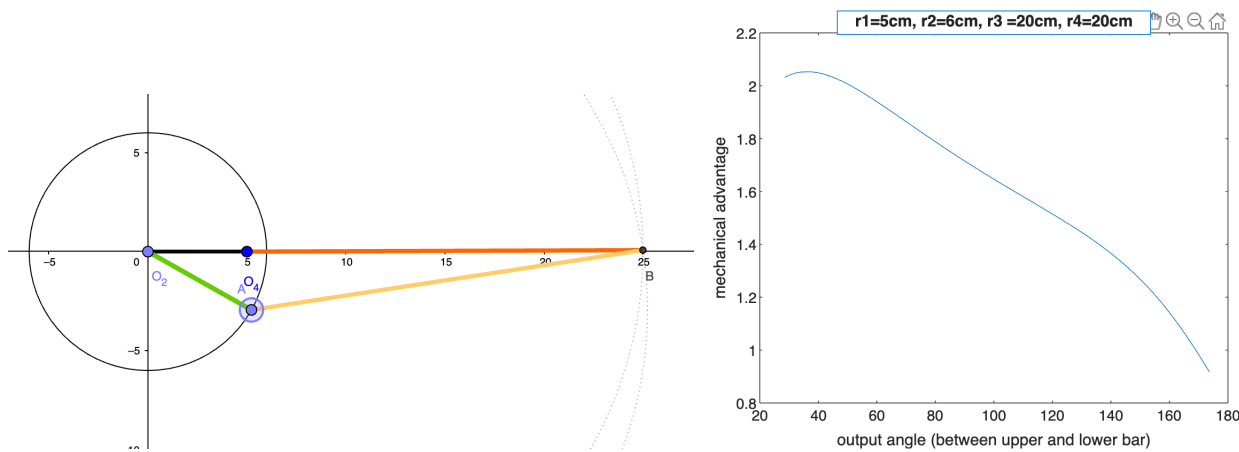


Figure 34: Alternate configuration with  $r_2$  slightly longer than  $r_1$ . Left: the configuration of the bars at output of  $180^\circ$ . Right: the mechanical advantage curve.

One solution to this problem is to make  $r_2$  slightly longer than  $r_1$ . The consequence of this is that the mechanical advantage drops off much faster at large angles. Figure 34 shows the configuration at a large output angle, and also the mechanical advantage vs output angle curve. Mechanical advantage drops to below 1 at above  $160^\circ$ , which means we are delivering less torque to the leg than is being generated by the motor.

#### *Selection of bar lengths.*

If it were absolutely necessary to design a four bar linkage for this purpose, and bar lengths must be chosen, then one set of appropriate bar lengths is:

- $r_1 = 5, r_2 = 6, r_3 = 20, r_4 = 20$

Then all that is left to do is to determine a suitable scale. This set of bar lengths guarantees a mechanical advantage of above 1 for all output angles below  $160^\circ$  (corresponding to most of the working range for physio exercises). This set of lengths also mitigates the problem of large internal forces in extended positions, so it is a valid design.

Importantly it should be considered how the angle of extension of the leg ( $\theta_4$ ) can be obtained. The easiest method is to (once the 4 lengths for our four bar linkage have been selected) produce a plot of output angle vs input angle by using my Matlab four bar linkage solver. This data can be imported into the system controller as a lookup table, so if we know the servo motor position we can quickly translate this to the knee extension angle. One thing worth noting here is that a four bar linkage usually has 2 possible configurations, so we must be careful to select the correct one, and this can be done by putting in an appropriate initial guess in the Matlab solver. We might also need to take a reference measurement with a known motor and four bar linkage configuration in order to calibrate the readings for our system.

### 7.1.3 Static forces

The final thing we might be interested in with a design of a four bar linkage is the static forces present in each member at equilibrium (tension, compression and bending moments).

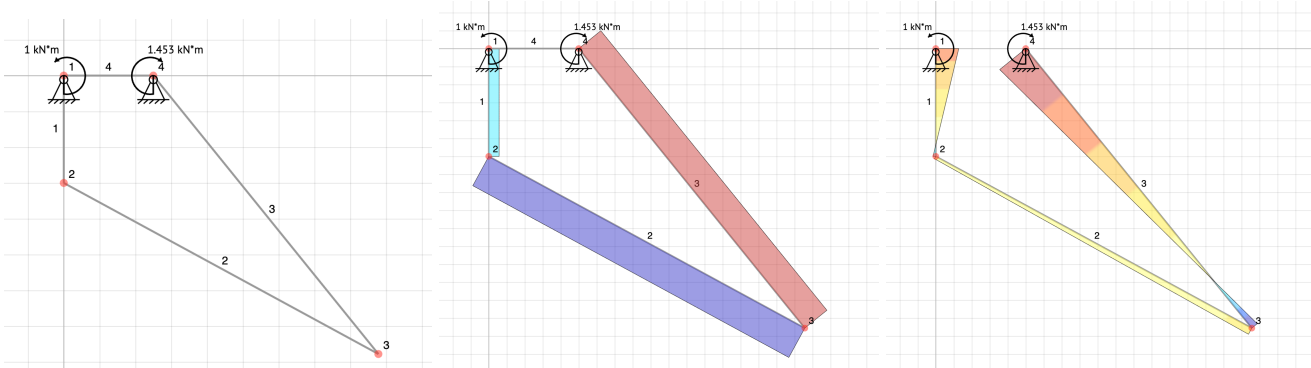


Figure 35: Loading (left), shear (middle) and bending (right) diagrams for four bar linkage

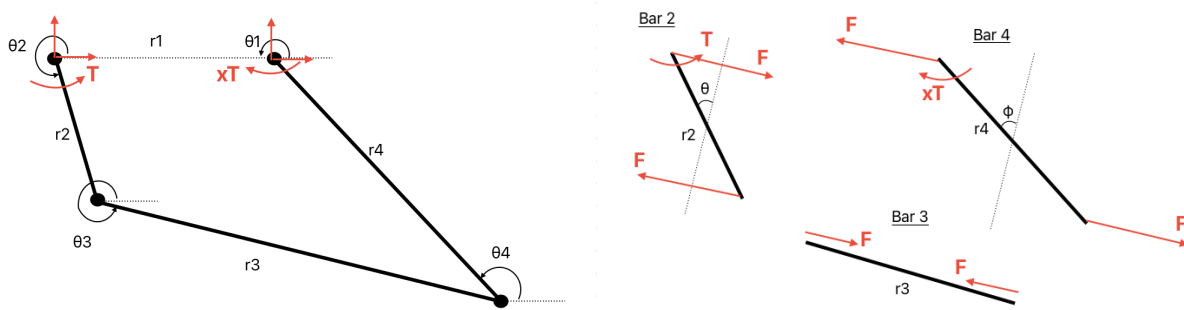


Figure 36: Overall loading on mechanism (left). Free body diagrams for each bar (right).

This analysis can be done by hand using conventional methods and force moment equilibrium. The analysis is done by first drawing the mechanism as a whole with all the external reaction forces and moments (noting that if a torque  $T$  is applied at input, a torque  $xT$  must be restoring at the output,

where  $x$  is the mechanical advantage). Then force and moment balance is considered for each bar in succession, working around the mechanism. From this analysis we can find the mechanical advantage,  $x$ , as the ratio of output to input torque required for equilibrium (see equation 37). The analysis is as follows:

Moments about bar 2 (see figure 36).

$$T = Fr_2 \cos \theta \quad (35)$$

By considering geometry, and with reference to angles  $\theta_1 \dots \theta_4$  as linkage angles anticlockwise from horizontal as before, it can be shown that:

$$\theta = 90^\circ + \theta_2 - \theta_3$$

Moments about bar 4.

$$xT = Fr_4 \cos \phi \quad (36)$$

Again from geometrical considerations:

$$\phi = 270^\circ + \theta_4 - \theta_3$$

It follows that our mechanical advantage is given by eq 36 divided by eq 35:

$$x = \frac{r_4}{r_2} \frac{\cos(270^\circ + \theta_4 - \theta_3)}{\cos(90^\circ + \theta_2 - \theta_3)} \quad (37)$$

The internal forces and reactions can easily be found. Given we know the configuration of the mechanism (angles and lengths of bars, which can be solved by the MATLAB script I wrote) and the input torque,  $T$ , then the internal force,  $F$ , can be calculated from equation 35. Finally, we can analyse the reactions and internal forces in terms of  $F$ :

- Reactions. Reactions at both pivots are simply the components of  $F$  acting in the opposite direction from that shown in the free body diagrams (angles can be found from geometry as before).
- Bar 2. Axial force is component of  $F$  parallel to bar, shear force is component of  $F$  normal to bar. Bending moments are the point moment at one end and then a linear drop to zero at the other end.
- Bar 3. Axial force only equal to  $F$ .

- Bar 4. Same as bar 2 but with different angles.

*Example.* Considering the limiting case where  $r_1$  and  $r_2$  are both small (say 1 unit), and  $r_3$  and  $r_4$  are both large (10 units), we wish to find  $F$ . With  $\theta_2 = 359^\circ$  (right at limit of mechanism), I used my MATLAB solver to find  $\theta_3 = 359.55^\circ$  and  $\theta_4 = 174.95^\circ$ . If the torque is 1Nm, we find that  $F = 104.17\text{N}$  (relatively large). This is what we expect as the input angle tends to the horizontal, and although the mechanical advantage is still approximately 2, the internal forces blow up in this case. So if we wanted to use a four bar linkage we should avoid the case where  $r_1 = r_2$  (and both small) and  $r_3 = r_4$  (and both large).

#### 7.1.4 Summary of four bar linkage

##### Advantages

- Simple to construct. Only requires 2 external bars and some pins. Can be fitted with a connection of the motor to the upper brace, and a connection of the coupler bar to the lower brace.
- Can provide some mechanical advantage over the range of leg motion, making the work for the motor easier. Mechanical advantage is however small at large output angles.
- Can repeat mechanism on both sides of the leg for double the torque.

##### Disadvantages

- The motor is mechanically fixed to the brace movement, so if the patient forces the mechanism against the motor, the gears in the motor experience large forces, and there will be lots of heating in the motor. Despite this, we still want a mechanical fixing, such that we can get robust angle measurements and better control of the mechanism.
- It is very hard to get a high mechanical advantage across a large range of output angles, and mechanical advantage drops off quickly at large output angles. A possible solution could be to work with a 5 bar linkage, and to see if the extra degree of freedom can be used to solve this challenge, however this will not be considered in this report.
- The design process for a four bar linkage is fiddly and not straightforward. While initial set of proposed lengths do provide good mechanical advantage, there is the possibility that bars will jam in the extended position, or flip into the alternate configuration. If bar lengths change to compensate for this, the mechanism cannot extend fully to  $180^\circ$ , or the mechanical advantage at this point becomes insufficient.

## 7.2 Preferred design - single joint exoskeleton

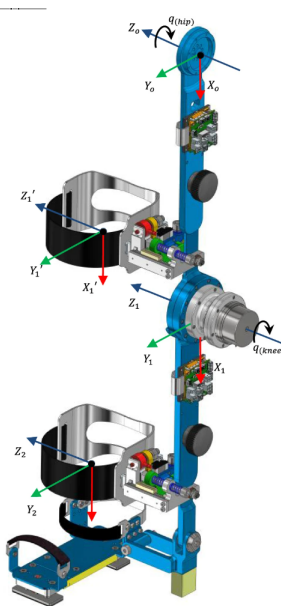


Figure 37: A single exoskeleton joint, from 'Nauman Masud, Sajid Rafique, Christian Smith and Magnus Isaksson' [70].

While a four bar linkage might offer increased mechanical advantage over a 1:1 connection design, it has a bulky design footprint and also makes control of torque more difficult (since we need to know the mechanical advantage profile of the mechanism to determine output torque).

The simplest, and perhaps most effective design is a 1:1 connected exoskeleton type mechanism. An example of what this might look like is illustrated in figure 37 which is taken from a paper designing an entire exoskeleton for human walking. Although we are not interested in assisting human walking, or creating an entire exoskeleton, our goal here is to assist rotation in a single joint, so this paper is a useful reference for what we might be able to design ourselves.

The basic design consists of an upper and lower compliant strap for the leg, which are connected by rigid bars to a motor in the middle. The motor is held in place to the upper bar, and its rotating shaft connects to the lower bar. This way when the motor is on, it can react against the fixed thigh in order to generate rotation of the shank about the knee.

Since we assume the patient is wearing a knee brace, it means we do not specifically have to focus on comfort or ergonomics, because as long as our mechanism transmits forces to the knee brace effectively, the knee brace will provide the comfort and safe motion path for the leg.

The design of the single joint exoskeleton assembly will be split into the following three stages.

1. Motor system selection and analysis.
2. Assembly of motor and gear with connecting bars.
3. Fixing of connecting bars onto the knee brace.

(N.b. Ryan Cherian will be designing the control and electronics for the motor. Additionally, dedicated housing for the electronics and battery is not considered in this design, but could be solved trivially by putting the components into a secured slot on the upper leg.)

### 7.2.1 Motor system selection and analysis

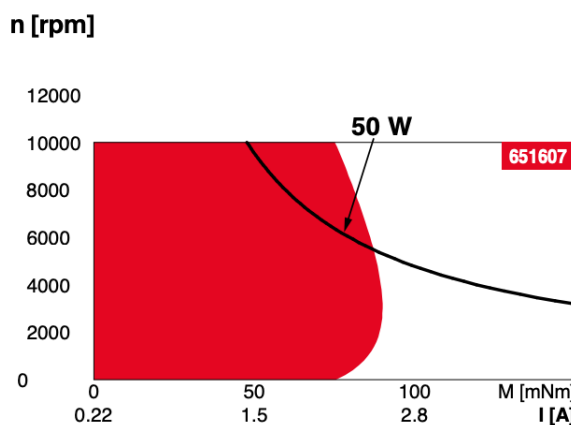


Figure 38: The continuous operating range for the EC 45 flat motor (in red) The maximum continuous operation is where the 50W rated power line meets the edge of the red region, and these values are given in the spec sheet.

In order to meet our torque specification of roughly 13Nm, we need to choose a motor and gearing which will be able to continuously output such a torque. We may also be interested in power consumption, speed and heating of the motor.

The motor we will use is the EC 45 flat by Maxon. Its operating range is shown in figure 38. The motor will be coupled with a strain wave gear (aka a harmonic drive gear). A harmonic drive gear is ideal for this application since it can produce very high reduction ratios in a compact space, without excess weight. Here is an outline of some the key parameters of the motor:

- Nominal voltage, 24V. Max continuous torque, 91.1mNm @ 5170 rpm and 2.52A. This will draw a power of about 60W.
- With a gearing of 150:1, the maximum continuous output torque will be 13.7Nm @ 34.5rpm. The output torque per Ampere is 5.4Nm/A, so we can specify torque by delivering a controlled current

between 0-2.5A.

### Important matters of safety

- The true rating of the motor allows up to 26A, which results in a stalling torque of 0.918Nm, or 137Nm after gearing. This is clearly far too high for our application, so our electronics must ensure that currents above, say 3A, are never delivered to the motor.
- If the user fully relaxes their leg and the maximum continuous current is delivered to the motor (2.5A), the output of the motor would be very fast (depending on resisting torque). Therefore the speed of the motor will need to be limited in the control system.

### Implementing control of motor

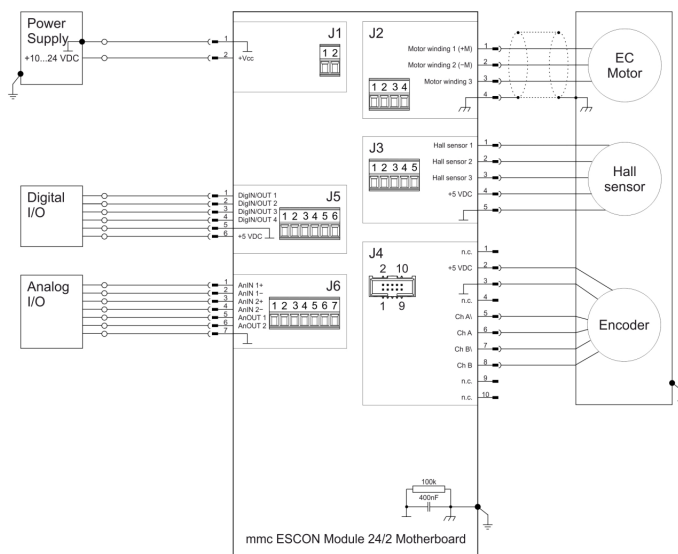


Figure 39: The connections between the 24/2 controller and the EC motor, hall sensor and encoder. Also shown are the configurable analogue and digital inputs and outputs (I/Os).

A compatible encoder can be fitted onto the motor to give position data at 2048 counts per turn. The motor should be driven by a compatible controller such as the ESCON 24/2, which provides either current (torque) or speed control. The controller gives us comprehensive safety features and allows easy integrated control with the main microprocessor on the device. The controller delivers a maximum continuous output current of 2A, which addresses our safety concern for the motor drawing too much current. Additionally, we can configure one of the digital pins with the 'enable' or 'stop' function to turn on and off the motor with a physical switch. The pin connections for the controller are shown in figure 39.

We can program the controller in two ways:

1. Using the ESCON software for initial setup. By USB connection between the controller and a PC, we can install specific instructions for the controller to implement. We can also use this software to specify what the controller's digital and analogue input controls do, which can be used for real time control of the device. The controller will retain these instructions even when disconnected from power.
2. Custom programming for real time control. If we want to control the motor in real time when our system is being used, and dynamically update parameters such as torque, speed and direction, then we need to send the controller instructions from a master controller, such as an Arduino, on board the device. The initial setup must still be completed, so that the controller knows the motor parameters, and the digital and analogue inputs are configured.

The system will be powered by a 24V dc rechargeable Li-ion battery pack.

### **Heating of the motor**

We might also be interested in the heating of the motor. The motor is quoted as about 80% efficient. We are also given that the thermal resistances from winding to housing is 8.28 K/W, and from housing to winding is 1.57 K/W. Since heat flows sequentially (in series) from winding to housing to ambient, the total heat flux resistance is the sum, 9.85 K/W.

This means that a temperature difference of 9.85K is required for 1 Watt of thermal flux between the motor winding and ambient conditions. If we operate our motor at its maximum current, 2A @ 24V, or about 50W, then the heat produced in the windings (due to inefficiency of motor) will be  $50 * (1 - 0.80) = 10\text{W}$ . This requires a temperature difference of  $10\text{W} * 9.85\text{K/W} = 98.5\text{K}$ . The maximum winding temperature is quoted as 125°C, so under continuous 2A motor current, we can operate in ambient temperatures up to  $125 - 98.5 = 26.5^\circ\text{C}$ , or a very warm room temperature. Since the motor will never be in continuous operation, due to the nature of the use of the system, we will not generate a continuous 10W of heating in the windings, and so we do not need to have any active cooling for the motor.

## Knee angle measurement

One key parameter we need for the control of the device, data gathering and machine learning model is the angle of the leg. We can calculate this parameter using the encoder in the motor. The encoder will send information about the position of the motor to the controller. We can configure the motor controller to output this signal through one of the chip's analogue output pins to the main microprocessor (Arduino). Since the encoder only measures relative position of the motor, we will need to begin every session at a fixed reference position, such as fully extended, and then we can track the angle of the leg, taking into account also the gear reduction of 150:1. This method assumes that the exoskeleton joint has the same angle as the knee brace, which could introduce a slight error in the angle measurement, depending on quality of build and correlation of exoskeleton joint angle and actual knee angle.

### 7.2.2 Assembly of motor and gear with connecting bars

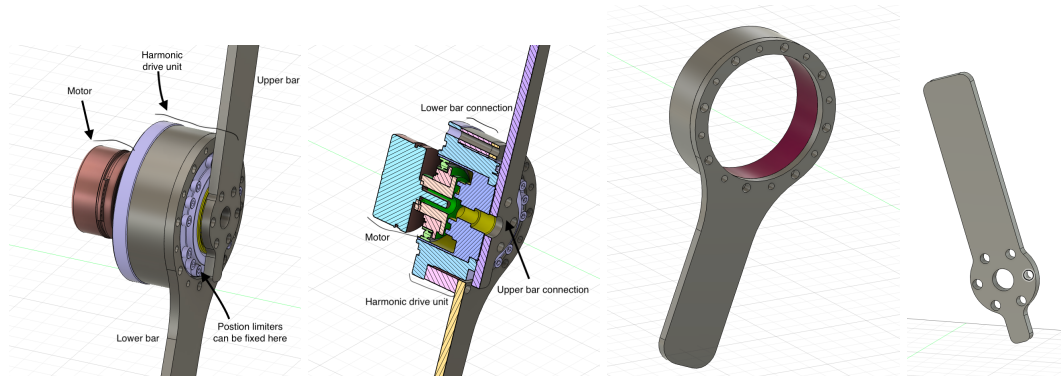


Figure 40: CAD modelling for exoskeleton joint. First (from left): completed joint module. Second: joint module slice, showing harmonic drive gear. Third: lower bar connector. Fourth: upper bar connector.

The next step in design is to connect the motor and harmonic drive gear to the connecting bars, ensuring that maximum stresses and forces are not exceeded. The connecting bars, harmonic drive and motor assembly was created in CAD software, as shown in figure 40. The upper and lower bars will be subsequently connected to the upper and lower sides of the brace, in order to complete the joint assembly.

This compact design is ideal for a joint actuator. By using a flat motor and a harmonic gear drive we can make an extremely compact and powerful actuator. While there do exist pre-made joint actuators on the market, by designing the actuator by its sub-components, more flexibility is achieved in the design. For example we have control over the motor input, gear ratio, output bar material and cross sections and also the position limiters, which will be designed and implemented shortly, when the joint is fixed to the brace.

### Basic bending analysis on connecting bars

We need to check that the cross sections and material selection for the connecting bars are suitable for the bending moments they will endure. Let's assume that the maximum bending moment in a bar will be 15Nm (just above the max torque we can deliver from the actuator), and this will be at the ends of the bars. The bars have rectangular cross section 5mmx25mm (upper bar) and 5mmx30mm (lower bar), so let's analyse the upper bar to be conservative, since its bending stiffness will be slightly lower.

$$I = \frac{bh^3}{12} = \frac{5 \times 25^3}{12} = 6510\text{mm}^4 = 6.5 \times 10^{-9}\text{m}^4$$

$$\sigma_{max} = \frac{My_{max}}{I} = \frac{15 \times 0.0125}{6.5 \times 10^{-9}} \approx 29\text{MPa}$$

Yield stress of high strength steel:  $\sigma_y = 400\text{MPa}$ . As expected, by bending the bars about their major principal axis, we have quite low stresses due to bending. The yield strength of 3D printed PLA is 26MPa, so by making the bars a bit thicker, e.g. 10mm as opposed to 5mm, we could prototype with 3D printed parts. This analysis has also assumed that the fixings between the harmonic drive and the connecting bars is not a failure point, which is a valid assumption if the fixings are designed securely, with multiple screws around the circumference of the connections, as illustrated in the CAD drawings in figure 40.

#### 7.2.3 Fixing of connecting bars onto the knee brace

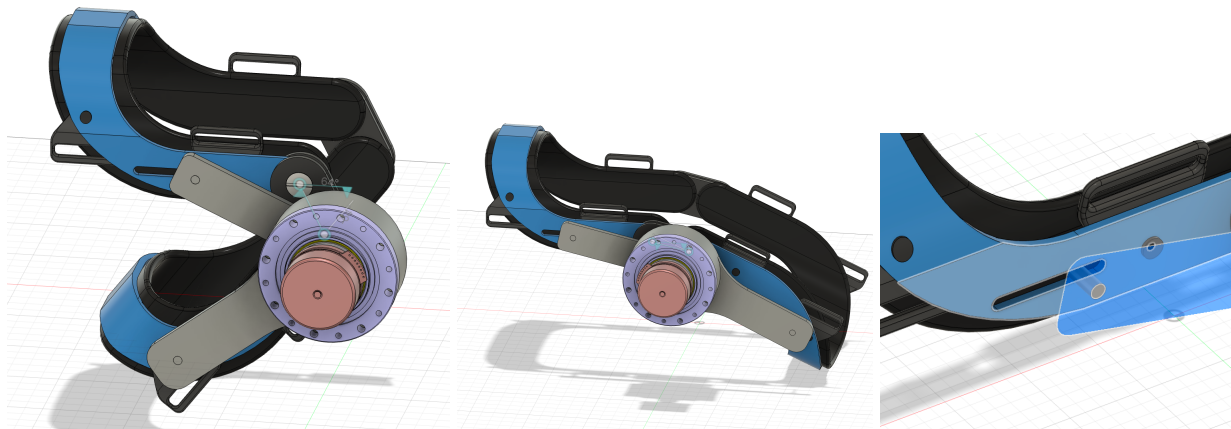


Figure 41: Full exoskeleton assembly with slot and pivot connection to brace. Left: assembly in flexion position. Centre: assembly in extended position. Right: Slot for upper bar.

### Design 1: Slot and pivot

The final step in this design is a method to fix the connecting bars onto the knee brace, at both the upper and lower sides. One possible design is shown in figure 41. The proposed connection involves a slot (pivot and slide) on the upper bar, and a pivot on the bottom bar.

The slot is not strictly necessary for compatible motion between the brace and joint, and indeed two simple pivots could complete the assembly by themselves, however, by adding an extra degree of freedom to the link, we increase the tolerance for the positioning of the pivots, and reduce the risk of locking out the mechanism, or having incompatible motion.

Note also that it isn't strictly necessary to have the upper bar at all, and an alternative design would be to fix the housing of the harmonic drive unit directly to the brace. This is not so easy, however, and using two bars, as done here, which easily connect to the actuator with the pre-drilled holes, is a more convenient design, since the same connections can be used for both upper and lower bars.

The drawback of this design is that it is knee brace specific and it permanently alters the knee brace. Certain knee braces might not have flat bars to drill into, and the lateral clearance (i.e. in the direction outwards from the pivot of the brace) might vary by model, meaning that the joint could collide with the brace pivot housing or other parts of the brace. In any case, we might not want to, or be able to, permanently modify the brace, for obvious reasons.

### Design 2: Non-permanent fixing

Figure 42 shows a possible design for a non permanent fixing of the exoskeleton joint onto the brace, using a padding on the lower bar and slots for Velcro straps cut into both connecting bars. The Velcro straps would be wound around the entire leg and brace in order to fix the bars onto the brace.

Compared to the slot and pivot connection discussed previously, using a non permanent fixing method such as Velcro straps might introduce unwanted friction during rotation. Friction will be introduced where the exoskeleton joint is in contact with the brace and is moving relative to it, neither of which can easily be avoided if we want the joint to be securely fastened to the brace.

Alternative approaches to fixing the joint to the brace could be considered, particularly fixing the actuator directly to the brace (eliminating the upper bar entirely), but for this project a couple of preliminary ideas have been discussed, both of which are relatively quick and easy to implement, and the overall structure

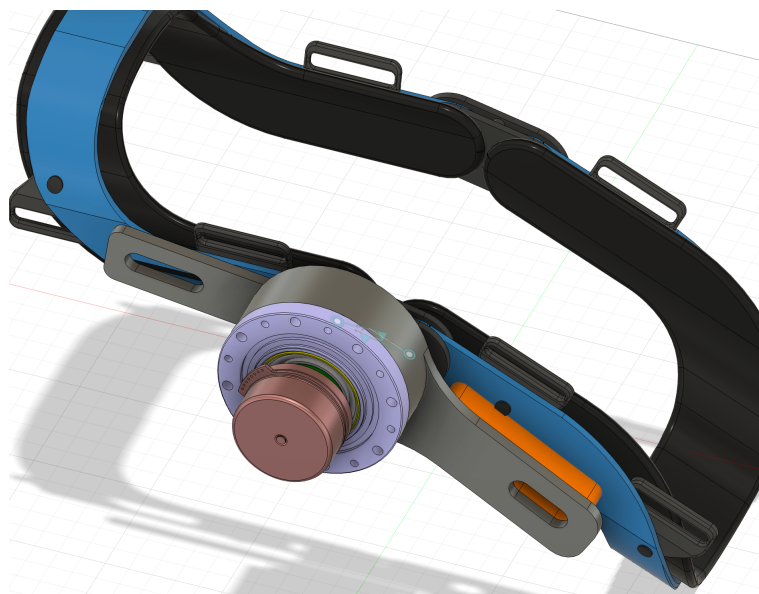


Figure 42: Non permanent fixing design. Orange material is a stiff padding, in order to reduce bending of lower bar towards brace.

of the design has been sufficiently explored.

### 7.3 Summary and scope of mechanism

The design of a mechanism to assist rotation of the knee has explored both the four bar linkage mechanism and a single joint exoskeleton actuator. With the four bar linkage it was possible to achieve some mechanical advantage, however this always changed (in fact it diminished) as the configuration of the linkage varied. This makes it impractical to implement in a control loop, since the output torque is not proportional to current, and depends on the configuration of the linkage. Hence it is a more practical design to use a fixed gearing ratio in an exoskeleton joint, as is conventional for robotics and mechatronics.

There are further areas which this module and control system could possibly be applied to. For example the use of our design (a universally fitting joint actuator with an integrated exertion control system) could be investigated for the following purposes:

- Recovery from other injuries which require strengthening or range of motion about a joint. E.g. tennis elbow and wrist injuries.
- Strengthening of leg or arm muscles. The exertion controller could be used to assist with strengthening of leg or arm muscles. This could be achieved by adding a variable damper to the joint, and improving the ergonomics of the fitting method to the body, by adding more padding and support.

# 8 Measuring muscle activity (John)

With reference to chapter 2.2.2, muscle strengthening around the knee is a key part of ACL rehabilitation. One method of monitoring muscle activity is through EMG signals. Amongst other indicators, AutoPhysio uses these to estimate patients' exertion (section 4) in order to: determine the torque to provide in sessions (chapter 3.3); and generate patients' rehabilitation plans (chapter 9). Thus, the aim of this chapter is to design an sEMG sleeve that collects and cleans EMG data from the pertinent muscles.

## 8.1 General specifications

### 8.1.1 Muscle Selection

Suitable muscles must be selected for placement of the bipolar pairs in the sEMG setup. Viewing the cross-section of the human thigh provides better spatial understanding of which muscles to include for AutoPhysio's sEMG sleeve. In Figure 43, the muscles closer to the skin surface are VM, RF, and VL for the quadriceps, and BFsh, ST, and SM for the hamstrings, and these are the ones suitable for better quality sEMG signals. Similar muscles have also been selected in other studies investigating thigh muscle activity using sEMG electrodes [47, 48, 71].

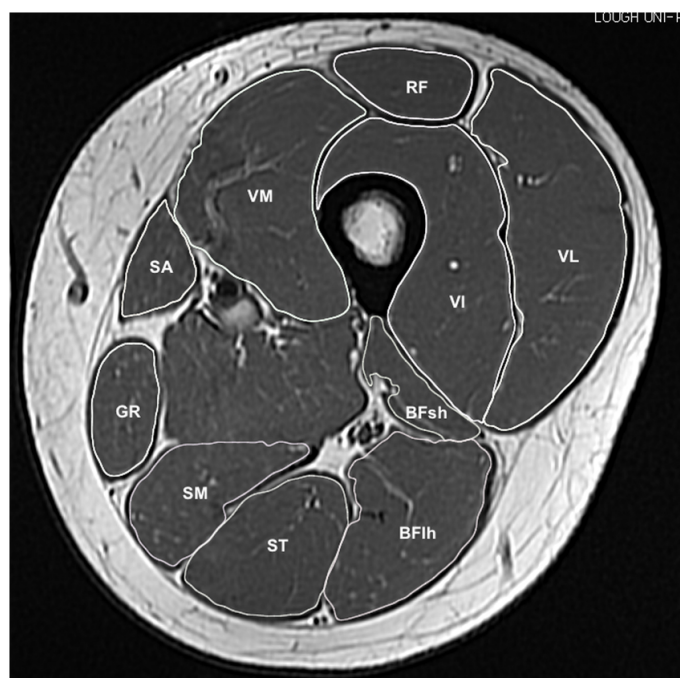


Figure 43: An MRI slice mid-thigh with the muscles segmented. Non-quadriceps or hamstrings muscles include the sartorius (**SA**) and the gracilis (**GR**) muscles. Adapted from Behan et al. 2018 [72].

### 8.1.2 Design goals

In the flow of EMG data from muscle fibres to user interface shown in figure 44, the design responsibility covers the first two blocks circled in red. The aforementioned sleeve design is chosen for three reasons. Firstly, the sleeve wraps the human thigh, which is where the pertinent muscles for measuring are. Secondly, the sleeve is compressive, meaning that the inner surface of the sleeve has good contact with the skin, making it an appropriate surface to place EMG electrodes. Thirdly, the sleeve's velcro is used for securing, a method that is more suitable for rehabilitation patients.

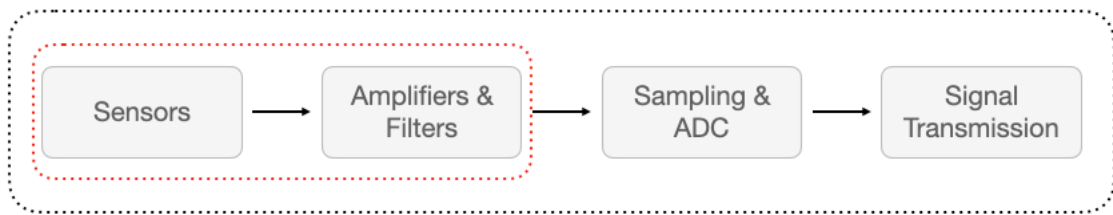


Figure 44: Block diagram of EMG data flow, with the processes to focus on circled in red.

For **sensors**, the AutoPhysio sEMG sleeve design can be achieved through locating accurate anatomical landmarks and having multiple possible electrode locations for dry Ag-AgCl electrodes (for patient ease & comfort). This would allow for cross-patient versatility in applying EMG electrodes to the selected muscles in 8.1.1.

For **amplifiers & filters**, information on EMG profile in 2.3.2 helps in deciding frequency ranges to attenuate. Attenuation is done via bandpass filtering as well as having a high common-mode rejection ratio (CMRR) at powerline frequency.

## 8.2 Sleeve design

Making use of the good skin contact of compressive fabrics for better quality EMG signals is an idea that has been implemented in both academia and industry, two examples shown in figure 45.



(a)



(b)

Figure 45: (a) A forearm band with EMG electrodes [41]. (b) An EMG band by startup exoSystems [22].

However, a common disadvantage in these is the lack of versatility. The prototypes released in academia tend to be custom made to target specific muscles of a participant or a group of participants. In industry, there is some flexibility afforded, but systems like the exoRehab by exoSystems fundamentally still rely on fixed positions on the sleeve for EMG recording. For sleeve design, the task is to create an ergonomic sleeve with flexibility of electrode placements built into its inner surface.

### 8.2.1 Design plans

To accommodate a wide audience without the need of customisation, the idea is to adapt a velcro compression thigh wrap with three major modifications:

1. To include perforations on the inner surface of the sleeve for flexible electrode placements.
2. To add a zipper on the outermost layer of the sleeve for easy access to electrodes.
3. To add an extension for the knee to act as reference electrode connection.

### 8.2.2 SENIAM guidelines

Upon specifying the pertinent muscles to measure from in 8.1.1, the general surface coordinates need to be determined for electrode placement. The SENIAM project (Surface EMG for the Non-Invasive Assessment of Muscles), a European concerted action in the Biomedical Health and Research Program (BIOMED II) of the European Union, provides anatomy-based recommendations on electrode placement for sEMG applications. For the six muscles (VM, RF, VL, BFlh, ST, SM), the specifications are stated in table 5 and table 6.

Table 5: Quadriceps electrode placement details [73].

	<b>VM</b>	<b>BF</b>	<b>VL</b>
Origin (L1)	Anterior spina iliaca superior	Anterior spina iliaca superior	Anterior spina iliaca superior
Insertion (L2)	Joint space front of anterior border of medial ligament	Superior part of patella	Lateral side of patella
Position between L1 and L2 (from L1)	80%	50%	66.7%
Max. electrode diameter	10 mm	10 mm	10 mm
Inter-electrode distance	20 mm	20 mm	20 mm

Table 6: Hamstrings electrode placement details [73].

	<b>BFlh</b>	<b>ST</b>	<b>SM</b>
Origin (L1)	Ischial tuberosity	Ischial tuberosity	Superolateral impression of ischial tuberosity
Insertion (L2)	Lateral epicondyle of tibia	Medial epicondyle of tibia	Medial epicondyle of tibia
Position between L1 and L2 (from L1)	50%	50%	50%
Max. electrode diameter	10 mm	10 mm	10 mm
Inter-electrode distance	20 mm	20 mm	20 mm

### 8.2.3 Sensitivity of electrode orientation

Apart from the general locations for electrode placement, their orientations need to be discussed. The ideal angle for orientation is the angle of pennation of the muscle being recorded [74, 75]. Angle of pennation refers to the angle between the orientation of muscle fibres and the attached tendon axis [76]. However, they are difficult to measure because they are different for every muscle, in every individual, and they change during contraction as well [75]. Fortunately, this mainly decreases the signal amplitude, and does not significantly affect signal shape [75, 77]. This is beneficial to AutoPhysio since relative (to previous sessions) and normalised amplitudes are used in data analysis. As long as the patient sticks to original electrode positions, misalignments will not affect AutoPhysio's function.

### 8.2.4 Inner surface modification

Based on findings expressed in chapter 8.2.3, the sleeve design can afford a tradeoff between orientation and position flexibility. Assuming this flexibility has been achieved (discussed later in this section), a doctor is necessary for deciding the origins and insertions for VM, RF, VL, BFlh, ST, SM, and then picking the best electrode placements from the available position options.

While designing for flexibility, SENIAM guidelines must be considered. Notably, commonalities among all muscles in table 5 and table 6 are the < 10 mm electrode diameters and 20 mm inter-electrode distances. A way to ensure that any two adjacent electrodes are 20 mm apart (centre-to-centre) is to arrange any three electrodes as vertices of an equilateral triangle.

The sleeve design aims to be compatible with commercially available dry Ag-AgCl electrodes (TDE-202). Therefore, a snap connection is used with the inner fabric layer between the electrode and the lead as shown in figure 46.

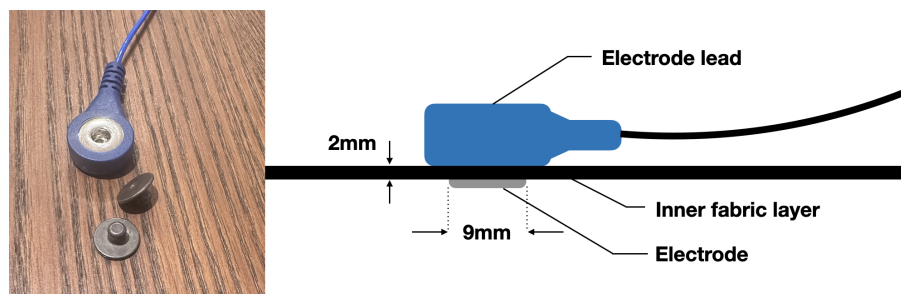


Figure 46: Left: a picture of TDE-202 snap electrodes (9mm diameter) and an electrode lead. Right: an illustration of how the parts on the left come together on the inner fabric layer of the sleeve.

Inspecting the connection between TDE-205 snap leads and TDE-202 snap electrodes reveals 2 mm of space that can be afforded for compressive material. To allow for connection to be made at all, a perforation must be created at the region of connection. The TDE-202 snap diameter measures < 5 mm, and to accommodate for manufacturing standards, a circular perforation of 6.3 mm ( $\frac{1}{4}$  inch) is used for each electrode position. To work with the equilateral triangle arrangement, the vertices will be arranged into columns, with alternating offsets to keep the tessellation of equilateral triangles. For easier identification of electrode positions, every column will have a unique letter and every row a unique number, all printed onto the fabric. This allows a doctor to record electrode positions by simply stating pairs (e.g. A1 - A2), and this yields figure 47.

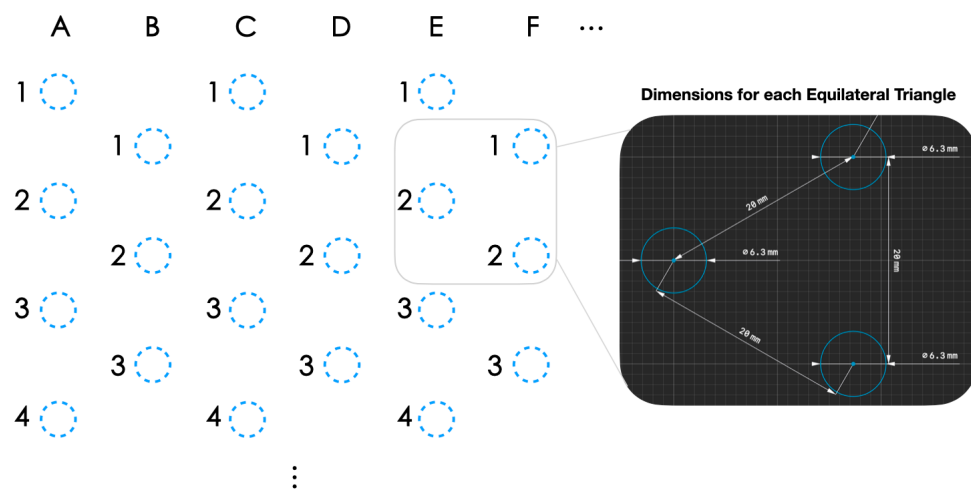


Figure 47: Concept electrode perforations on inner fabric layer along with their dimensions.

### 8.2.5 Outer surface modification

For some clarity on the layers involved in the AutoPhysio sEMG sleeve, figure 48 demonstrates how a standard electrode lead would fit in between the inner and outer fabric layers. The outer fabric layer provides further compressive support to the sleeve, improving the contact between the inner surface and the skin. To succeed in this basic function, the outer fabric layer must not be loose, and should be remain tight and close to the inner fabric layer as seen in the illustration. However, if the electrode leads are trapped between two fabric layers, there emerges a problem of leads accessibility.

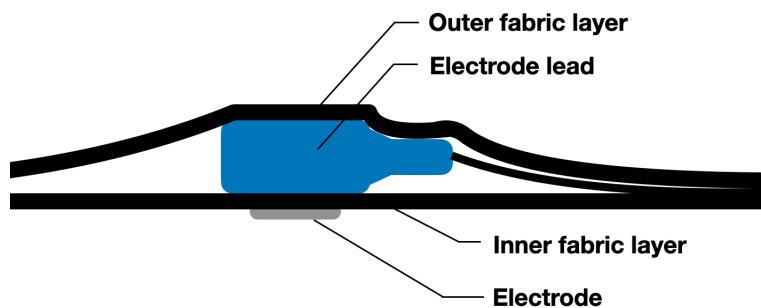


Figure 48: The electrode lead sits in between the inner and outer fabric layers.

A solution to this is to add zippers on the outer fabric layer shown in figure 49. This allows for the outer fabric layer to be in either a tight or loose state while enabling access to electrode leads. A curved zipper is used on both the quadriceps side and the hamstrings side so that the outer fabric layer can open up for visibility of electrode leads. Since lead wires will converge into an external bus connector just above the patella, a zipper is also included there for easy removal of electronics for washing.

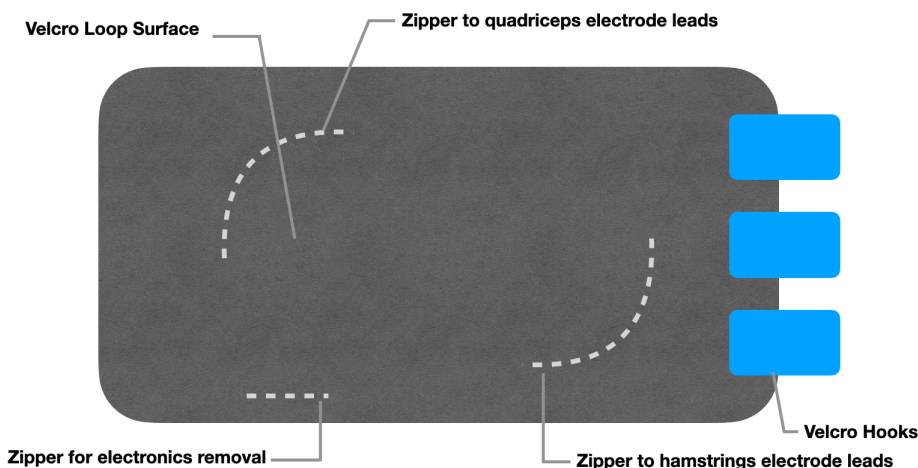


Figure 49: Labelled concept for outer fabric layer with zipper locations (right thigh).

### 8.2.6 Extension for reference electrode

Studies often select between two locations as a common reference point for all EMG recordings: the patella (kneecap) and the tibia [47, 78, 79, 80, 81]. To decide on which, consider Figure 50.

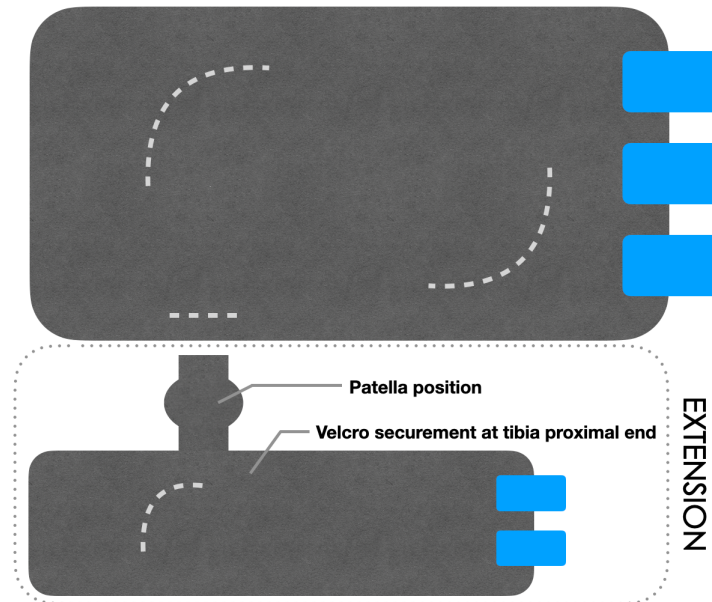


Figure 50: Outer fabric layer extension for reference electrode (right thigh).

While the extension covers both candidate positions, only the tibial area has velcro, allowing for better skin - electrode contact. Conversely, due to slight anatomical differences and overall movement during exercise, the patella connection might slip, making the proximal tibial reference the preferred option. Perforations like those in figure 47 will be made on the tibial part below the patella to allow for different tibial attachment locations. Figure 51 demonstrates a proof of concept on the VL muscle for this design.

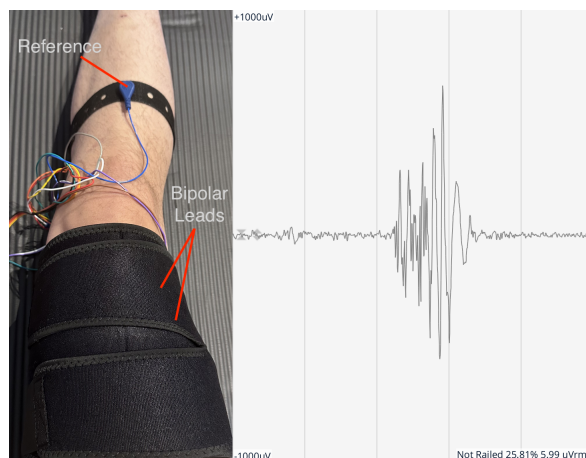


Figure 51: Left: a labelled picture of compression wrap proof of concept. Right: the corresponding EMG signal upon muscle flexion (compare with figure 4).

An additional zipper is included as shown in figure 50 to allow for adjustment of the reference electrode lead. However, fixing the attachment point will not cover the anatomical difference across patients. Thus, the extension is detachable, connectable to an extension electrode lead at the upper thigh sleeve (i.e. changing the bottom electrode in figure 48 to a connector from the reference electrode).

With this, the process for electrode placement begins with the doctor locating the origins and insertions of the six muscles and suggesting regions for electrode placement using SENIAM guidelines in table 5 and table 6. Next, a suitable sleeve size is picked based on the patient's thigh circumference (standard sizes XS: up to 40.6 cm, S: 40.6 cm - 55.9 cm, M: 55.9 cm - 71.1 cm, L: 71.1 cm - 91.4 cm) [82]. On the chosen sleeve, the appropriate 13 perforations (two for each muscle + one for reference connection) will be recorded. In preparation for a session, the patient connects electrodes to leads based on records. An expansion bus that emerges from the bottom zip of the upper thigh sleeve is then connected to the main board for data transmission.

## 8.3 Connection design

### 8.3.1 Design plans

The aim in this part is to establish clarity for the patient when connecting electrodes. This will involve:

1. Connecting all wires into an expansion bus.
2. Creating a housing for each bipolar electrode pair.

### 8.3.2 Expansion bus

Many existing EMG recording setups are not user-friendly, one reason being the mess of wires. Experimental and clinical setups involving these are not fit for commercial sale as they are difficult to set up and prone to improper connection.

Inspired by high-density EMG sensor designs, the connections will be reduced to a single connection to the main board via an expansion bus. It will involve a total of 13 wires flushed into a compact form factor, with a matching set of pins on the main board. The expansion bus will be accessible through the bottom zip in figure 49, above the extension piece in figure 50.

### 8.3.3 Bipolar electrode housing

Another user-friendly feature to add is grouping and labelling of bipolar electrode pairs. With medical professionals, labels, in this contexts, serve more as useful reminders since placement is determined by anatomical landmarks. However, for patients (where medical knowledge is not expected), these provide necessary instructions for smooth and systematic preparation of the EMG device.

To create the housing, some dimensions need to be taken from the TDE-205 snap lead. Measurements of the button reveal a diameter of 12.5 mm and a height of 3 mm. The bottom part design is shown in figure 52a. The buttons' centres are separated 20 mm apart as mentioned in the SENIAM guidelines and designed for in figure 47. To allow for connection, there is an opening for each button at the connection end. Since the TDE-202 snap electrode is 9 mm in diameter, a hole of diameter 10 mm was used for each, allowing for connection and also preventing the button from dropping out. To accommodate the wires, the middle is cut empty, and a circular hollow section is made for the wires to exit the housing.

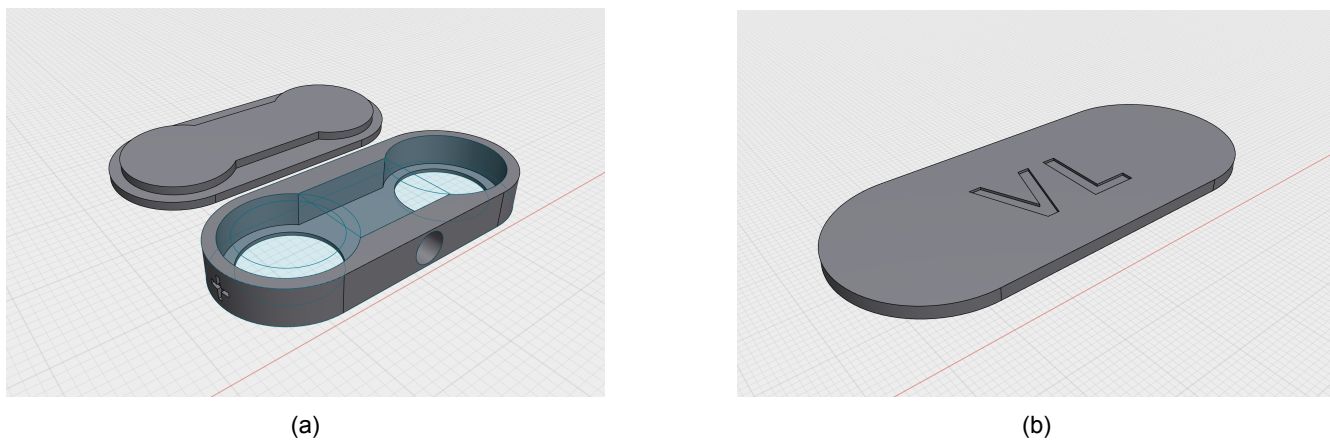


Figure 52: (a) Bottom and top parts of housing. (b) Label for corresponding muscle (VL).

The top part serves as the cover for the housing through gluing. It is designed to keep the buttons in place without vertical rattling during movement. The muscle label will be clearly shown on this top layer. In figure 52b, it is the top case for VL. The sides are also labelled positive and negative to specify the polarity of each side. Overall, this increases the ease of attachment for the patient at home.

The perforations will not lie on a flat surface during operation since the sleeve is meant to wrap around the patient's thigh. Given the nonnegative Gaussian curvature of the sleeve's inner fabric layer during operation, some flexibility in the material is required for expansion. For a balance between rigidity and softness, these can be made via 3D printing with softer filaments such as thermoplastic elastomers (TPEs).

## 8.4 Filter design

Filter design will be based on the EMG features discussed in chapter 2.3.2. To capture the bulk of an EMG signal's energy spectrum, a bandpass filter is applied from its lower bound of 20 Hz to its upper bound of 350 Hz. Filtering of mains frequency should be done digitally in the user interface for flexibility. Therefore, EMG signals will only go through a bandpass filter after instrumentation amplification.

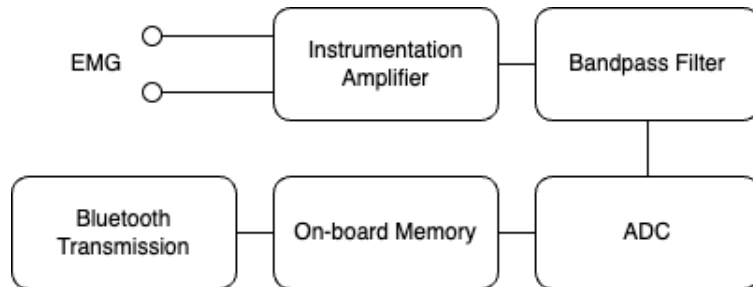


Figure 53: Flow of EMG signals in hardware.

### 8.4.1 Filter specifications

The bandpass filter is constructed with two filters concerning separate purposes: high pass and low pass filtering, both using the Sallen-Key topology that encourages cascading for combination in figure 54.

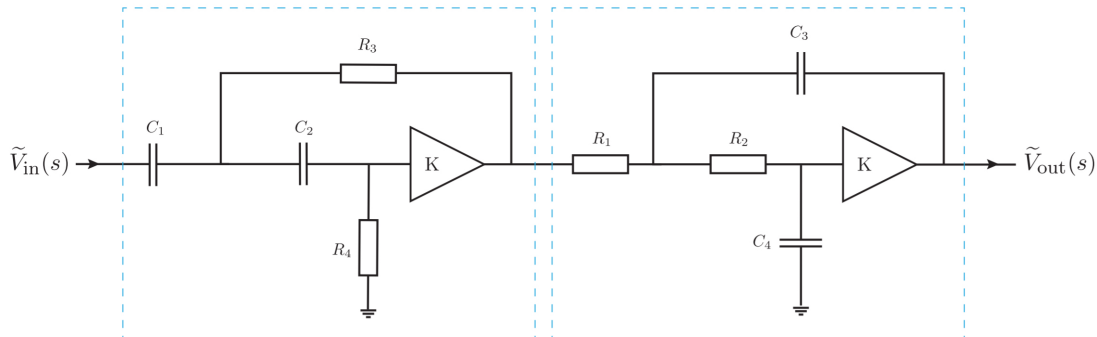


Figure 54: An active high pass filter circuit cascaded with an active low pass filter circuit to create an active bandpass filter circuit [83].

As such, the design task is to specify resistance and capacitance values for each filter. International standard values (BS 2488 E24) shown in table 7 will be considered in this design.

Table 7: BS 2488 E24 series standard values [84].

#### International standard values

Appropriate for tolerance $\pm 5\%$ or narrower
10, 11, 12, 13, 15, 16, 18, 20, 22, 24, 27, 30, 33, 36, 39, 43, 47, 51, 56, 62, 68, 75, 82, 91

Figure 54 demonstrates the second-order nature of both filters involved, suggesting that second-order filter coefficients will be helpful in design. The Butterworth filter approach is opted here given its desirable behaviour in out-of-band frequencies. Given the transfer function of a second-order system with unity gain in equation 38 (for high pass filter) and equation 39 (for low pass filter), the filter coefficients for the Butterworth filter are  $a = 1.4142$  and  $b = 1$ .

$$G_{hpf}(s) = \frac{1}{1 + a\frac{1}{s} + b\frac{1}{s^2}} \quad (38)$$

$$G_{lpf}(s) = \frac{1}{1 + as + bs^2} \quad (39)$$

#### 8.4.2 High pass filter design

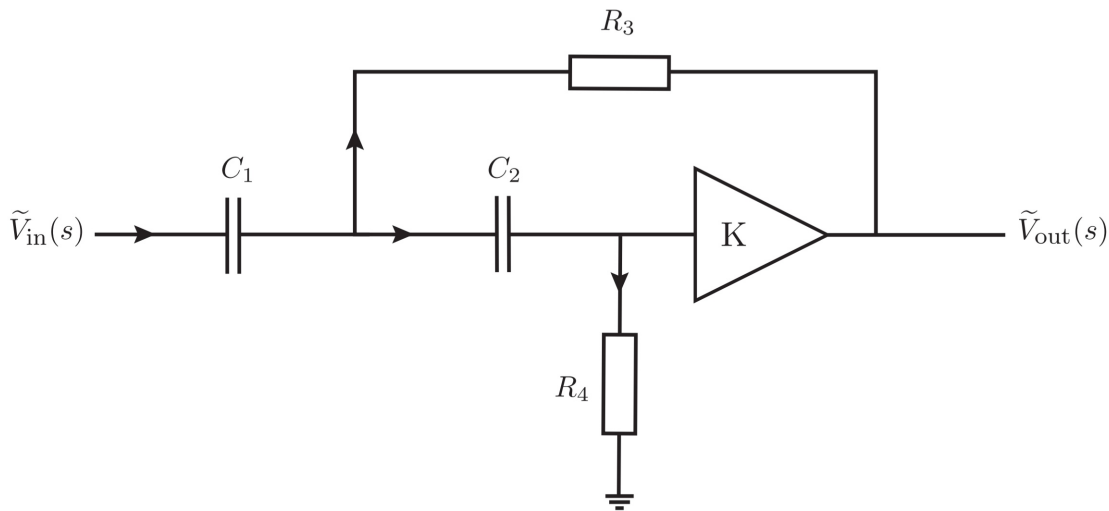


Figure 55: Second-order high pass filter using the Sallen-Key topology, with gain  $K$  [83].

As a preliminary constraint,  $C_1 = C_2 = C = 100\text{nF}$  and  $K = 1$ . The transfer function for the high pass filter is shown in equation 40, meaning  $a = \frac{2}{\omega_c R_4 C}$  and  $b = \frac{1}{\omega_c^2 R_3 R_4 C^2}$ .

$$G_{hpf}(s) = \frac{1}{1 + \frac{2}{\omega_c R_4 C} \frac{1}{s} + \frac{1}{\omega_c^2 R_3 R_4 C^2} \frac{1}{s^2}} \quad (40)$$

With  $f_c = 20\text{Hz}$ , this yields the following resistance values:

Table 8: High pass filter resistance values

	$R_3$	$R_4$
Ideal Resistance ( $\text{k}\Omega$ )	56.27	112.54
Achievable Resistance ( $\text{k}\Omega$ )	56	$22 + 91 = 113$

### 8.4.3 Low pass filter design

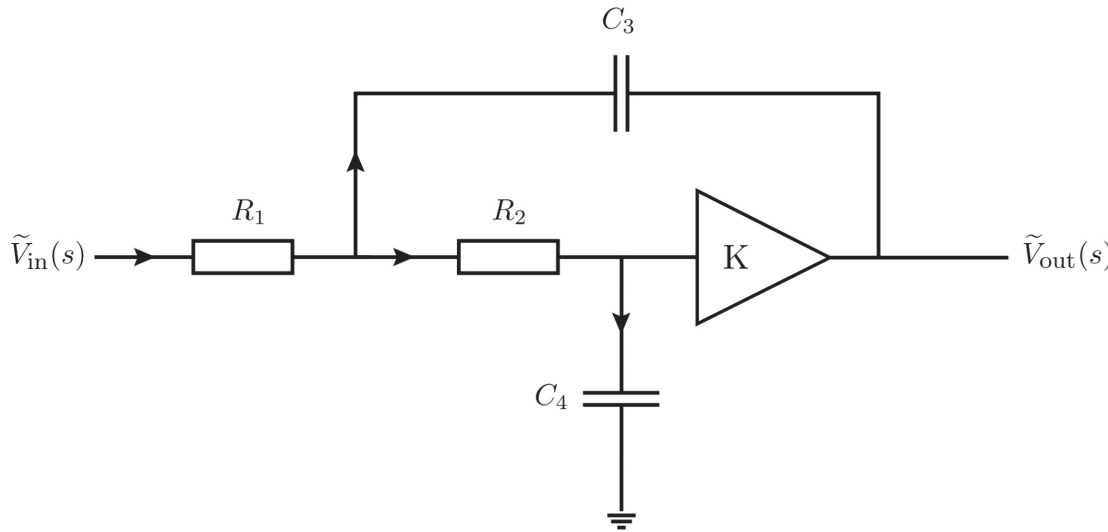


Figure 56: Second-order low pass filter using the Sallen-Key topology, with gain  $K$  [83].

As a preliminary constraint,  $C_4 = 10\text{nF}$  and  $K = 1$ . The transfer function for the high pass filter is shown in equation 41, meaning  $a = \omega_c C_4(R_1 + R_2)$  and  $b = \omega_c^2 R_1 R_2 C_3 C_4$ .

$$G_{lpf}(s) = \frac{1}{1 + \omega_c C_4(R_1 + R_2)s + \omega_c^2 R_1 R_2 C_3 C_4 s^2} \quad (41)$$

Given this, the resistance values can be calculated through:

$$R_{1,2} = \frac{a C_3 \mp \sqrt{a^2 C_3^2 - 4 b C_3 C_4}}{2 \omega_c C_3 C_4}$$

To prevent imaginary solutions, a further constraint arises for  $C_3$ , namely that  $C_3 \geq 4 \frac{b}{a^2} C_4$ . To satisfy this constraint,  $C_3 \geq 20\text{nF}$ , so  $C_3 = 30\text{nF}$ . With  $f_c = 350\text{Hz}$ , this yields the following resistance values:

Table 9: Low pass filter resistance values

	$R_1$	$R_2$
Ideal Resistance ( $\text{k}\Omega$ )	13.59	50.72
Achievable Resistance ( $\text{k}\Omega$ )	13	51

### 8.4.4 Bandpass filter design

Results from section 8.4.2 and 8.4.3 are compiled into table 10. By applying these values to the template shown in figure 54, the final bandpass filter is obtained in figure 57.

Table 10: Filter component values

	Capacitors (nF)	Resistors (kΩ)		
High pass filter	$C_1$ 100	$C_2$ 100	$R_3$ 56	$R_4$ 113
Low pass filter	$C_3$ 30	$C_4$ 10	$R_1$ 13	$R_2$ 51

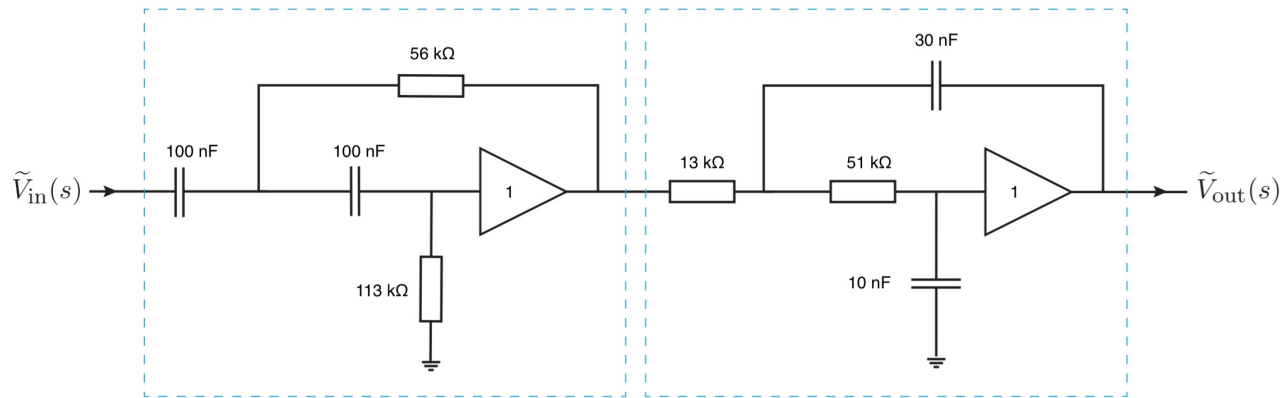


Figure 57: Bandpass filter constructed with previously designed high pass and low pass filters.

The resulting bandpass filter has a transfer function that is the product between the transfer functions of the high pass and low pass filters. It yields desirable results as shown in the bode plot in figure 58, reaching -3dB at 19.2 Hz and 350 Hz while maintaining 0 dB between these cutoffs frequencies.

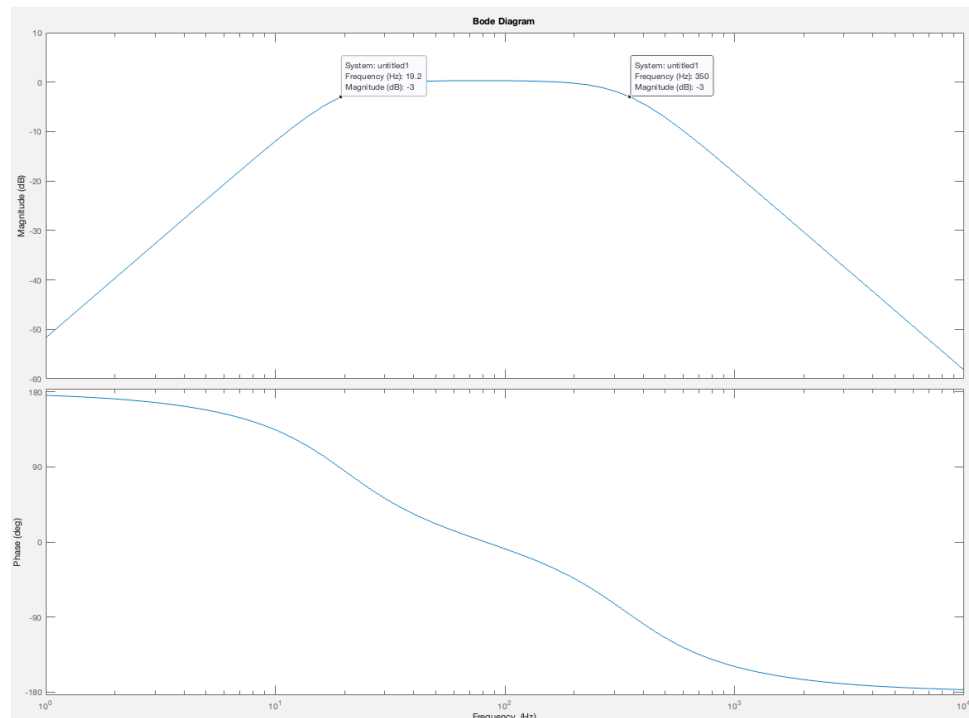


Figure 58: Bode plots (magnitude and phase) of the proposed bandpass filter.

## 8.5 Areas for improvement

For the sEMG sleeve design, while SENIAM does suggest 20 mm for inter-electrode distance, some experimentation could be done to discover optimal values for each muscle across a substantial population. This might then encourage the bipolar electrode housing to be extendable in length. Furthermore, while orientation of electrodes might not play a large role in the EMG waveform, the loss of EMG amplitude could deprive the system of potentially useful information. Applying component analysis could reveal further insights on the ideal orientation for capturing signals while avoiding cross-talk.

One concern that arises in this setup is the amount of data that can be captured by bipolar electrode pairs. This could be significantly improved by applying high-density EMG electrode grids as shown in figure 59. While the orientations are not standardised, there is more activity captured over the same surface area, allowing for finer information to be used in training schedule suggestion and the real-time control system.

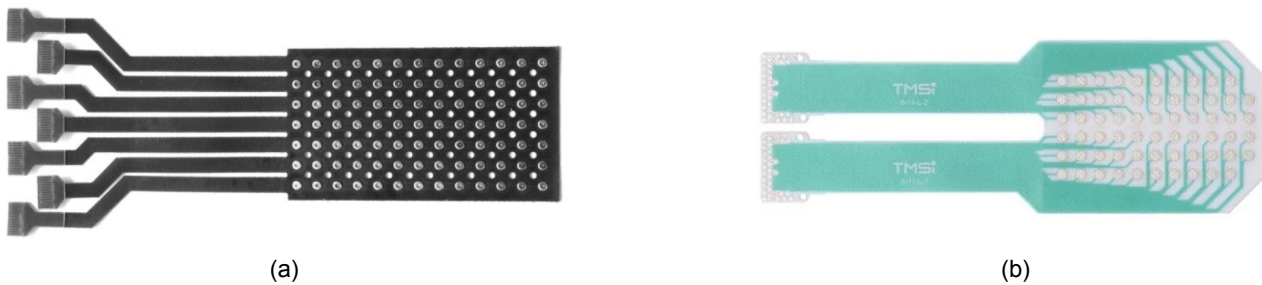


Figure 59: (a) High density EMG electrode grid used in research [85]. (b) An example of electrode grids used in industry (manufactured by TMSi) [86].

Another fundamental limitation of the current setup is the fact that it is non-invasive. While it is crucial for comfort, it misses deeper muscles such as the Vastus Intermedius which could present further information on muscle health and overall patient recovery.

For EMG signal filtering, while a bandpass does work, it might be interesting to explore digital filters that deal with removing EMG-related noise with greater sophistication. The attenuation performance of 40 dB/decade on out-of-band frequencies could also be improved using other filter configurations.

## 9 Machine learning for personalised rehabilitation (Yoon-sang)

*Application of machine learning can enhance the efficiency of rehabilitation programs [87]. We can recommend optimal load and motor support settings tailored to each patient's needs by utilising data collected during rehabilitation training sessions. Furthermore, by analysing aggregated data gathered from recovery processes of multiple patients, we can forecast rehabilitation outcomes and design customised rehabilitation programs that optimise recovery trajectories. This data-driven approach will personalise treatment and improve the overall effectiveness of rehabilitation strategies.*

### 9.1 Theoretical data generation for initial training

Machine learning can be applied to the AutoPhysio device to monitor and support a patient's rehabilitation training. As patients repeat the training and data is accumulated from various patients, the machine learning based rehabilitation training program will become more refined. However, when the device first developed and applied to patients, there will be insufficient data. Also, due to privacy concerns, the amount and quality of data collected may be limited. Therefore, at the initial stage of development, a theoretical model dataset should be created based on existing research results and conventional simulations. The theoretical model data will be used as a basis on which we can continuously add clinical data to improve the machine learning model [88]. Other studies endorse the use of theoretical data as a practical resource in the medical field [89, 90]. The data needed for machine learning can be divided into two types. The first dataset includes simulated sequences of range of motion for individual therapy sessions designed to model single-session progressions. The second dataset will chart the daily maximum range of motion, providing a theoretical framework for patient improvement throughout the rehabilitation timeline.

#### 9.1.1 In-session range of motion sequences

To simulate and generate theoretical range of motion data for ACL rehabilitation planning, the smart actuator Dynamixel was used. Dynamixel, known for its precision, control, and comprehensive design featuring a DC motor, controller, driver, sensor, and reduction gear, offers unparalleled capabilities for fine-tuning settings and ensuring robust position, velocity, and torque control [91]. The motor has a low

gear ratio of 32:1. A low gear ratio is needed to mitigate the risk of damage from resistance during range of motion exercises. This distinct combination renders them exceptionally adept at replicating the nuanced movements of human joints, making them an ideal choice for mimicking the knee or arm movements in range of motion exercises. However, since the motor lacks the strength needed for the actual product, it will be used solely for data generation.

Given the challenges of collecting actual data, creating theoretical data becomes indispensable for applying machine learning models effectively [92]. To this end, simulating knee joint behaviors using arm movements emerges as a pragmatic approach, given the fundamental kinematic principles they share [93]. By integrating a Dynamixel motor with an Arduino board, we can simulate and record arm movements that mirror the rehabilitation exercises typically prescribed for ACL recovery. This setup facilitates the generation of a robust dataset that covers a broad spectrum of range of motion scenarios and deepens the understanding of the kinematic patterns crucial for charting successful recovery trajectories in ACL rehabilitation.

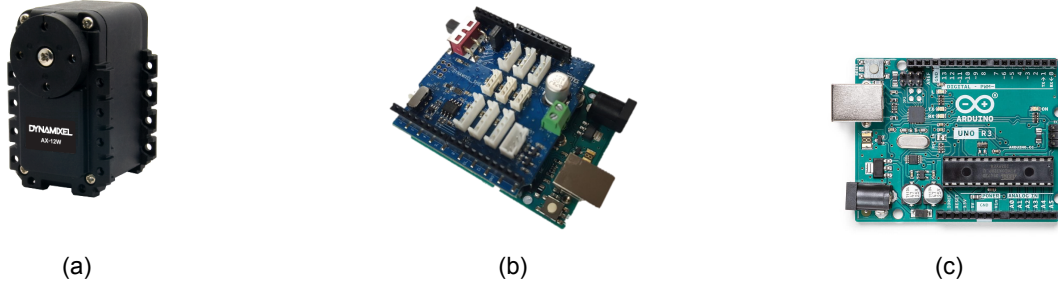


Figure 60: (a) Dynamixel AX-12W (b) Dynamixel Shield (c) Arduino Uno R3 [91]

The materials required consist of the Dynamixel AX-12W motor, the Dynamixel Shield, and an Arduino Uno R3 board (shown in figure 60). The central function of the Dynamixel Shield is to serve as an intermediary interface between the Dynamixel motor and the Arduino board. This interface simplifies the connection and communication procedures, facilitating smooth data transfer and efficient management of the power supply between the two devices. Moreover, the shield introduces an additional layer of protection for the actuators and the Arduino board, shielding them from potential electrical hazards and guaranteeing consistent operation throughout the data collection. Arduino Uno R3 was used since the Dynamixel is incompatible with new models like Arduino Uno R4.

Key settings for the Dynamixel AX-12W motor include a baud rate adjustable from 7843 bps to 1Mbps and an operating voltage range of 9-12V [94]. We used a baud rate of 9600 and a 12V power source.

Calibration of the Dynamixel's built-in sensors is essential to accurately track the arm movements' position, velocity, and torque, reflecting the dynamics encountered during rehabilitation exercises. The Arduino Uno board controls the Dynamixel AX-12W via the Dynamixel Shield to initialize the movement and record sensor data using the Dynamixel2Arduino library.

The process starts with mounting the Dynamixel AX-12W motor to an arm support mechanism, ensuring it allows for a full range of motion. This mimics the lifting and lowering movements akin to knee exercises in ACL rehabilitation [93]. The next step involves integrating the Dynamixel Shield with the Arduino Uno board by matching the correct pins. The data collection protocol includes defining arm movement patterns that effectively mimic the targeted knee exercises for ACL rehabilitation [93], including the range of motion, speed, and repetitions for each exercise simulation. As the system executes these movements, the Dynamixel's sensors meticulously track and record detailed metrics, which are then stored for further analysis. The Arduino serial monitor shows the angles in time intervals of 0.1 seconds. Figure 61 shows samples of a range of motion sequence.

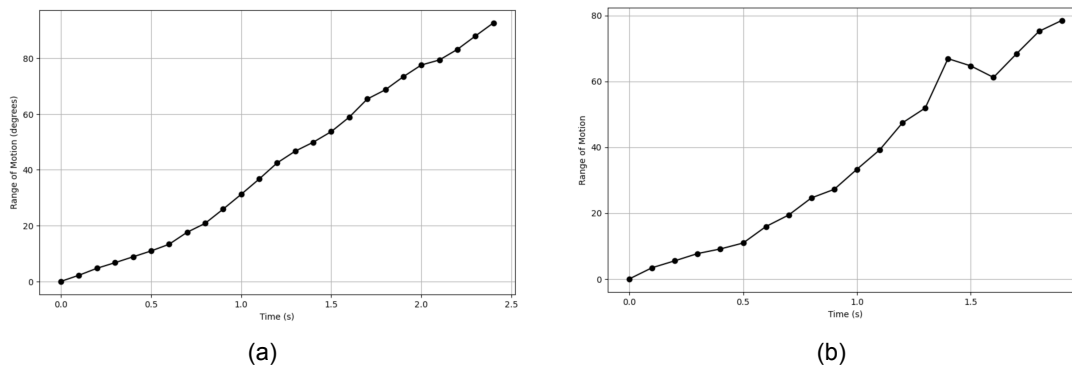


Figure 61: (a) Stable session (b) Unstable session with flinching

Analysing the collected data helps understand the kinematic patterns and their implications for ACL rehabilitation. This analysis is crucial for identifying the trends, anomalies, or specific characteristics of the simulated rehabilitation exercises. The generated dataset is used to train machine learning models to optimise rehabilitation strategies, predict outcomes, and tailor rehabilitation plans to individual needs.

### 9.1.2 Daily maximum range of motion progression

The daily maximum range of motion is the maximum angle that a patient reaches in sessions throughout the day. It is important to account for the individual differences in recovery speed among patients. The synthetic data will be generated using Python. By generating a diverse set of possible theoretical data, we can cover the broad spectrum of possible recovery trajectories. This will enable the development of

a machine learning model that can adapt to each patient's unique rehabilitation recovery trend. Figure 62 shows five theoretical recovery trajectories.

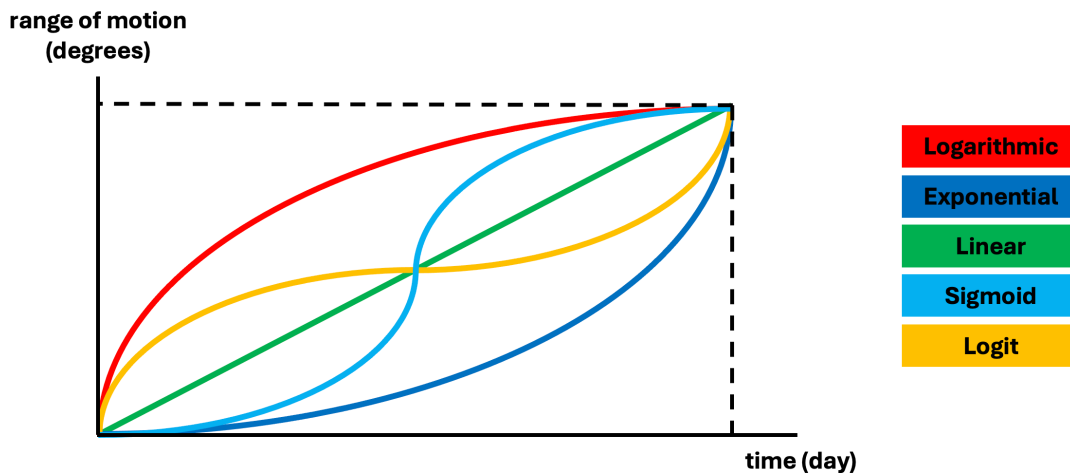


Figure 62: Possible recovery trajectories

I have surveyed the “Cruciate Ligament and Knee Patient Rehabilitation Community” on Naver [95], an influential Korean web portal, to find the typical recovery trajectories experienced by patients. They were requested to select which among the five depicted recovery trends they underwent and the duration it took to attain full knee extension.

Table 11: Recovery trajectories distribution among patients

Recovery trend	Number of participants	Percentage of participants (%)
Logarithmic	18	15.9
Exponential	14	12.3
Linear	6	5.3
Sigmoid	71	62.8
Logit	1	0.9
Other	3	2.7

The results displayed the following distribution of recovery trends among participants (shown in table 11): 18 people (15.9%) reported a logarithmic trend marked by quick initial improvement that slows over time; 14 people (12.3%) reported an exponential trend with minimal early gains that increase significantly with ongoing rehabilitation; 6 people (5.3%) reported a linear trend of steady and constant range of motion increase; 71 people (62.8%) reported a sigmoid trend, which mirrors the common recovery pattern of a slow start and finishes with a faster middle phase; 1 individual (0.9%) reported a logit trend, characterized by swift initial progress, a slower intermediate phase, and an accelerated final improvement phase. An additional 3 participants (2.7%) selected 'Other,' indicating varied or unclassified recovery patterns.

Table 12: Time required to achieve full range of motion

Time	Number of participant	Percentage of participants (%)
4 weeks	46	40.7
5 weeks	39	34.5
6 weeks	22	19.5
3 weeks (Other)	6	5.3

Usually, reaching the full range of motion, around 120 degrees, should take around 4 to 6 weeks [96]. The responses from the survey were as follows (shown in table 12): 46 participants (40.7%) achieved full range of motion in 4 weeks, 39 participants (34.5%) in 5 weeks, 22 participants (19.5%) in 6 weeks, and 6 participants (5.3%) answered the ‘other’ option and reported 3 weeks.

Based on the information collected, we can generate theoretical data. Figure 63 shows examples of synthetic data.

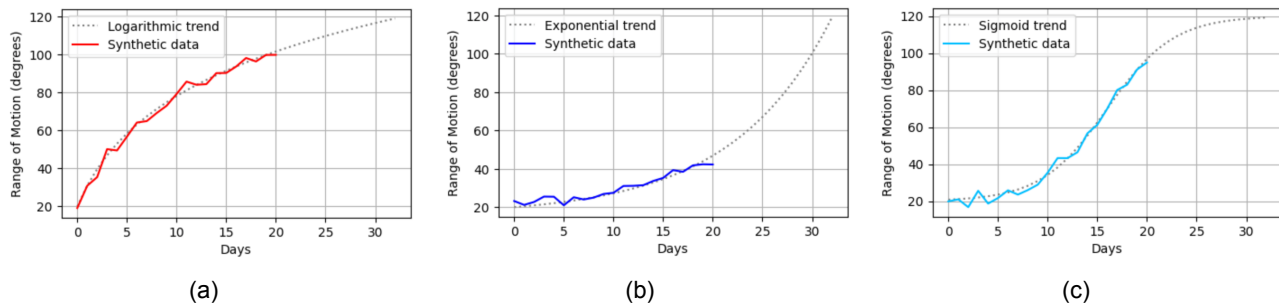


Figure 63: Synthetic data for (a) Logarithmic (b) Exponential (c) Sigmoid

For a given recovery pattern and time range, we make a function that reflects the overall shape of the recovery trend. This creates a theoretical recovery model, assuming an ideal progression without individual variations. To add realism to the synthetic data and simulate individual differences among patients, random noise sampled from a normal distribution was added to the theoretical values. This mimics real-world variations in daily measurements due to individual patient conditions and day-to-day inconsistencies. Despite the efforts to create realistic data, it remains challenging to fully capture the complex, human-like variability in patient recovery trajectories. To address this, further refinement could involve incorporating more statistical models or machine learning techniques that can learn from actual patient data [97, 98]. Moreover, collecting and integrating more data on patient behaviours, treatment adherence, and other physiological factors could enhance the data’s accuracy and realism.

## 9.2 Predictive analysis for recovery progress

Predictive analysis can give therapists and patients the expected progression of recovery, allowing for more accurate planning and effective management of rehabilitation activities [99]. This approach helps the patient set daily goals for range of motion and provides a clearer timeline for the end of rehabilitation.

### 9.2.1 Support Vector Regression prediction model

The Support Vector Regression (SVR) model is used in AutoPhysio's predictive analysis. The SVR model is a machine learning algorithm that predicts continuous outcomes and improves accuracy by using special functions called kernels to adapt to different types of data [100]. The SVR model is suitable for AutoPhysio for the following two reasons. First, the SVR model is robust against overfitting and can handle non-linear regression effectively, as evidenced by its application in post-stroke rehabilitation predictive models [99]. This capability is based on the use of kernel functions, which transform the input data into a higher-dimensional space where linear regression can be applied to non-linear relationships in the lower-dimensional space. Additionally, the SVR model uses kernel functions which allows for accurate modelling of complex physiological recovery curves, such as those observed in upper limb recovery [101].

To implement the SVR model effectively, we integrate patterns based on the three most relevant recovery trends as identified from table 11: sigmoid, logarithmic, and exponential. When applying a regression model to predict the future range of motion, we can include terms that allow the model to adjust to the given trends:

$$\Phi_{\text{sigmoid}}(x) = \frac{L}{1 + e^{-k(x-x_0)}}, \quad (42)$$

$$\Phi_{\text{logarithmic}}(x) = \log(x + \epsilon), \quad (43)$$

$$\Phi_{\text{exponential}}(x) = e^{\frac{(x-\mu)}{\sigma^2}}, \quad (44)$$

where  $L$  is the expected maximum range of motion,  $k$  is the steepness of the curve,  $x_0$  is the inflection point,  $\epsilon$  is the term to avoid the logarithm of zero,  $\mu$  is the mean, and  $\sigma^2$  is the variance of the days.

The transformations above will be used to integrate into the SVR model through a composite kernel approach [102]. The composite kernel can be written as

$$K(x, y) = \beta_1 \times K_{\text{sigmoid}}(x, y) + \beta_2 \times K_{\text{logarithmic}}(x, y) + \beta_3 \times K_{\text{exponential}}(x, y), \quad (45)$$

The training of the SVR model involves optimising the coefficients  $\beta_1$ ,  $\beta_2$ , and  $\beta_3$  along with the regularisation parameter and the loss function to minimise the loss function. This minimises the empirical risk and prevents overfitting. Figure 64 shows the recovery progress prediction for a sigmoid recovery trend.

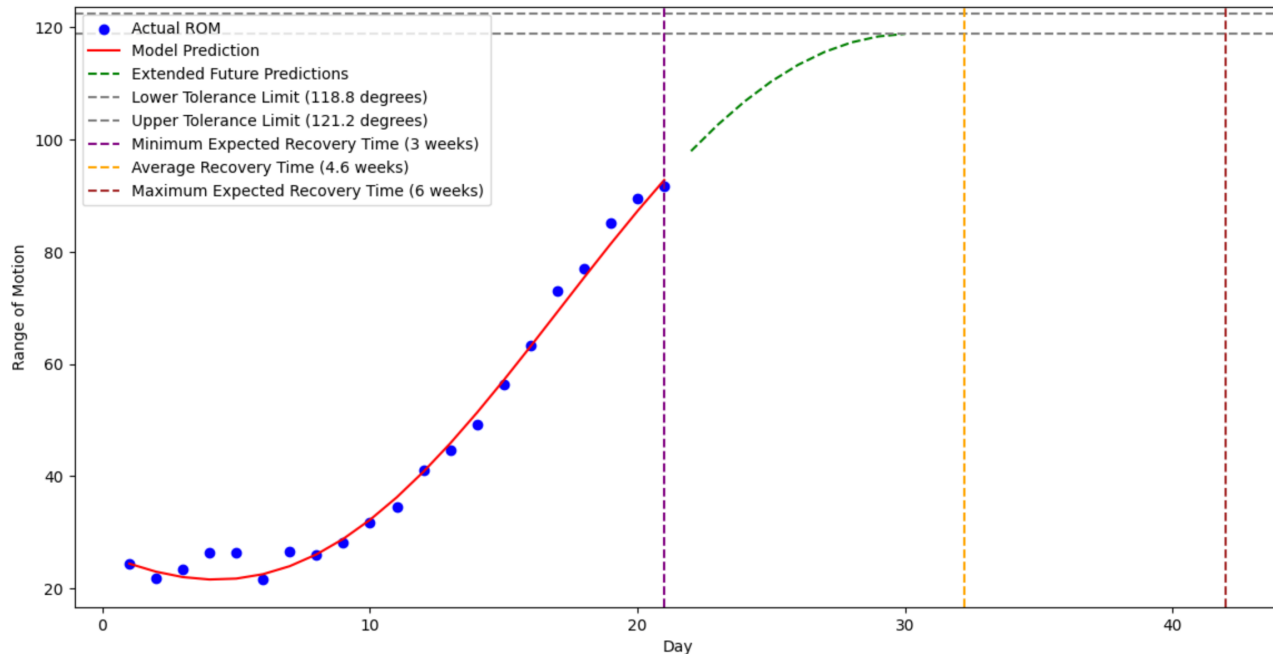


Figure 64: Recovery progress prediction for sigmoid trend

Furthermore, three additional safeguards are incorporated to enhance the model. First, the model stops predictions once the estimated range of motion approaches the goal, within a chosen error margin - in this case, a margin of 1% around a goal of 120 degrees. This ensures the predictions have realistic recovery outcomes, aligning with clinical expectations for patient recovery. Secondly, the model is constrained to predict a continually increasing range of motion. This reflects the typical recovery trajectory, where improvements, even if sometimes slow, are expected to progress without regression, unless there is a new injury in the patient. Lastly, the model's prediction is within the clinically realistic time range of 3 to 6 weeks. Patients with deviations from this range should review with the therapist ensuring that the prediction remains aligned with the therapeutic expectations.

### 9.2.2 Addressing model limitation with solutions

Even with these safeguards, the SVR model faces several limitations that affect the accuracy and reliability when available data is limited. For example, with only 10 days of data, the model inaccurately predicts recovery trajectories, often converging on an angle significantly lower than the target range of motion or suggesting a significantly short recovery period.

One simple way to mitigate this is to increase the frequency of measurements or extend the observation period. However, this does not solve the problem of getting accurate predictions with the limited data initially available. A better solution is to leverage data from other patients who had similar treatments. This method provides comparative insights and improves prediction accuracy even with limited data.

Pooling data from multiple patients allows identification of broader recovery trends and enhances the robustness of the model by integrating a wider array of recovery trajectories [103]. This ensures that the model is not overly reliant on limited data points from a single patient, which can skew predictions. By analysing collected data, the model can learn to recognise patterns and variations in recovery that are more universally applicable, thus improving its predictive accuracy across new patients.

However, this strategy also implies that the initial few patients may not benefit from the predictive model, as their data would be used to train and refine the model's accuracy. This raises ethical considerations regarding the equity of treatment and the informed consent process. Patients should be aware that their data will contribute to a more accurate and robust predictive model for future patients. There will be three phases - initial, data aggregation, and full implementation.

In the initial phase, we will establish the baseline performance of the SVR model using the existing theoretical data and any available clinical data. The model will be implemented in a controlled clinical setting with a small group of patients, and initial data collection will focus on recovery trajectories and range of motion. This stage will help us gain a preliminary understanding of the model's capabilities and limitations with minimal patient data.

During the data collection phase, we aim to expand the dataset by incorporating recovery data from a larger patient cohort, enhancing the model's predictive power. The scale-up of data collection across multiple treatment centres will lead to a more diverse set of recovery trajectories. Data from patients undergoing similar treatments will also be included to improve comparative insights. Continuous refinement of the SVR model based on incoming data and feedback will be crucial during this phase.

The full implementation phase involves optimising and deploying the model for real-time predictive use in clinical practice. This will include finalising model adjustments based on comprehensive data analysis and validation against clinical outcomes. The optimised model will then be implemented across all participating clinics and treatment centres. A training program for clinical staff will be developed to ensure effective use of the new predictive tool. All ethical considerations, such as informed consent and data

privacy, will be thoroughly addressed.

This structured approach will allow us to effectively manage the development and integration of the predictive model while addressing both technical and ethical considerations. Continuous monitoring and feedback from healthcare providers will enable ongoing refinement of the model, ensuring it remains reliable and useful in clinical settings. Through this gradual and careful implementation, the model's accuracy and utility in aiding patient recovery planning will be maximised.

## 9.3 Personalised rehabilitation training plans

### 9.3.1 Range of motion goals

Upon receiving the projected range of motion from the SVR model discussed in section 9.2.1, the value is established as the patient's daily goal. This method ensures that each goal is personalised and dynamically adjusted daily, reflecting the patient's most recent performance and overall progression in recovery. Instead of treating the projected range as a fixed target, the system uses it as a flexible benchmark that adjusts to the patient's changing abilities. Setting the daily goal in this adaptive manner promotes steady and continuous improvement in joint mobility, ensuring that patients are challenged without exceeding safe exertional limits.

### 9.3.2 Effort estimation

In the AutoPhysio system, a patient rehabilitation is personalized through the precise estimation of the effort level required during therapy sessions. This estimation is guided by a Gradient Boosting Machine (GBM) model, a machine learning algorithm known for its precision in regression tasks and handling of complex datasets. The GBM model enhances prediction accuracy by sequentially building decision trees, each correcting the errors of its predecessor [104].

The GBM model integrates with the torque determination data as described in chapter 4. It utilises feedback from torque sensors, that measure the mechanical force applied by and on the patient's knee, offering a direct measure of the patient's physical exertion. These data, coupled with historical exertion metrics, form a comprehensive dataset for the model.

Key inputs to the GBM model include measured torque levels from the session, the patient's range of motion and movement speed, and historical exertion data. The measured torque level from the session provides a quantitative measure of current effort. The patient's range of motion and movement speed

helps assess the physical state of recovery. Historical exertion data tracks the progress and response of the patient over time.

To enhance the accuracy of the model, extensive feature engineering is applied to the raw data inputs. The torque signal is smoothed using a moving average filter to minimize noise and emphasize underlying trends, which are crucial for assessing patient effort. Additionally, changes in torque and the range of motion between sessions are calculated to document the dynamic aspects of the patient's recovery. Interaction terms, such as the products of torque and angular velocity, are computed to further understand the complex bio-mechanical loads experienced by the patient.

The effort estimation is directly linked to the motor control system discussed in chapter 5. The motor control system employs a control algorithm that translates the effort prediction into actionable torque adjustments. This adjustment is calculated using the formula:

$$\text{Torque adjustment} = k \times (\text{predicted effort} - \text{baseline effort}), \quad (46)$$

where  $k$  is a calibration constant that adjusts the effort levels into specific torque settings [105]. This equation ensures that adjustments are both responsive and proportional to the predicted requirements.

The motor control adjusts the mechanical support provided during exercises based on the effort level predicted by the GBM model. This integration allows the device to offer more support if the patient is unable to meet the prescribed effort level due to fatigue or discomfort, or less support if the patient is performing well and can safely handle more physical challenge.

This real-time adjustment is crucial for aiding rehabilitation and encouraging natural muscle recovery, thereby optimising the therapeutic impact of each session. The system's adaptability ensures that the rehabilitation process is continuously tuned to match the patient's capabilities and recovery history.

### 9.3.3 Further enhancements and personalisation

Future iterations of the AutoPhysio system will focus on integrating additional data points such as gender, height, weight, and specific injury characteristics. This comprehensive data collection will facilitate a more nuanced understanding of each patient's unique rehabilitation needs. For instance, incorporating data on muscle mass distribution and bone density could provide critical insights into the mechanical forces appropriate for each patient, adjusting the therapy to accommodate individual physical structures.

To leverage the enriched dataset, clustering algorithms such as k-means clustering and hierarchical clustering will be used to categorise patients into distinct groups based on their demographic and physiological profiles. Each cluster will represent a subset of patients who share similar traits and, potentially, recovery patterns.

K-means clustering method groups dataset into K distinct clusters. It assigns each data point to the cluster whose centroid is nearest [100]. K-means clustering will be used to identify compact clusters based on quantifiable attributes like age, weight, and the severity of injury. Additionally, K-means clustering method can also group patients based on their recovery progress or in-session performance, grouping the individuals with similar traits and rehabilitation needs. The k-means algorithm is particularly effective for handling large datasets and will enable quick grouping of new patients into existing clusters.

For more detailed segmentation, hierarchical clustering will be applied. Hierarchical clustering, also known as agglomerative clustering, is a method of building a hierarchy of clusters [100]. This method will help identify nested clusters at various levels of similarity, providing an in-depth stratification of patient groups. This could be particularly useful for understanding subtle variations in recovery within broadly similar groups.

With patients segmented into distinct groups, AutoPhysio will customise its rehabilitation protocols for each cluster. For example, patients in a cluster characterised by higher body mass might receive protocols that emphasise gradual torque incrementation, considering the additional stress on joints. Conversely, clusters comprising patients with faster recovery patterns might see a progression in their exercise regimen more quickly.

Each cluster's data will also refine the system's predictive models, enabling more accurate forecasts of recovery trajectories and optimal exertion levels. This will not only enhance the effectiveness of individual sessions but also minimise the risk of injuries due to overexertion.

Beyond mechanical adjustments, the system will also recommend specific exercises tailored to the physiological characteristics of each cluster. These recommendations will be dynamically updated based on ongoing data analysis, ensuring that the rehabilitation exercises evolve in line with patient feedback.

# 10 Machine learning for device safety

(Yoonsang)

*Safety is important in designing a wearable device, especially for a rehabilitation medical wearable device where patients are in a delicate phase of recovery. Unsafe equipment can lead to re-injury or complicate the recovery process, potentially resulting in long-term disability or increased pain. Therefore, ensuring safety is very important to protect patients from additional harm and to build trust in the technology that supports their recovery. Beyond the physical designs and software safeguards, incorporating machine learning can elevate the safety protocols [106].*

## 10.1 Anomaly detection in movement patterns

### 10.1.1 Basic implementation (2D movements)

There are expected standard movements and patterns in each rehabilitation exercise. By identifying deviations from expected movement patterns, anomaly detection can find potential wrong movements that can lead to injury. For example, a patient can do the exercise in a wrong way or inadvertently extend beyond the recommended range of motion, risking injury. Anomaly detection can alert them or the therapist to correct the movement.

For practical implementation, we will use the theoretical dataset referred to in section 9.1.1, which records the range of motion over time in a single session. The initial step in our anomaly detection involves calculating the absolute differences between consecutive measurements of the range of motion:

$$\text{Absolute Difference}_i = |\text{range of motion}_i - \text{range of motion}_{i-1}|, \quad (47)$$

where  $i$  ranges from 1 to  $n - 1$  with  $n$  being the total number of measurements in the session. These differences help us understand the rate of change in the range of motion, which is critical for identifying unusual movements.

Following the calculation of absolute differences, we compute the mean and standard deviation of these values across the session. Anomalies are identified by detecting points where the change in the range of motion is significantly different from the typical behavior. This is determined using the following criteria:

$$\text{Absolute Difference}_i > \text{Mean Difference} + 1.5 \times \text{Standard Deviation} \quad (48)$$

This threshold is chosen to identify changes that are not just above average but significantly higher, suggesting a potential issue in the exercise movement. However, 1.5 is an initial setting and can be adjusted based on specific medical backgrounds or the observed variability in patient responses during rehabilitation. This flexibility allows for customisation of the system to better match the sensitivity needed for each individual's condition and recovery progress.

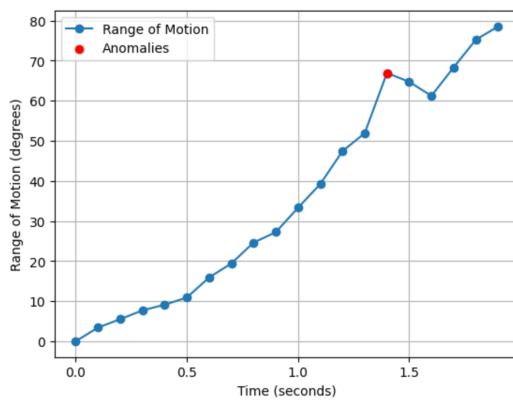


Figure 65: Anomaly detection

In the given range of motion data shown in figure 65, the mean difference between consecutive data points is approximately 4.73 degrees. The standard deviation, which measures the variation from the mean, is around 3.10 degrees. In this case, one such anomaly was identified at time  $t = 1.3$  seconds. The difference at this point was about 15 degrees, which is significantly higher than the threshold set by the mean plus 1.5 times the standard deviation. This specific difference was approximately 5.62 degrees above the anomaly detection threshold, showing a sudden increase in the range of motion.

We can also do multivariate analysis by considering multiple parameters simultaneously [107]. For instance, incorporating data from other sensors like EMG, muscle strain gauges or balance measurements could provide a multivariate perspective, enhancing the detection capabilities by identifying anomalies across different dimensions of movement and physiological data.

### 10.1.2 Further implementation (3D movements)

To further enhance detection capabilities, integrating 3D modelling can provide more detailed observation [108] of patient movements during rehabilitation. Employing a combination of diverse sensors, such as accelerometers and gyroscopes, we can create detailed three-dimensional models of each patient's movements. This method is particularly beneficial for analyzing movements in all directions, including lateral (side-to-side) movements, allowing us to identify potentially harmful actions outside of the typical

vertical (up-and-down) plane.

Accelerometers detect changes in speed and direction, while gyroscopes measure angular velocity, which is crucial for identifying rotations and twists that may not be within the clinically acceptable range. These data collectively feed into the 3D modeling system, enabling dynamic visual analysis of patient movements.

Effective anomaly detection within 3D framework utilizes advanced machine learning algorithms. Supervised learning models, trained on datasets labeled as 'correct' or 'incorrect' by physiotherapists, allow for precise identification of deviations. Models such as Convolutional Neural Networks (CNNs) and Recurrent Neural Networks (RNNs) are particularly effective, due to their ability to process spatial and temporal data [109]. These models excel at recognising complex patterns and anomalies in movement that may indicate a risk of injury or incorrect exercise execution.

Specifically, anomaly detection algorithms suitable for 3D movement analysis include sequence modelling and feature-based classification. Sequence modelling, often conducted using RNNs or their variants like Long Short-Term Memory networks (LSTMs), tracks movements over time to detect anomalies in sequences of movements that deviate from learned patterns [110]. Feature-based classification involves extracting key features from the 3D movement data, such as maximum rotation angles or sudden accelerations, and analysing them using classifiers like Support Vector Machines (SVMs) or decision trees to identify outliers [108].

The integration of these sophisticated machine learning techniques into the 3D modeling framework allows for a nuanced analysis of rehabilitation exercises. This methodology not only aids in identifying and correcting improper movements more efficiently but also assists in customising the rehabilitation process to better suit the individual needs of patients, thereby enhancing the overall effectiveness and safety.

#### **10.1.3 Real-time implementation**

Continuous monitoring will be done during the rehabilitation sessions. When an anomaly is detected the system triggers an immediate alert. This alert can be communicated visually or audibly to both the patient and the therapist. The therapist can then intervene to correct the patient's movement, potentially adjusting the exercise protocol to prevent the recurrence of risky movements. Additionally, these anomalies are logged into the patient's treatment history, providing valuable insights for further customization of the rehabilitation plan.

## 10.2 Intelligent sound analysis for pain detection

The intelligent sound analysis module within AutoPhysio aims to augment the safety mechanisms by detecting vocal expressions of discomfort or pain. The pain recognition system is already used to help detect patients' pain during surgery [111], so we will bring it to post-surgery rehabilitation. Through a combination of audio signal processing and machine learning, the system is trained to recognize specific sounds associated with pain, such as sharp intakes of breath, groans, or the word "Ouch!". Upon detection, the system can initiate a response, such as pausing the rehabilitation exercise, thus preventing further strain or injury.

The process begins with meticulous audio data acquisition. Place the microphones near the patient to capture the patient's vocalizations clearly while advanced signal processing techniques filter out irrelevant background noise. This ensures that the machine learning model receives high-quality input for accurate feature extraction. Then, we have a feature extraction as the next step. We will use Mel-Frequency Cepstral Coefficients (MFCCs) to distill the unique timbral qualities of human speech that signal the pain [112].

Machine learning models can be trained on labeled datasets containing both pain and non-pain vocalizations. Possible algorithms for classification are Support Vector Machines or Convolutional Neural Networks. Then, we can use sequential models like RNNs or LSTMs to add a layer of recognition, enhancing the system to distinguish pain sounds from the other signals.

In AutoPhysio, we will use a CNN-based pain detection system [113]. The CNN is capable of capturing hierarchical patterns in the data, and this capability makes it suitable for identifying complex features in audio signals [114]. First, we will define some parameters specific to pain sounds. We will need input features, which would be the MFCCs derived from audio clips captured by the microphone. These MFCCs represent the critical frequencies associated with pain expressions, groans or sharp intakes of breath, which are indicative of discomfort or pain. Then, we have weights and biases, which are optimized during training to best differentiate between pain and non-pain sounds based on the labeled dataset specifically created from patient interactions with the AutoPhysio device. The CNN architecture has several convolutional layers, each designed to extract higher-level features from the input features. The first layer might use filters of small size to capture basic features. Each convolutional operation can

be represented by the equation:

$$y = f(W * x + b), \quad (49)$$

where  $*$  denotes the convolution operation,  $x$  is the input feature,  $W$  is the weight kernel,  $b$  is the bias, and  $f$  is the activation function. We can use Rectified Linear Unit (ReLU) as our activation function which is commonly incorporated in sound recognition models [115].

To adapt to various sensitivity needs in pain detection, a dynamic threshold adjustment mechanism can be included. The dynamic threshold is adjusted continuously based on the real-time analysis of audio signals collected by the microphone [116]. For example, if there is a series of uncertain pain indications like soft groans or ambiguous vocalisations, the threshold might be lowered to increase the sensitivity and make sure no pain expression is missed. Over time, the device learns from the specific vocal characteristics of the patient's pain expressions. Some patients may express pain less vocally than others, so in this case, the dynamic threshold adapts to the patient's expression. There are many ways to express dynamic threshold, but the simplified form can be written as

$$\theta(t+1) = \alpha\theta(t) + (1 - \alpha)f(\theta(t), \Delta y(t)), \quad (50)$$

where  $\theta(t+1)$  is the threshold for the next time step,  $\theta(t)$  is the current threshold,  $\Delta y(t)$  is the difference between the predicted and the observed pain expression,  $\alpha$  is the coefficient that balances the contribution of the previous threshold and the volatility function  $f$  [116].  $\alpha$  adjusts how sensitively the threshold reacts to changes in detected pain levels. For example, if a patient typically expresses pain subtly, a lower  $\alpha$  could be used to place more weight on the new data rather than the current threshold. This stabilises the threshold adjustments, preventing drastic changes due to anomalies or outliers in pain detection.

Lastly, to train the CNN, a cross-entropy loss function is applied, which is particularly effective for binary classification tasks such as pain detection:

$$L = -[y \log(\hat{y}) + (1 - y) \log(1 - \hat{y})], \quad (51)$$

where  $y$  is the true label and  $\hat{y}$  is the predicted probability of pain presence from the network. Then, we

can use an optimisation algorithm to minimise the loss function. We will use Adam optimiser, which has combined advantages of two stochastic gradient descents - Adaptive Gradient Algorithm (AdaGrad) and Root Mean Square Propagation (RMSProp) [117].

Following the application of the cross-entropy loss function and optimisation via the Adam optimiser, further enhancements can be made to the intelligent sound detection algorithm within the AutoPhysio device. These improvements aim to increase the accuracy, adaptability, and responsiveness of the system, thereby providing more reliable and effective patient care.

Enhanced data collection and labeling techniques should be employed to broaden the diversity of the audio dataset [118]. By incorporating vocal expressions from a wide range of demographic groups, the model can be trained to recognize pain indicators across various ages, genders, and cultural backgrounds [119]. Regular updates with new data can help refine the model's accuracy over time and prevent drift, ensuring the system remains effective as patient demographics and behaviors evolve.

Additionally, exploring advanced feature extraction methods can provide deeper insights into audio signals [120]. While MFCCs serve as a robust baseline, integrating additional features such as Chroma and Spectral Contrast could capture more complex vocal patterns associated with pain expressions [121, 122].

The integration of cutting-edge deep learning architectures, like attention-based models including transformers, could also enhance performance [123]. These models focus on the most relevant parts of an audio signal, potentially improving the system's ability to distinguish subtle pain sounds from other non-pain related sounds.

Lastly, expanding the model to include multimodal data integration, such as physiological signals like heart rate or muscle tension, could significantly improve pain detection [124]. This multimodal approach would not only rely on audio cues but also incorporate other relevant data, providing a more comprehensive assessment of the patient's condition. Advanced noise reduction algorithms could also be applied to ensure the system's performance remains consistent, regardless of environmental noise variations.

By implementing these enhancements, the AutoPhysio device can become more than just a tool for rehabilitation; it can be an integral part of a patient-centered approach that prioritises safety, comfort, and efficiency in the recovery process.

# 11 App design

(John)

As mentioned in section 1.2, the patient uses a mobile application to interact with the physical device when using AutoPhysio during rehabilitation. This chapter focuses on the design of this app, both the user interface and the system details associated with deployment. The user interface is developed in Swift, but these will be used as visual aids in the discussion to avoid language-specific or platform-specific details. System design will cover the architecture for realising a robust experience, concerning overall connections and database options.

## 11.1 Purpose of App

The aim of the mobile application is to serve as the primary method for interacting with the physical rehabilitation device. To fulfil this, it needs to grant users a certain amount of control of the motor, access to visualisations, receipt of alerts, training results, and personalised training schedules. On top of the basic requirements, as discussed in section 2.2.2, the app should also gamify the recovery journey as a way of motivating patients to adhere consistently to the personalised training schedule.

## 11.2 Frontend design

The app follows the Model-View-View Model (MVVM) for creating components [125].

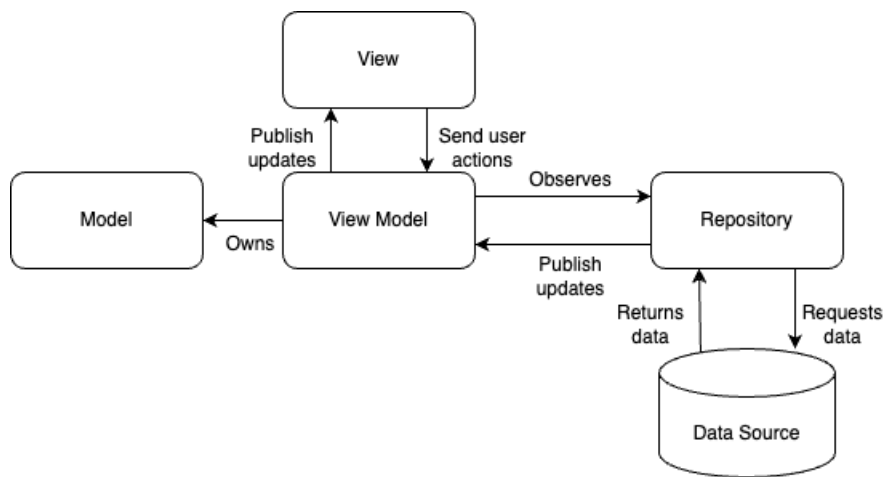


Figure 66: Model-View-View Model design pattern

Models represent the entities that need to be managed on the app. Views are the visual elements of the app and are responsible for displaying the data within models. View Model transforms data within models into a displayable form, enabling the relationship between models and views. Repository is the

abstraction that handles communication with the data source. The View Model communicates with the Repository to perform data operations and also notifies views about changes in the data. This design pattern maintains the separation of concerns to keep views and models agnostic from data sources.

### 11.2.1 App features

#### Warm-up calibration

Prior to every session, the patient is prompted to do warm-up. This has two main purposes: to prepare the patient for training, and to calibrate the device for a new training session. Calibration aims to capture EMG values when the patient is at maximal voluntary contraction (MVC). These values serve as normalisation constants for the session to gauge progress overall multiple sessions. MVC is performed through three successful (hits easy target angle) reps of an unassisted knee extension. The MVC EMG values used for normalisation is the average of the three. These would be used in the real-time control system as well as the CCI in section 2.3.1 that serves as input for ML training suggestion.

A session is contained within an in-session view in the app, and exiting it would mean concluding the session. Within this view, AutoPhysio is in an **ON** state as mentioned in section 3.1, involving the three components within the session loop, with the warm-up check being done by ascertaining that the MVC EMG fields are not empty. Upon exit, there is also an option to rate the training session on a scale from 1 to 5. This serves both as user feedback on performance of AutoPhysio and input weights for the given session into the ML model.

#### Gamification

Gamification aims at user retention and in-session focus. The former is achieved through an adapted “streaks” feature that is implemented via a counter that increments everytime the patient completes an AI-generated session. The reason for not following a daily usage model is that sufficient rest that could span days is required between sessions. This constraint is issued before the healthcare professional provides the patient with AutoPhysio. In-session effort is motivated through displaying target metrics (e.g. best range of motion angle, best torque, target angle) on the home screen and in the session view.

#### Considerations for healthcare providers

Upon opening the app, the user is greeted by a login or registration page in figure 67. For registration, a further identity verification is done, this being particularly important for doctors on the app. As seen in figure 67b, there is a toggle for indicating whether the user registering is the healthcare professional

involved. The reason for this inclusion is that while AutoPhysio aims to facilitate home-based recovery, there remains the need for expert consultation. This is true in the existing methodology in which patients schedule appointments with both their physiotherapists and surgeons for updates on rehabilitation progress (consulted with Dr. Lim Jit Kheng in Mount Elizabeth hospital in Singapore). Therefore, the included features must account for two user types: patients and doctors.

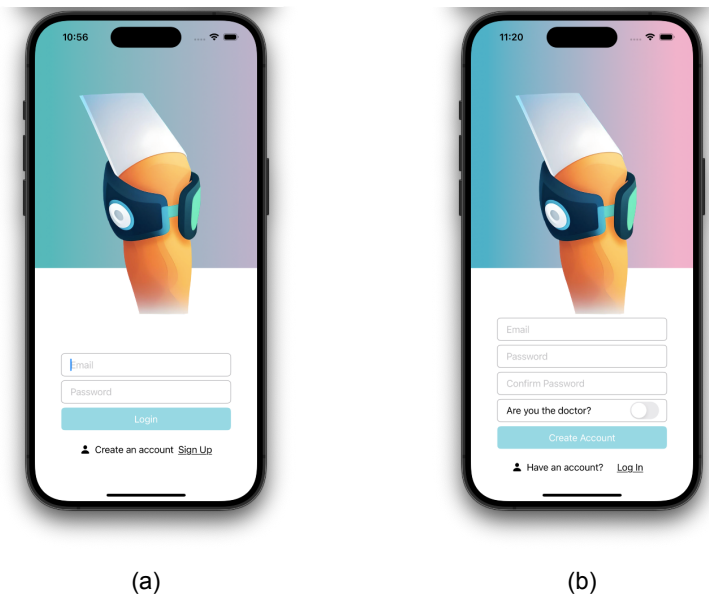


Figure 67: (a) Login page. (b) Registration page.

Table 13 shows the different levels of access given to either user types for interaction features. This is defined as app-to-user features that define how users interact with the app itself.

Table 13: Interact app features

	Patient	Doctor
Interact with visualisations	✓	✓
View AI-generated targets	✓	✓
View and download summary data	✓	✓
View and download full data		✓
Manual target setting		✓
Access to physical device		✓

Both user types are able to interact with visualisations that play during sessions and on the dashboard. Data can be downloaded for further analysis, but only the healthcare providers are given access to full data. This difference exists to strike a balance between user needs and overall download bandwidth.

limits. Apart from the AI-generated targets, the healthcare provider is also entitled to set achievable goals for the patient. To improve device safety, only the patient can access the physical knee brace with the app; this lessens the chance of remote access of physical functions.

Table 14 demonstrates methods for user-to-user interaction between patients and their healthcare providers. While both user types receive data-driven alerts generated by in-built rules or the ML model, only the healthcare provider can create alerts. The healthcare provider also has multi-patient view, allowing for a one-to-many connection, while patients maintains one-to-one connection with their specified healthcare provider. Communication can be done via comments on targets or performance metrics.

Table 14: Collaboration app features

	Patient	Doctor
Receive data-driven alerts	✓	✓
Create alerts		✓
Multi-patient view		✓
Create comments	✓	✓

## 11.3 Backend system design

One crucial observation is that bulk of the data is training parameters (e.g. angle, angular speed, and CCI in section 2.3.1), and fewer target objects such as target angle can be said to describe a datapoint (metadata). The former has greater data variety and is unlikely to experience heavy alterations, while the latter will experience many changes so as to reflect the daily progress made by the patient. The overall application is depicted by the system architecture diagram in figure 68. A standard load balance cluster consisting of web servers and a load balancer connects the user Repository in figure 66 to the databases. The two databases are tailored to exploit the aforementioned distinct data behaviours, splitting into parameters and metadata.

### 11.3.1 Choice of database

Parameters occupy larger space as entries are over the course of a session, meaning storage must be scalable in pricing per unit storage and data variety. Upon storage, the data must be highly accessible for on-cloud computation. Schema-less databases are better suited for this purpose due to low-cost infrastructure and configurable high read operation speeds. Storage is in the JSON format, allowing for further flexibility. Examples include Apache Cassandra and Amazon Simple Storage Service (AWS S3).

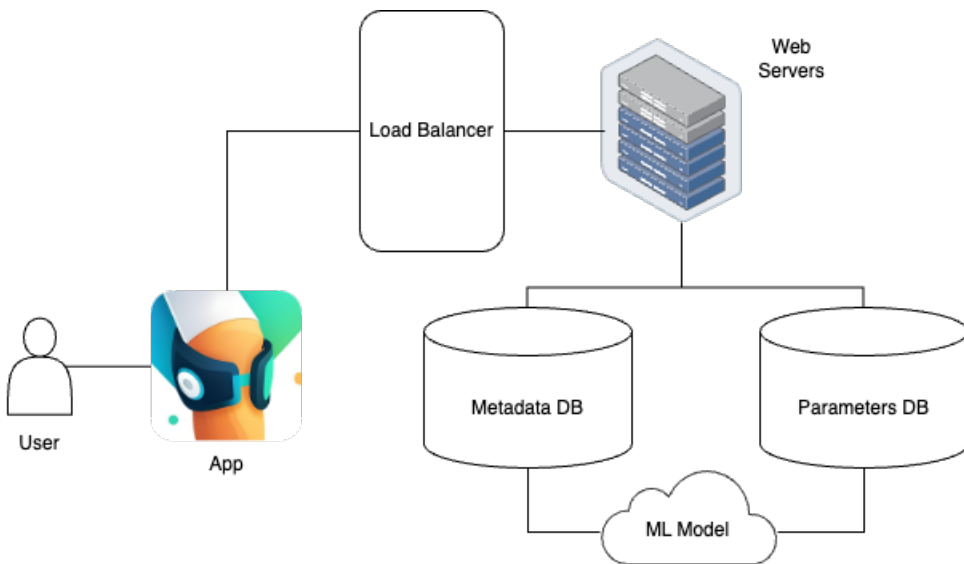


Figure 68: App system architecture

Metadata, in the context of AutoPhysio, does not take up much storage space. As such, the system can afford higher pricing per unit storage. However, it gets updated more frequently, and plays an active role in the MVVM pattern. Thus, both read and write operations need to be fast and accessible. Relational databases work better here since querying is faster in a highly structured environment, with the acceptable downside of pricier storage scaling.

### 11.3.2 Data security

To satisfy UK GDPR, one feature to be implemented to satisfy this is to request for users' consent of the app's use of their personal data in the onboarding process. Apart from this, identifiable data needs to be well-protected during transit and at rest. Applying Transport Layer Security (TLS) ensures that data is protected going to and from the database, and using server-side encryption (often in-built in state-of-the-art database services) manages data that is at rest.

## 11.4 Areas for improvement

User testing would be key in ascertaining the features provided for each user type. This would mean delivering a minimally viable product (MVP) to users and iterating on it based on feedback, and this involves both patients and healthcare providers. For backend implementation, a trial run of the product provides information of the bandwidths required for the data stream, thereby informing the decision of simply adding more web servers to the load balancing cluster or issuing new clusters altogether to sustain the traffic.

## 12 Conclusion

(co-authored)

### 12.1 Risk assessment (Yoonsang)

The development and implementation of medical devices involve a thorough understanding and management of potential risks to ensure patient safety and device efficacy. The AutoPhysio device, an innovative solution designed for patients recovering from ACL injuries, incorporates several high-tech components and software algorithms that pose unique challenges in terms of safety and performance. To safeguard users and optimize therapeutic outcomes, a comprehensive risk assessment is crucial. This assessment not only identifies potential hazards but also proposes mitigation strategies to address these risks, ensuring that the device adheres to the highest standards of medical device safety. The following table 15 provides a detailed overview of the potential risks associated with the AutoPhysio device, the existing controls in place, their assessed risk levels, and further actions recommended to minimise these risks.

Table 15: Risk Assessment for the AutoPhysio device

Potential Harm	Risk Controls in Place (Existing Safety Precautions)	Risk Level	Further Actions Needed to Reduce Risk
Injury due to device malfunction	Regular software updates and safety settings; Emergency shutoff mechanism	Medium	Implement real-time monitoring systems to detect anomalies
Skin irritation or damage from brace	Hypoallergenic materials; Adjustable brace design	Low	Regularly update material based on patient feedback
Incorrect rehabilitation data leading to improper therapy	Machine learning model validation; Data accuracy checks	Medium	Continuous algorithm training with new data and expert review
Data privacy issues	Encryption; Compliance with data protection regulations	High	Strengthen cybersecurity measures and conduct regular audits
Dependency on device leading to reduced manual physiotherapy	Device is an adjunct, not a replacement; Clear guidelines on usage	Low	Educate patients and therapists on the complementary nature of the device

## 12.2 Project ethics (Yoonsang)

Ethics play a pivotal role in the development and deployment of medical devices, where the primary concern is always the safety and well-being of the patient. The AutoPhysio device, designed to aid in the rehabilitation of ACL injuries, must adhere to stringent ethical standards throughout its design, testing, and eventual use.

Ensuring patient safety is the foremost ethical obligation. The device must be rigorously tested for safety and efficacy through controlled trials that are conducted with informed consent from participants. These trials must be designed to comprehensively assess potential risks without exposing subjects to undue harm.

The AutoPhysio device collects and analyses personal health data to tailor rehabilitation efforts. It is imperative to implement robust data protection measures to secure sensitive information against unauthorized access and breaches. Compliance with healthcare regulations such as HIPAA in the U.S. or GDPR in Europe is essential [126]. Additionally, patients should be fully informed about what data is collected, how it is used, and who has access to it.

Ethical considerations also include the accessibility of the device to all patients in need, regardless of socio-economic status. Efforts should be made to ensure that the device is affordable and available widely to prevent disparities in healthcare outcomes. Moreover, the device should be adaptable to various physical needs to accommodate a diverse patient population.

Maintaining transparency with stakeholders—including patients, healthcare providers, and regulatory bodies—is crucial. This involves honest reporting of device performance and potential limitations, ensuring that all parties have accurate information to make informed decisions.

Considering the long-term impacts of the device on patients and the healthcare system is also an ethical necessity. This includes evaluating how the technology might affect traditional physiotherapy practices and ensuring it complements rather than replaces human care.

The project team must take responsibility for continual monitoring of the device's performance and impact and be ready to intervene if unforeseen issues arise. Ethical responsibility also means being accountable for the device's effects on patients and the broader healthcare landscape.

### 12.3 Summary (John)

In this report, we have introduced the AutoPhysio, a companion active knee brace for early phase home-based ACL rehabilitation. Our solution comprises a motorised knee brace, an EMG recording sleeve, and a mobile application to facilitate training sessions. Training sessions are managed by a real-time sensor-based algorithm that automatically determines user states. Training goals are then set online through access to the on-cloud machine learning model.

As it is, the device's degree of freedom allows for exercises that strengthen the hamstrings (e.g. single-legged squats) to be considered. This requires the motor to apply torque in the opposite direction, necessitating an updated control system, but providing more space for personalisation through the ML model's inferences. In fact, if both directions are functional, the device has the potential to cover all large muscle-strengthening (hamstrings and quadriceps) requirements for early-phase rehabilitation.

The physical device can also be significantly improved by considering additional degrees of freedom. As of now, the actuator in chapter 7 only supports movement along the flexion-extension axis. Other important features of the knee are valgus and varus orientations, and its ability to support internal and external rotations; movements along axes that are not currently possible with the current design. Modifications through additional actuators can enable this behaviour on the device to cover a larger range of strengthening and stability exercises. A successful implementation of AutoPhysio could inspire these design modifications for other exercises mentioned in section 2.2.2 as well as rehabilitation for other knee injuries such as injuries involving the other three ligaments in figure 3.

Beyond rehabilitation and strength restoration, as this design is strongly inspired by exoskeletons, future developments could even provide strength enhancements, benefiting the warehouse workers, house movers in lifting heavy objects, and giving strength to the elderly to regain movement.

For the current purpose of facilitating home-based early-phase rehabilitation, the next step would be to construct an MVP of the product and get supervised user testing, both from patients and their healthcare providers. This will provide critical information on the features that should be added or removed, the product-market fit, and the best way to market such a device to reach the intended audience.

## 13 References

- [1] Letha Griffin et al. "Understanding and Preventing Noncontact Anterior Cruciate Ligament Injuries: A Review of the Hunt Valley II Meeting". In: *American Orthopaedic Society for Sports Medicine* 34 (Sept. 2006). DOI: 10.1177/0363546506286866.
- [2] Stephanie R. Filbay and Hege Grindem. "Evidence-based recommendations for the management of anterior cruciate ligament (ACL) rupture". In: *Best Practice and Research Clinical Rheumatology* 33.3 (Feb. 2019), pp. 33–47. DOI: 10.1016/j.berh.2019.01.018.
- [3] Di Miceli R, Marambio CB, Zati A, Monesi R, Benedetti MG. "Do knee bracing and delayed weight bearing affect mid-term functional outcome after anterior cruciate ligament reconstruction?" In: 5 (2017), pp. 202–6.
- [4] Bordes P, Laboute E, Bertolotti A. "No beneficial effect of bracing after anterior cruciate ligament reconstruction in a cohort of 969 athletes followed in rehabilitation". In: *Ann Phys Rehabil Med* 60 (2017), pp. 230–6.
- [5] Rodríguez-Merchán EC. "Knee bracing after anterior cruciate ligament reconstruction". In: *Orthopedics* 39 (2016), e602–9.
- [6] Lowe WR, Warth RJ, Davis EP, Bailey L. "The influence of functional knee bracing on the anterior cruciate ligament strain biomechanics in weightbearing and nonweightbearing knees". In: *Am J Sports Med* 28 (2000), pp. 815–824.
- [7] Marx RG, Jones EC, Angel M, Wickiewicz TL, Warren RF. "Beliefs and attitudes of members of the American Academy of Orthopaedic Surgeons regarding the treatment of anterior cruciate ligament injury". In: *Arthroscopy* 19 (2003), pp. 762–770.
- [8] Fleming BC, Renstrom PA, Beynnon BD, Engstrom B, Peura G. "The influence of functional knee bracing on the anterior cruciate ligament strain biomechanics in weightbearing and nonweightbearing knees". In: *Am J Sports Med* 28 (2000), pp. 815–824.
- [9] Clare Ardern et al. "Psychological responses matter in returning to preinjury level of sport after anterior cruciate ligament reconstruction surgery". In: *Am J Sports Med* 41.7 (July 2013). DOI: 10.1177/0363546513489284.
- [10] David Flanigan et al. "Fear of Reinjury (Kinsephobia) and Persistent Knee Symptoms Are Common Factors for Lack of Return to Sport After Anterior Cruciate Ligament Reconstruction". In: *The Journal of Arthroscopic and Related Surgery* 29 (Aug. 2013). DOI: 10.1016/j.artro.2013.05.015.
- [11] Faleide, A.G.H. and Inderhaug E. "It is time to target psychological readiness (or lack of readiness) in return to sports after Anterior Cruciate Ligament tears". In: *Journal of Experimental Orthopaedics* 10 (2023), p. 94. URL: <https://doi.org/10.1186/s40634-023-00657-1>.
- [12] "Clinical Research Progress of Internal Brace Ligament Augmentation Technique in Knee Ligament Injury Repair and Reconstruction: A Narrative Review". In: *Stomatology* 12.5 (2023), pp. 1999–1999. DOI: 10.3390/jcm12051999.
- [13] "Innovative rehabilitative bracing with applied resistance improves walking pattern

- recovery in the early stages of rehabilitation after ACL reconstruction: a preliminary investigation.” In: *BMC Musculoskeletal Disorders* 21.1 (2020), pp. 1–9. DOI: 10.1186/S12891-020-03661-Z.
- [14] VynZ Research. *Global Knee Braces Market – Analysis and Forecast (2025-2030)*. Market Analysis Report VRHC1215. VynZ Research, Dec. 2023.
- [15] American Academy of Orthopaedic Surgeons. *The Use of Knee Braces*. Position Statement. Rosemont, IL: American Academy of Orthopaedic Surgeons, 2003.
- [16] Bauerfeind. <https://www.bauerfeind-sports.uk>.
- [17] Ossur. <https://www.ossur.com/en-gb>.
- [18] Spring-Loaded. <https://www.springloaded.com>.
- [19] Mariam Faizullabhoy. *Knee Braces Market Share*. Gobal Market Insights, June 2023.
- [20] Guidera KJ, Hontas R, Ogden JA. “Use of continuous passive motion in pediatric orthopedics”. In: *J Pediatr Orthop* 10.1 (1990), pp. 120–123.
- [21] Soma Y, Mutsuzaki H, Yoshioka T, Kubota S, Shimizu Y, Kanamori A, Yamazaki M. “Single-joint Hybrid Assistive Limb in Knee Rehabilitation after ACL Reconstruction: An Open-label Feasibility and Safety Trial”. In: *Prog Rehabil Med* 7 (2022), p. 20220036. DOI: 10.2490/prm.20220036.
- [22] Eun-Lee Lee et al. “Home-Based Remote Rehabilitation Leads to Superior Outcomes for Older Women With Knee Osteoarthritis: A Randomized Controlled Trial”. In: *The Journal of Post-Acute and Long-Term Care Medicine* 24 (Oct. 2023). DOI: 10.1016/j.jamda.2023.08.013.
- [23] Jia Z, Zhang Y, Zhang W. “Efficacy and safety of continuous passive motion and physical therapy in recovery from knee arthroplasty: a systematic review and meta-analysis”. In: *Journal of Orthopaedic Surgery and Research* 19 (2024), p. 68. DOI: 10.1186/s13018-024-04536-y.
- [24] R. Morales-Avalos et al. “ACL anatomy: Is there still something to learn?” In: *Revista Española de Cirugía Ortopédica y Traumatología* (Feb. 2023). DOI: 10.1016/j.recot.2023.02.005.
- [25] V. B. Duthon et al. “Anatomy of the anterior cruciate ligament”. In: *Knee Surgery, Sports Traumatology, Arthroscopy* 14.3 (Oct. 2005), pp. 204–213. DOI: 10.1007/s00167-005-0679-9.
- [26] Walter L. Calmbach and Mark Hutchens. “Evaluation of Patients Presenting with Knee Pain: Part I. History, Physical Examination, Radiographs, and Laboratory Tests”. In: *American Family Physician* 68.5 (Sept. 2003), pp. 907–912.
- [27] Thomas Fridén et al. “Review of Knee Proprioception and the Relation to Extremity Function After an Anterior Cruciate Ligament Rupture”. In: *Journal of Orthopaedic and Sports Physical Therapy* 31.10 (Oct. 2001), pp. 567–576. DOI: 10.2519/jospt.2001.31.10.567.
- [28] Konstantinos Banios et al. “Anterior and Posterior Cruciate Ligaments Mechanoreceptors: A Review of Basic Science”. In: *Diagnostics* 12.331 (Jan. 2022). DOI: 10.3390/diagnostics12020331.
- [29] Royal United Hospitals Bath NHS Foundation Trust. *Prehabilitation Programme for an Anterior Cruciate Ligament (ACL) Injury*. Patient Information Leaflet. Aug. 2020.

- [30] Royal United Hospitals Bath NHS Foundation Trust. *Post-operative advice after Anterior Cruciate Ligament (ACL) Reconstruction*. Physiotherapy Patient Information. Dec. 2021.
- [31] Derwin Chan et al. "Patient Motivation and Adherence to Postsurgery Rehabilitation Exercise Recommendations: The Influence of Physiotherapists' Autonomy-Supportive Behaviors". In: *Arch Phys Med Rehabil* 90 (2009). DOI: 10.1016/j.apmr.2009.05.024.
- [32] A. Sulfikar Ali, Ashokan Arumugam, and Senthil Kumaran D. "Effectiveness of an intensive, functional, gamified Rehabilitation program in improving upper limb motor function in people with stroke: A protocol of the EnteRtain randomized clinical trial". In: *Contemp Clin Trials* 105 (June 2021). DOI: 10.1016/j.cct.2021.106381.
- [33] Jenna Tosto-Mancuso et al. "Gamified Neuromotor Strategies for Post-stroke Motor Recovery: Challenges and Advantages". In: *Curr Neurol Neurosci Rep* 22.3 (Mar. 2022). DOI: 10.1007/s11910-022-01181-y.
- [34] Fábio Marcos Alfieri et al. "Gamification in Musculoskeletal Rehabilitation". In: *Curr Rev Musculoskelet Med* 15.6 (Oct. 2022). DOI: 10.1007/s12178-022-09797-w.
- [35] BIOPAC Systems. *Introductory EMG Guide*.
- [36] Marianne Boyer et al. "Reducing Noise, Artifacts and Interference in Single-Channel EMG Signals: A Review". In: *Sensors* 23.6 (Mar. 2023). DOI: 10.3390/s23062927.
- [37] B. A. Alkner, P. A. Tesch, and H. E. Berg. "Quadriceps EMG/force relationship in knee extension and leg press". In: *Med Sci Sports Exerc*. 32.2 (Feb. 2000). DOI: 10.1097/00005768-200002000-00030.
- [38] Thomas Roberts and Annette Gabaldón. "Interpreting muscle function from EMG: lessons learned from direct measurements of muscle force". In: *Integrative and Comparative Biology* 48 (June 2008). DOI: 10.1093/icb/icn056.
- [39] Miriam González-Izal et al. "Electromyographic models to assess muscle fatigue". In: *Journal of Electromyography and Kinesiology* 22 (Aug. 2012). DOI: 10.1016/j.jelekin.2012.02.019.
- [40] A. Vijayvargiya et al. "A Hybrid WD-EEMD sEMG Feature Extraction Technique for Lower Limb Activity Recognition". In: *IEEE Sensors Journal* 21.18 (Sept. 2021). DOI: 10.1109/JSEN.2021.3095594.
- [41] Jing Jie et al. "High dimensional feature data reduction of multichannel sEMG for gesture recognition based on double phases PSO". In: *Complex and Intelligent Systems* 7 (Mar. 2021). DOI: 10.1007/s40747-020-00232-6.
- [42] K. S. Rudolph, M. J. Axe, and L. Snyder-Mackler. "Dynamic stability after ACL injury: who can hop?" In: *Knee Surg Sports Traumatol Arthroscopic*. 8.5 (2000). DOI: 10.1007/s001670000130.
- [43] L. A. Setton, V. C. Mow, and D. S. Howell. "Mechanical behaviour of articular cartilage in shear is altered by transection of the anterior cruciate ligament". In: *Journal of Orthopaedic Research* 13 (1995). DOI: 10.1002/jor.1100130402.
- [44] R. Chowdhury et al. "Surface Electromyography Signal Processing and Classification Techniques". In: *Sensors* 13 (2013). DOI: 10.3390/s130912431.
- [45] N. Nazmi et al. "A Review of Classification Techniques of EMG Signals during Isotonic

- and Isometric Contractions". In: *Sensors* 16 (Aug. 2016). DOI: 10.3390/s16081304.
- [46] R. Merletti and G. Cerone. "Tutorial. Surface EMG detection, conditioning and pre-processing: Best practices". In: *Journal of Electromyography and Kinesiology* 54 (Oct. 2020). DOI: 10.1016/j.jelekin.2020.102440.
- [47] Ann-Katrin Stensdotter et al. "Quadriceps Activation in Closed and in Open Kinetic Chain Exercise". In: *Medicine and Sports in Sports and Exercise* 35.12 (Dec. 2003). DOI: 10.1249/01.MSS.0000099107.03704. AE.
- [48] Derek Pamukoff et al. "Quadriceps Function and Hamstrings Co-Activation After Anterior Cruciate Ligament Reconstruction". In: *Journal of Athletic Training* 52.5 (May 2017). DOI: 10.4085/1062-6050-52.3.05.
- [49] M. Raez, M. Hussain, and F. Mohd-Yasin. "Techniques of EMG signal analysis: detection, processing, classification and applications". In: *Biological Procedures Online* 8 (Mar. 2006). DOI: 10.1251/bpo115.
- [50] Banff Sport Medicine. *Post Operative Rehabilitation Program for Anterior Cruciate Ligament Reconstruction*. Patient Information Leaflet. Sept. 2011.
- [51] University of New Mexico School of Medicine. *Post-operative Rehabilitation Protocol*. 2017. URL: [https://hsc.unm.edu/medicine/departments/ortho-rehab/orthopaedics/fellowships/sports/\\_id\\_docs/sports-medicine-protocols.pdf](https://hsc.unm.edu/medicine/departments/ortho-rehab/orthopaedics/fellowships/sports/_id_docs/sports-medicine-protocols.pdf).
- [52] University of Colorado Sports Medicine. *ACL and Meniscus Repair Rehabilitation Guidelines*. 2023. URL: [https://medschool.cuanschutz.edu/docs/librariesprovider65/eric-mccarty/rehab-protocols/acl-and-meniscus-repair-protocol-2024.pdf?sfvrsn=f9fdc1bb\\_0](https://medschool.cuanschutz.edu/docs/librariesprovider65/eric-mccarty/rehab-protocols/acl-and-meniscus-repair-protocol-2024.pdf?sfvrsn=f9fdc1bb_0).
- [53] Meghan Kelley. *Structured Training Versus All-Out Efforts*. 2023. URL: <https://www.trainerroad.com/blog/structured-training-versus-all-out-efforts/>.
- [54] Corbin Hett et al. "Blood Flow Restriction Enhances Rehabilitation and Return to Sport: The Paradox of Proximal Performance". In: *REHABILITATION AND RETURN TO SPORT IN ATHLETES* 4.1 (2022). DOI: <https://doi.org/10.1016/j.asmr.2021.09.024>.
- [55] University of Oxford Dept. of Computer Science. *Models of Computation*. 2023. URL: <https://www.cs.ox.ac.uk/teaching/courses/2022-2023/modelsofcomputation/>.
- [56] University of Cambridge Dept. of Engineering. *Digital Electronics*. 2022. URL: <https://teaching.eng.cam.ac.uk/content/engineering-tripos-part-iia-3b2-integrated-digital-electronics-2021-22>.
- [57] Ehh (<https://math.stackexchange.com/users/133303/eh>). *How to control a nonlinear system with a PID controller*. Mathematics Stack Exchange. URL: <https://math.stackexchange.com/q/1509193> (version: 2015-11-02). eprint: <https://math.stackexchange.com/q/1509193>.
- [58] Korol G Karniel A Melzer I Ronen A. "Relation between Perceived Effort and the Electromyographic Signal in Localized Effort Activities of Forearm Muscles". In: *Journal of Ergonomics* (2017).
- [59] Yanagisawa N. "EMG for study of involuntary movements". In: *Nihon Rinsho*. (1993).

- [60] Morrison S Kavanagh J Obst SJ Irwin J Haseler LJ. "he effects of unilateral muscle fatigue on bilateral physiological tremor". In: *Exp Brain Res* (2005).
- [61] Loren G Martin. "Why do muscles tremble after strenuous exercise?" In: *Scientific American* (1999).
- [62] Lee SW Vermillion BC Dromerick AW. "Toward Restoration of Normal Mechanics of Functional Hand Tasks Post-Stroke: Subject-Specific Approach to Reinforce Impaired Muscle Function". In: *IEEE Trans Neural Syst Rehabil Eng* (2019).
- [63] Levy A et al Oliveira. "Movement Velocity as an Indicator of Mechanical Fatigue and Resistance Exercise Intensity in Cross Modalities". In: *Research Quarterly for Exercise and Sport* (2023).
- [64] Asa Ben-Hur et al. "Support Vector Clustering". In: *Journal of Machine Learning Research* 2 (2001).
- [65] University of Oxford Dept. of Engineering Science. *Information Theory*. 2023.
- [66] X. Jiaqun and C. Haotian. "Regenerative brake of brushless DC motor for light electric vehicle". In: *18th International Conference on Electrical Machines and Systems (ICEMS)* (2013).
- [67] Jaime et al Hislop. "Validation of 3-Space Wireless Inertial Measurement Units Using an Industrial Robot". In: *Sensors* (2021).
- [68] Stanley Plagenhoef, F. Gaynor Evans, and Thomas Abdelnour. "Anatomical Data for Analyzing Human Motion". In: *Research Quarterly For Exercise and Sport* 54.2 (1983), pp. 169–178. DOI: 10 . 1080 / 02701367.1983.10605290.
- [69] Simon Barrué-Belou et al. "Absolute and Normalized Normative Torque Values of Knee Extensors and Flexors in Healthy Trained Subjects: Asymmetry Questions the Classical Use of Uninjured Limb as Reference". In: *Arthroscopy, Sports Medicine, and Rehabilitation* (2024). DOI: 10.1016/j.asmr.2023.100861.
- [70] Nauman Masud et al. "Design control and actuator selection of a lower body assistive exoskeleton with 3-D passive compliant supports". In: *Journal of the Brazilian Society of Mechanical Sciences and Engineering* (2022). DOI: 10 . 1007 / s40430 – 023 – 04480 – 8.
- [71] Joo-Hyun Lee et al. "Differences in the muscle activities of the quadriceps femurs and hamstrings while performing various squat exercises". In: *BMC Sports Science, Medicine and Rehabilitation* 14.12 (Jan. 2022). DOI: 10 . 1186 / s13102 – 022 – 00404 – 6.
- [72] Fearghal Behan et al. "Sex differences in muscle morphology of the knee flexors and knee extensors". In: *PLoS ONE* 13.1 (Jan. 2018). DOI: 10 . 1371 / journal . pone . 0190903.
- [73] H. Herman, B. Freriks, and R. Merletti. "European Recommendations for Surface Electromyography: Results of the SENIAM Project". In: (1999).
- [74] Joseph Weir et al. "Influence of electrode orientation on electromyographic fatigue indices of the vastus lateralis". In: *Journal of Exercise Physiology* 2.3 (July 1999).
- [75] Felipe Torres Miranda Oliveira et al. "Effects of pennation angle, electrodes orientation and knee angle on surface electromyography of vastus lateralis during isometric con-

- tractions". In: *Sport Sci Health* 13 (2017). DOI: 10.1007/s11332-017-0388-z.
- [76] Dongwoon Lee et al. "A three-dimensional approach to pennation angle estimation for human skeletal muscle". In: *Computer Methods in Biomechanics and Biomedical Engineering* 18.13 (2015). DOI: 10.1080/10255842.2014.917294.
- [77] Diptasree Ghosh et al. "A computational model to investigate the effect of pennation angle on surface electromyogram of Tibialis Anterior". In: *PLoS ONE* 12.12 (Dec. 2017).
- [78] Guido Belli et al. "Electromyographic Analysis of Leg Extension Exercise during Different Ankle and Knee Positions". In: *Journal of Mechanics in Medicine and Biology* 15.2 (2015). DOI: 10.1142/S0219519415400370.
- [79] T. G. Balshaw et al. "Reliability of quadriceps surface electromyography measurements is improved by two vs. single site recordings". In: *Eur J Appl Physiol* 117.6 (Apr. 2017). DOI: 10.1007/s00421-017-3595-z.
- [80] Hiv Lofti, Afsun Nodehi Moghadam, and Mohsen Shati. "Electromyography Activity of Vastus Medialis Obliquus and Vastus Lateralis Muscles During Lower Limb Proprioceptive Neuromuscular Facilitation Patterns in Individuals with and without Patellofemoral Pain Syndrome". In: *Phys Ther Res* 24.3 (July 2021). DOI: 10.1298/ptr.E10094.
- [81] Javier Rodriguez-Falces et al. "The influence of the reference electrode location on the M-wave characteristics in the quadriceps". In: *Journal of Electromyography and Kinesiology* 66 (2022). DOI: 10.1016/j.jelekin.2022.102681.
- [82] *Kendall SCD Sequential Compression Comfort Sleeves*. CardinalHealth. 2018. URL: <https://www.cardinalhealth.co.uk/content/dam/corp/web/documents/brochure/cardinal-health-sequential-compression-comfort-sleeves-brochure.pdf>.
- [83] Paul Stavrinou. *Operational Amplifiers and Circuits*. 2022.
- [84] A. M. Howatson, P. G. Lund, and J. D. Todd. *Engineering Tables and Data*. Department of Engineering Science, 2009.
- [85] B. Lapatki et al. "A thin, flexible multielectrode grid for high-density surface EMG". In: *J Appl Physiol* 96 (Sept. 2003). DOI: 10.1152/japplphysiol.00521.2003.
- [86] *HD-EMG Electrodes*. <https://www.tmsi.com/products/hd-emg-electrodes/>. Accessed: 2024-04-30.
- [87] "The Use of Machine Learning for Inferencing the Effectiveness of a Rehabilitation Program for Orthopedic and Neurological Patients". In: *International Journal of Environmental Research and Public Health* 20.8 (2023), pp. 5575–5575. DOI: 10.3390/ijerph20085575.
- [88] "A Machine Learning-Based Initial Difficulty Level Adjustment Method for Balance Exercise on a Trunk Rehabilitation Robot". In: *IEEE Transactions on Neural Systems and Rehabilitation Engineering* 31 (2023), pp. 1857–1866. DOI: 10.1109/tnsre.2023.3260815.
- [89] *Applying Information Theory Analysis for the Solution of Biomedical Data Processing Problems*. 2014. DOI: 10.3844/AJBSP.2014.17.29.
- [90] "Synthetic data in medical research". In: *BMJ Medicine* 1.1 (2022), e000167–e000167. DOI: 10.1136/bmjmed-2022-000167.

- [91] *Dynamixel*. <https://www.dynamixel.com/index.php>.
- [92] *Medical Time-Series Data Generation Using Generative Adversarial Networks*. Springer, Cham, 2020, pp. 382–391. DOI: 10.1007/978-3-030-59137-3\_34.
- [93] Sylos-Labini F, Ivanenko YP, MacLellan MJ, Cappellini G, Poppele RE, Lacquaniti F. “Locomotor-Like Leg Movements Evoked by Rhythmic Arm Movements in Humans”. In: *PLoS ONE* 9.3 (2014). URL: <https://doi.org/10.1371/journal.pone.0090775>.
- [94] *Dynamixel AX-12W e-manual*. <https://emanual.robotis.com/docs/en/dxl/ax/ax-12w/>.
- [95] *Naver ACLKnee Community*. <https://cafe.naver.com/aclknee>.
- [96] Emory Healthcare. *ACL Recovery Guidelines: Weeks 4-6*. 2022.
- [97] “Generation of realistic synthetic data using Multimodal Neural Ordinary Differential Equations”. In: 5.1 (2022). DOI: 10.1038/s41746-022-00666-x.
- [98] “A Method for Machine Learning Generation of Realistic Synthetic Datasets for Validating Healthcare Applications”. In: *medRxiv* (2021). DOI: 10.1101/2021.02.11.21250741.
- [99] “Improvement of predictive accuracies of functional outcomes after subacute stroke inpatient rehabilitation by machine learning models”. In: *PLOS ONE* 18.5 (2023), e0286269–e0286269. DOI: 10.1371/journal.pone.0286269.
- [100] Christopher M. Bishop. *Pattern Recognition and Machine Learning*. Springer, 2006.
- [101] “Support Vector Machine for Stroke Risk Prediction”. In: *Highlights in Science, Engineering and Technology* 38 (2023), pp. 917–923. DOI: 10.54097/hset.v38i.5977.
- [102] *Support Vector Machine with Composite Kernels for Time Series Prediction*. Springer, Berlin, Heidelberg, 2007, pp. 350–356. DOI: 10.1007/978-3-540-72395-0\_45.
- [103] “Regression for Pooled Testing Data with Biomedical Applications”. In: (2019).
- [104] *Understanding Gradient Boosting Machine*. <https://towardsdatascience.com/understanding-gradient-boosting-machines-9be756fe76ab>.
- [105] “A Comparative Study of Machine Learning Algorithms for Controlling Torque of Permanent Magnet Synchronous Motors through a Closed Loop System”. In: (2019), pp. 1–6. DOI: 10.1109/INTELLECT47034.2019.8955467.
- [106] Olyanasab, Ali, and Mohsen Annabestani. “Leveraging Machine Learning for Personalized Wearable Biomedical Devices: A Review”. In: *Journal of Personalized Medicine* 14.2 (2024), p. 203.
- [107] “Anomaly detection using spatial and temporal information in multivariate time series”. In: *Dental science reports* 13.1 (2023). DOI: 10.1038/s41598-023-31193-8.
- [108] *Anomaly Detection of Motion Capture Data Based on the Autoencoder Approach*. 2023, pp. 611–622. DOI: 10.1007/978-3-031-36021-3\_59.
- [109] “Anomaly detection for multivariate times series through the multi-scale convolutional recurrent variational autoencoder”. In: *Expert systems with applications* 231 (2023),

- pp. 120725–120725. DOI: 10 . 1016 / j . eswa . 2023 . 120725.
- [110] “Anomaly Detection Using Prediction Error with Spatio-Temporal Convolutional LSTM”. In: *The University of Danang - Journal of Science and Technology* (2022), pp. 7–12. DOI: 10 . 31130 / ud - jst . 2022 . 289e.
- [111] American Society of Anesthesiologists. *AI Pain Recognition System*. Oct. 2023. URL: <https://www.asahq.org/about-asa/newsroom/news-releases/2023/10/ai-pain-recognition-system> (visited on 04/15/2023).
- [112] Sahar Borna et al. “A Review of Voice-Based Pain Detection in Adults Using Artificial Intelligence”. In: *Bioengineering* 10.4 (2023). ISSN: 2306-5354. DOI: 10 . 3390 / bioengineering10040500. URL: <https://www.mdpi.com/2306-5354/10/4/500>.
- [113] Rasha M. Al-Eidan, Hend Al-Khalifa, and AbdulMalik Al-Salman. “Deep-Learning-Based Models for Pain Recognition: A Systematic Review”. In: *Applied Sciences* 10.17 (2020). ISSN: 2076-3417. DOI: 10 . 3390 / app10175984.
- [114] Ossama Abdel-Hamid et al. “Convolutional neural networks for speech recognition”. In: *IEEE/ACM Transactions on Audio, Speech, and Language Processing* 22.10 (2014), pp. 1533–1545.
- [115] Geoffrey Hinton et al. “Deep neural networks for acoustic modeling in speech recognition: The shared views of four research groups”. In: *IEEE Signal Processing Magazine* 29.6 (2012), pp. 82–97.
- [116] Xiaofei Li et al. “Voice activity detection based on statistical likelihood ratio with adaptive thresholding”. In: *2016 IEEE International Workshop on Acoustic Signal Enhancement (IWAENC)*. 2016, pp. 1–5. DOI: 10 . 1109/IWAENC . 2016 . 7602911.
- [117] Diederik P. Kingma and Jimmy Ba. “Adam: A Method for Stochastic Optimization”. In: *CoRR* abs/1412.6980 (2014). URL: <https://api.semanticscholar.org/CorpusID:6628106>.
- [118] “Extending Radio Broadcasting Semantics through Adaptive Audio Segmentation Automations”. In: *Knowledge* 2.3 (2022), pp. 347–364. DOI: 10 . 3390 / knowledge2030020.
- [119] “Semi-Supervised Audio Classification with Partially Labeled Data.” In: *arXiv: Sound* (2021).
- [120] “A Robust Feature Extraction Method for Sound Signals Based on Gabor and MFCC”. In: (2022), pp. 49–55. DOI: 10 . 1109/ICCIS56375 . 2022 . 9998146.
- [121] “Accurate extraction of chroma vectors from an audio signal”. 2017.
- [122] “Enhanced representation of spectral contrasts in the primary auditory cortex”. In: *Frontiers in Systems Neuroscience* 7 (2013), pp. 21–21. DOI: 10 . 3389 / FNSYS . 2013 . 00021.
- [123] “Comparative analysis between application of transformer and recurrent neural network in speech recognition”. In: *Applied and Computational Engineering* 6.1 (2023), pp. 629–634. DOI: 10 . 54254 / 2755-2721 / 6 / 20230879.
- [124] “Multimodal physiological sensing for the assessment of acute pain”. In: *Frontiers in pain research* 4 (2023). DOI: 10 . 3389 / fpain . 2023 . 1150264.

- [125] Michael Stonis. *Enterprise Application Patterns Using .NET MAUI*. 1.0. Microsoft Developer Division, .NET, and Visual Studio product teams, 2022.
- [126] “Compliance with HIPAA and GDPR in Certificateless-Based Authenticated Key Agreement Using Extended Chaotic Maps”. In: *Electronics* 12.5 (2023), pp. 1108–1108. DOI: 10.3390/electronics12051108.

## 14 List of Figures

1	Three types of braces by materials . . . . .	8	23	Overall schematic for AutoPhysio . . . . .	45
2	Examples of electronic rehabilitation devices . . . . .	9	24	Knee pivots (external) . . . . .	49
3	An anatomy of the knee. . . . .	10	25	Knee pivots (internal) . . . . .	49
4	sEMG electrodes . . . . .	13	26	Illustrations of alternative mechanisms	50
5	Example sessions . . . . .	16	27	Maximum muscular flexion and extension . . . . .	53
6	Session flowcharts . . . . .	17	28	Simplified leg dynamics . . . . .	54
7	Remaining flowcharts . . . . .	17	29	Four bar linkage mechanism . . . . .	55
8	Flowchart of the procedure during a repetition . . . . .	19	30	Loop closure angles convention. . . . .	57
9	AutoPhysio’s user interface . . . . .	21	31	MATLAB solution to four bar linkage	58
10	The system to be controlled in the Assist state . . . . .	23	32	Mechanical advantage by four bar linkage . . . . .	58
11	Finite State Machine for the motor - safety transitions not illustrated for clarity . . . . .	24	33	Testing four bar mechanical advantage	59
12	Extension and flexion setting . . . . .	28	34	Robust four bar linkage . . . . .	60
13	Accounting for multi-variate and multi-modal data . . . . .	31	35	Static forces (software) . . . . .	61
14	Example collected data (simplified to 2D) . . . . .	32	36	Static forces (by hand) . . . . .	61
15	Clusters . . . . .	33	37	Exoskeleton joint . . . . .	64
16	Class posterior PDF . . . . .	34	38	Motor curve . . . . .	65
17	Integral over the volume split by the hyperplane at $F^*$ perpendicular to $\bar{v}$ . . . . .	35	39	Controller connections . . . . .	66
18	Equivalent circuit for a separately-excited DC generator . . . . .	41	40	CAD modelling for exoskeleton joint	68
20	Overall Schematic . . . . .	42	41	Full exoskeleton joint assembly . . . . .	69
21	System for the control of motor torque to a desired torque . . . . .	43	42	Non permanent fixing . . . . .	71
22	Block reduction from a cascaded to an integrated control system . . . . .	44	43	Cross-section of the human thigh . . . . .	72
			44	EMG data flow . . . . .	73
			45	Existing use of EMG within sleeves . . . . .	73
			46	Snap connection illustration . . . . .	76
			47	Electrode perforations illustration . . . . .	76
			48	Fabric layers illustration . . . . .	77
			49	Concept for outer fabric layer . . . . .	77
			50	Reference extension outer fabric layer	78
			51	Basic sleeve proof of concept . . . . .	78
			52	Bipolar electrode case. . . . .	80

53	Flow of EMG signals in hardware . . . . .	81	62	Possible recovery trajectories . . . . .	89
54	Bandpass filter template . . . . .	81	63	Synthetic data - daily maximum range of motion progression . . . . .	90
55	High pass filter template . . . . .	82	64	Recovery progress prediction for sigmoid trend . . . . .	92
56	Low pass filter template . . . . .	83	65	Anomaly detection . . . . .	98
57	Bandpass filter . . . . .	84	66	Model-View-View Model design pattern . . . . .	103
58	Bandpass filter bode plot . . . . .	84	67	Login screen . . . . .	105
59	High density EMG electrode grids . . . . .	85	68	App system architecture . . . . .	107
60	Materials for data generation . . . . .	87			
61	In-session range of motion theoretical data . . . . .	88			

## 15 List of Tables

1	Summary of the physical and psychological roles of physiotherapy sessions . . . . .	15	7	BS 2488 E24 series standard values	81
2	The desired functionality for the four modes of AutoPhysio's operation . . . . .	20	8	High pass filter resistance values . . . . .	82
3	Summarising the implementations for each state's output torque calculation . . . . .	23	9	Low pass filter resistance values . . . . .	83
4	Anatomical data (relevant data indicated) . . . . .	52	10	Filter component values . . . . .	84
5	Quadriceps electrode placement details . . . . .	74	11	Recovery trajectories distribution among patients . . . . .	89
6	Hamstrings electrode placement details . . . . .	75	12	Time required to achieve full range of motion . . . . .	90
			13	Interact app features . . . . .	105
			14	Collaboration app features . . . . .	106
			15	Risk Assessment for the AutoPhysio device . . . . .	108